Acta Cryst C STRUCTURAL CHEMISTRY

ISSN 2053-2296

Crystal structures of hybrid completely reduced phosphomolybdates and catalytic performance applied as molecular catalysts for the reduction of chromium(VI)

Xuerui Tian, Xing Xin, Yuanzhe Gao, Dandan Dai, Jinjin Huang and Zhangang Han*

College of Chemistry and Material Science, Hebei Normal University, Yuhua District South Second Ring Road 20, Shijiazhuang, Hebei 050024, People's Republic of China. *Correspondence e-mail: hanzg116@126.com

Received 21 May 2018
Accepted 14 September 2018

Edited by J. R. Galán-Mascarós, Institute of Chemical Research of Catalonia (ICIQ), Spain

Keywords: polyoxometalates; crystal structure; catalytic performance; hexavalent chromium.

CCDC references: 1842298; 1842297; 1842296

Supporting information: this article has supporting information at journals.iucr.org/c

The exploration of highly efficient and low-cost catalysts for the treatment of hexavalent chromium Cr^{VI} in environmental remediation is currently one of the most challenging topics. Here, three phosphomolybdate hybrid compounds have been successfully isolated by the hydrothermal method and been applied as supramolecular catalysts for the reduction of Cr^{VI}. Single-crystal X-ray diffraction revealed their formulae as $(H_2bpp)_2[Fe(H_2O)][Sr(H_2O)_4]_2\{Fe[Mo_6O_{12}(OH)_3(H_2PO_4)(HPO_4)(PO_4)_2]_2\}\cdot 5H_2O$ (**1**), $(H_2bpp)_2[Na(H_2O)(OC_2H_5)][Fe(H_2O)_2][Ca(H_2O)_2]_2\{Fe[Mo_6O_{12}(OH)_3(H_2PO_4)(HPO_4)(PO_4)_2]_2\}\cdot 4H_2O$ (**2**) and $(H_2bpe)_3\{Fe[Mo_6O_{12}(OH)_3(HPO_4)_3(H_2PO_4)]_2\}\cdot 8H_2O$ (**3**) [bpp is 1,3-bis(pyridin-4-yl)propane ($C_{13}H_{14}N_2$) and bpe is *trans*-1,2-bis(pyridin-4-yl)ethylene ($C_{12}H_{10}N_2$)]. The three hybrids consist of supramolecular networks built up by noncovalent interactions between $\{Fe[P_4Mo_6{}^VO_{31}]_2\}^{22-}$ polyanions and protonated organic cations. This kind of hybrid polyoxometalate could be applied as heterogeneous molecular catalysts for the reduction of Cr^{VI}. It was found that the organic moiety plays a vital role in influencing the catalytic activity of the polyanions. Organic bpp-containing hybrids **1** and **2** are highly active in the catalytic reduction of heavy metal Cr^{VI} ions using HCOOH as reductant, while bpe-containing hybrid **3** is inactive to this reaction. This work is significant for the design of new catalysts, as well as the exploration of reaction mechanisms at a molecular level.

1. Introduction

In recent years, the large-scale natural water environment is suffering some degree of pollution with the rapid development of industry, in which heavy metal ions are especially dangerous due to their toxicity. Chromium, a trace element essential for the human body, is one of the most common heavy metal pollutants in the environment (Gong *et al.*, 2015*a*,*b*). It is widely used in industries such as electroplating, leather making, metallurgy, printing and dyeing, textile, medicine and ceramics. Chromium pollution is characterized by its nonnatural biodegradability and can enter the body through the digestive tract, respiratory tract and skin (Linos *et al.*, 2011). Generally, chromium is often present in two stable oxidation states, *i.e.* Cr^{VI} and Cr^{III} (Han *et al.*, 2004). The toxic Cr^{VI} ion is highly migratory in soils and aqueous environments, while the less toxic Cr^{III} ion is insoluble in water and poor in mobility. Therefore, the chemical reduction of Cr^{VI} to the less toxic and easily removed Cr^{III} is an effective way of treating chromium-containing wastewater (Shao *et al.*, 2017). In this regard, the development of new catalysts and green reaction systems is a key challenge in chemical research.

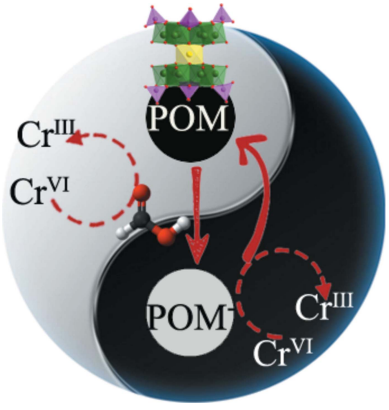

Polyoxometalates (POMs) are transition metal–oxide clusters of d^0 or d^1 metal ions bridged *via* O atoms (Walsh *et al.*, 2016). In the POM library, the hourglass-type $\{M(P_4Mo_6O_{31})_2\}$ (abbreviated as $\{M(P_4Mo_6)\}$) polyanionic cluster is unique and is formed from two $(P_4Mo_6O_{31})$ (abbreviated as $\{P_4Mo_6\}$) subunits bridged by one metal atom *M* (Chang *et al.*, 2006; Hao *et al.*, 2010; Zhang *et al.*, 2007*a*,*b*). This kind of polyanionic structure has a larger specific surface area and richer surface O atoms than common 'spheroidal' anionic clusters. These surface O atoms can act as potential active coordination sites to bond with various metal linkers (Dolbecq *et al.*, 2010; Han & Hill, 2007). More especially, all Mo atoms are in the +5 oxidation states, representing a reduced polyanionic metal–oxygen cluster. Therefore, both their shape and electronic structure endow them with many applications in catalysis, semiconductors and materials science. The design and synthesis of novel $\{P_4Mo_6\}$-based POMs have become an important research area for POM chemists (Miras *et al.*, 2014; Zhang *et al.*, 2015; Lin *et al.*, 2008; Chen *et al.*, 2007). During the synthesis of hybrid $\{P_4Mo_6\}$-based POMs, organic amines not only play an important role as structure-directing agents to induce the final packaging arrangements (Streb *et al.*, 2007), but also act as reductants to reduce Mo^{VI} to Mo^{V}.

POM-based catalysts have been widely researched in the laboratory and even applied in industry. Although there are many examples using $\{P_4Mo_6\}$-based POMs as catalysts (Gkika *et al.*, 2006; Liang *et al.*, 2015; Yu *et al.*, 2012; Fu *et al.*, 2012; Zhang *et al.*, 2014), the field still remains undeveloped. Our research has focused on the design, synthesis and application of new $\{P_4Mo_6\}$-based supramolecular hybrids and has shown that the central metal atom *M* has important effects on the catalytic performance of crystalline materials (Gong *et al.*, 2015*a*,*b*; He *et al.*, 2015). Our experiments showed that the transition-metal Fe atom, as the connecting unit to construct these $\{P_4Mo_6\}$-based hybrid materials, is a positive factor for the catalytic properties of crystal materials. Here, three examples of $\{Fe[P_4Mo_6{}^{V}O_{31}]_2\}^{n-}$-containing hybrid supramolecular phosphomolybdates, *i.e.* $(H_2bpp)_2[Fe(H_2O)][Sr(H_2O)_4]_2\{Fe[Mo_6O_{12}(OH)_3(H_2PO_4)(HPO_4)(PO_4)_2]_2\}\cdot 5H_2O$ (**1**), $(H_2bpp)_2[Na(H_2O)(OC_2H_5)][Fe(H_2O)_2][Ca(H_2O)_2]_2\{Fe[Mo_6O_{12}(OH)_3(H_2PO_4)(HPO_4)(PO_4)_2]_2\}\cdot 4H_2O$ (**2**), $(H_2bpe)_3\{Fe[Mo_6O_{12}(OH)_3(HPO_4)_3(H_2PO_4)]_2\}\cdot 8H_2O$ (**3**) [bpp is 1,3-bis(pyridin-4-yl)propane and bpe is *trans*-1,2-bis(pyridin-4-yl)ethylene], have been isolated successfully through hydrothermal reactions. All of them present supramolecular networks formed through numerous intermolecular interactions between organic and inorganic moieties. Hybrids **1** and **2** consist of protonated bpp cations and $\{Fe(P_4Mo_6)_2\}$ polyanionic clusters, while hybrid **3** is composed of protonated bpe cations and polyanionic clusters. The three $\{Fe(P_4Mo_6)_2\}$ hybrids were used as supramolecular catalysts to catalyze the reaction of Cr^{VI} to Cr^{III} with formic acid (FA) as reductant. It was found that the organic moiety plays a critical role in adjusting the catalytic activity of the polyanions. Bpp-containing hybrids **1** and **2** are active in the catalytic redox reaction of Cr^{VI}–FA, while bpe-containing hybrid **3** is inactive in this reaction. This work is significant for the design of new catalysts, as well as for exploring the reaction mechanism at a molecular level.

2. Experimental

2.1. Materials and measurements

All the chemical reagents were obtained through commercial channels, and were used as received. FT–IR spectra (KBr pellet) were recorded with an FTIR-8900 IR spectrometer in the range 400–4000 cm^{-1}. Thermogravimetric analyses (TG) were carried out with a PerkinElmer Pyris Diamond TG/DTA instrument. UV–Vis spectra were measured with a U3010 UV–Vis spectrophotometer (Shimadzu). Powder X-ray diffraction (XRD) analyses were carried out on a Bruker D8 Advance diffractometer. Cyclic voltammograms (CV) were performed on a PARC Model 384B polarographic analyzer.

2.2. Syntheses of hybrids 1–3

2.2.1. Hybrid 1. A mixture of $Na_2MoO_4\cdot 2H_2O$ (0.24 g, 1.00 mmol), bpp (0.04 g, 0.20 mmol), $FeCl_2\cdot 4H_2O$ (0.10 g, 0.50 mmol), $SrCl_2\cdot 6H_2O$ (0.10 g, 0.38 mmol), H_3PO_4 (0.50 ml, 7.5 mmol) and H_2O (8.0 ml, 0.44 mol) was stirred for 30 min and the pH was adjusted to 2.50 with NaOH. The mixture was

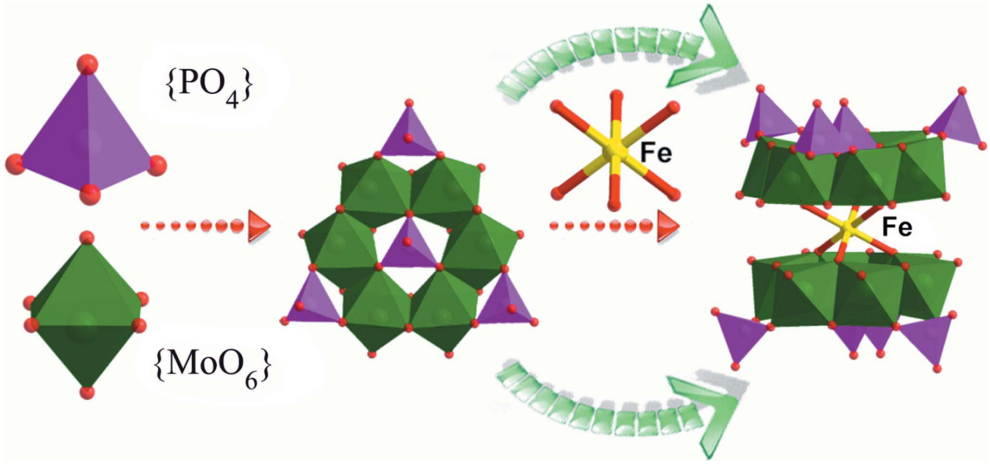

Figure 1
Polyhedral diagram showing the assembly of the hourglass-type cluster $\{Fe(P_4Mo_6O_{31})_2\}$.

Table 1
Experimental details.

	1	2	3
Crystal data			
Chemical formula	$(C_{13}H_{16}N_2)_2[Fe(H_2O)][Sr(H_2O)_4]_2\{Fe[Mo_6O_{12}(OH)_3(H_2PO_4)(HPO_4)(PO_4)_2]_2\}\cdot 5H_2O$	$(C_{13}H_{16}N_2)_2[Na(H_2O)(C_2H_5O)][Fe(H_2O)_2][Ca(H_2O)_2]_2\{Fe[Mo_6O_{12}(OH)_3(H_2PO_4)(HPO_4)(PO_4)_2]_2\}\cdot 4H_2O$	$(C_{12}H_{12}N_2)_3\{Fe[Mo_6O_{12}(OH)_3(HPO_4)_3(H_2PO_4)]_2\}\cdot 8H_2O$
M_r	3338.82	3260.77	3159.85
Crystal system, space group	Triclinic, $P\overline{1}$	Monoclinic, $C2/c$	Monoclinic, $P2_1/c$
Temperature (K)	296	296	296
a, b, c (Å)	11.385 (3), 14.121 (3), 15.126 (4)	21.317 (7), 18.533 (6), 22.838 (8)	11.8121 (9), 22.6484 (16), 16.0089 (12)
α, β, γ (°)	69.259 (3), 82.422 (4), 88.086 (4)	90, 95.130 (5), 90	90, 98.701 (1), 90
V (Å^3)	2254.0 (9)	8986 (5)	4233.5 (5)
Z	1	4	2
Radiation type	Mo $K\alpha$	Mo $K\alpha$	Mo $K\alpha$
μ (mm^{-1})	3.35	2.31	2.16
Crystal size (mm)	0.17 × 0.15 × 0.13	0.19 × 0.17 × 0.15	0.19 × 0.15 × 0.13
Data collection			
Diffractometer	Bruker SMART CCD area detector	Bruker SMART CCD area detector	Bruker SMART CCD area detector
Absorption correction	Multi-scan (*SADABS*; Bruker, 2008)	Multi-scan (*SADABS*; Bruker, 2008)	Multi-scan (*SADABS*; Bruker, 2008)
T_{min}, T_{max}	0.571, 0.647	0.652, 0.708	0.685, 0.756
No. of measured, independent and observed [$I > 2\sigma(I)$] reflections	10357, 7715, 5705	19982, 7781, 7629	20768, 7432, 7075
R_{int}	0.033	0.022	0.018
$(\sin \theta/\lambda)_{max}$ (Å^{-1})	0.595	0.595	0.595
Refinement			
$R[F^2 > 2\sigma(F^2)]$, $wR(F^2)$, S	0.057, 0.161, 1.05	0.038, 0.111, 1.06	0.020, 0.050, 1.07
No. of reflections	7715	7781	7432
No. of parameters	616	616	628
No. of restraints	0	3	0
H-atom treatment	H-atom parameters constrained	H atoms treated by a mixture of independent and constrained refinement	H atoms treated by a mixture of independent and constrained refinement
$\Delta\rho_{max}$, $\Delta\rho_{min}$ (e Å^{-3})	2.59, −1.40	1.89, −0.73	0.72, −0.60

Computer programs: *SMART* (Bruker, 2008), *SAINT* (Bruker, 2008), *SHELXTL* (Sheldrick, 2008) and *SHELXL2014* (Sheldrick, 2015).

then transferred to a Teflon-lined reactor and kept at 160 °C for 5 d. After the reactor was cooled to room temperature at a rate of 10 °C h^{-1}, red cubic crystals were obtained, washed with distilled water and air-dried to give a yield of 70% (based on Mo). Elemental analysis calculated for $C_{26}H_{72}Fe_2Mo_{12}N_4O_{76}P_8Sr_2$ (%): C 9.34, H 2.17, N 1.68; found: C 9.32, H 2.19, N 1.65.

2.2.2. Hybrid 2. A mixture of $Na_2MoO_4\cdot 2H_2O$ (0.24 g, 1.00 mmol), bpp (0.04 g, 0.20 mmol), $FeCl_2\cdot 4H_2O$ (0.10 g, 0.50 mmol), $CaCl_2$ (0.10 g, 0.90 mmol), H_3PO_4 (0.50 ml, 7.5 mmol) and H_2O (8.0 ml, 0.44 mol) was stirred for 30 min, and the pH was adjusted to 2.00∼3.50 with NaOH. The mixture was then transferred to a Teflon-lined reactor and kept at 160 °C for 5 d. After the reactor was cooled to room temperature at a rate of 10 °C h^{-1}, red cubic crystals were obtained, washed with distilled water and air-dried to give a yield of 80% (based on Mo). Elemental analysis calculated for $C_{28}H_{71}Ca_2Fe_2Mo_{12}N_4NaO_{74}P_8$ (%): C 10.31, H 2.19, N 1.72; found: C 10.29, H 2.22, N 1.70.

2.2.3. Hybrid 3. A mixture of $Na_2MoO_4\cdot 2H_2O$ (0.12 g, 0.50 mmol), bpe (0.04 g, 0.22 mmol), $FeCl_2\cdot 4H_2O$ (0.18 g, 0.90 mmol), $CaCl_2$ (0.10 g, 0.90 mmol), H_3PO_4 (0.50 ml, 7.5 mmol) and H_2O (8.0 ml, 0.44 mol) was stirred for 30 min, and the pH was adjusted to 0.20 with H_3PO_4. The mixture was then transferred to a Teflon-lined reactor and kept at 160 °C for 5 d. After the reactor was cooled to room temperature at a rate of 10 °C h^{-1}, red acicular crystals were obtained, washed with distilled water and air-dried to give a yield of 70% (based on Mo). Elemental analysis calculated for $C_{36}H_{68}FeMo_{12}N_6O_{70}P_8$ (%): C 13.68, H 2.17, N 2.66; found: C 13.65, H 2.19, N 2.65.

2.3. X-ray crystallography

Non-H atoms were refined anisotropically in all three structures. The instructions used for the final refinements are included in the CIF, available as supporting information. Some representative bond lengths in hybrids **1–3** are listed in Tables S1–S3. All the crystallographic data and structure refinement details for hybrids **1–3** (CCDC 1842296–1842298) are summarized in Table 1. The hydroxyl H atoms in **1–3** were located from difference Fourier maps and refined with a fixed model. H atoms attached to N atoms in **1–3** were fixed in riding modes. The water H atoms were not defined, but were included in the final formula.

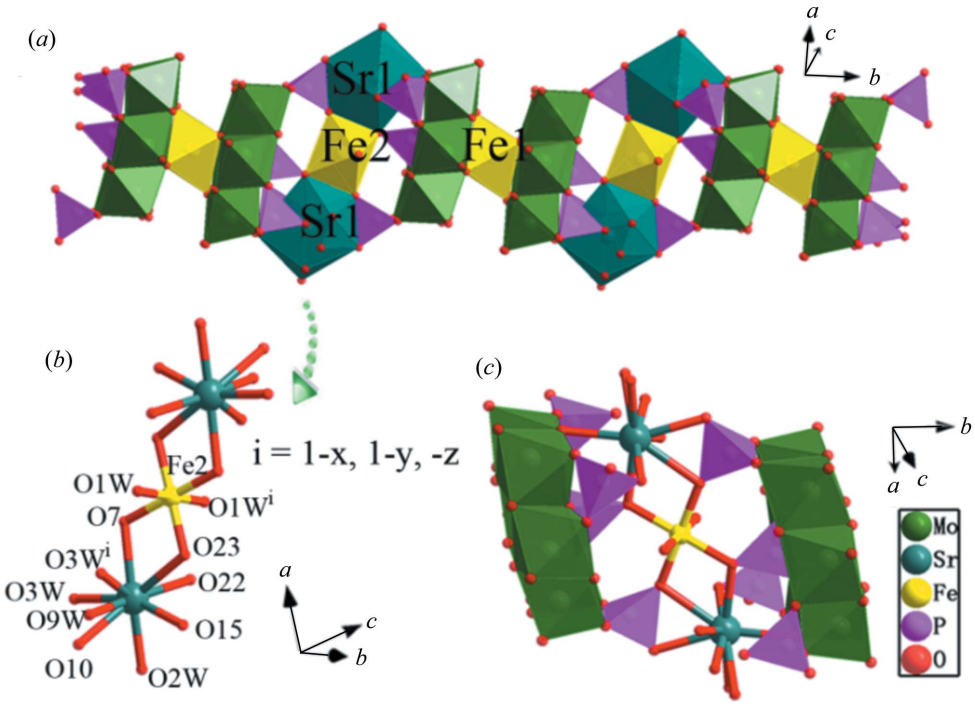

Figure 2
(*a*) Polyhedral representation showing the 1D chain of $\{Fe(P_4Mo_6)_2\}$ units and $\{Sr_2Fe\}$ linkers in **1**. (*b*) The trinuclear cationic fragment of $\{Sr_2Fe\}$ in **1**, showing the coordinated environments of the Fe and Sr atoms. (*c*) The trinuclear $\{Sr_2Fe\}$ unit bridging two adjacent $\{P_4Mo_6\}$ clusters in **1**.

2.4. Preparation of carbon paste electrodes (CPEs) modified with hybrids 1–3

For the preparation of **1**-modified carbon paste electrodes (labelled as **1**-CPE), graphite powder (0.100 g) and hybrid **1** (0.010 g) were mixed and ground in an agate mortar, and then two drops of liquid paraffin were added while stirring with a glass rod. Finally, the paste-like mixture was added to a glass tube with an inner diameter of 3 mm and pressed tightly with a copper bar inserted as a conductor. The procedures for **2**-CPE and **3**-CPE were identical to that for **1**-CPE.

2.5. Catalytic study of the Cr^{VI} reduction reaction

To assess the catalytic activity of the POMs, we investigated the aqueous-phase reduction of Cr^{VI} to Cr^{III} using FA as the reducing agent. The redox reaction of $K_2Cr_2O_7$ and FA catalyzed by hybrids **1**, **2** or **3** was carried out in a glass reactor of 80 ml capacity. The initial concentrations of $K_2Cr_2O_7$ and FA were 4.4×10^{-4} and 4.6×10^{-2} *M*, respectively. 20 mg of the $\{P_4Mo_6\}$-based catalysts and 0.5 ml of FA were added to the Cr^{VI} solution (50 ml). The system was stirred magnetically at different temperatures. After 30, 60, 90, 120, 150 and 180 min, a 3 ml aliquot was sampled and centrifuged to remove any particles of catalyst. The reaction kinetics and the progress of the reaction were monitored by UV–Vis spectrophotometry at 348 nm absorption as a function of reaction time. The spectra of the blank experiments in the absence of any catalyst were also recorded. The ionic equation for the redox reaction is shown in equation (1) (Liang *et al.*, 2014; Omole *et al.*, 2007).

$$Cr_2O_7^{2-} + 8H_3O^+ + 3FA \leftrightarrow 2Cr^{3+} + 3CO_2 + 15H_2O \quad (1)$$

The conversion rate of Cr^{III} was calculated from the formula $([C_0] - [C_i])/C_0 \times 100\%$, where $[C_0]$ is the initial concentration and $[C_i]$ is the interim concentration at each time point. Concentrations were determined by absorbance. Detailed information can be found in the supporting information (Fig. S1).

3. Results and discussion

3.1. Synthesis

Different from the classical Keggin- and Dawson-type polyanions, all the Mo sites in $\{P_4Mo_6\}$ are in the +5 oxidation state. This means that $\{P_4Mo_6\}$ may be one of the few anionic clusters with reducing properties in this large family of polyanions. In the process of synthesizing new $\{P_4Mo_6\}$-based supramolecular assemblies, we have realized the influence of the reaction conditions on the final structures and properties of new crystals. Thus, the reaction parameters for the successful synthesis of the hourglass-like anionic clusters have a regulatory role. Hybrids **1–3** were obtained by changing the type of organic moiety and metal chloride, as well as the pH value of the solution. Experiments showed that the transition-metal Fe atom, as the connecting unit in the construction of these hourglass-type $\{P_4Mo_6\}$-based hybrid materials, should be a positive factor for the catalytic properties of crystalline materials. Furthermore, alkali-metal ions usually act as another type of linker because of their more flexible bonding modes and low positive charge number, and can effectively adjust the acidity–alkalinity of the polyanionic cluster (Huang *et al.*, 2003; Zhang *et al.*, 2007*a*,*b*).

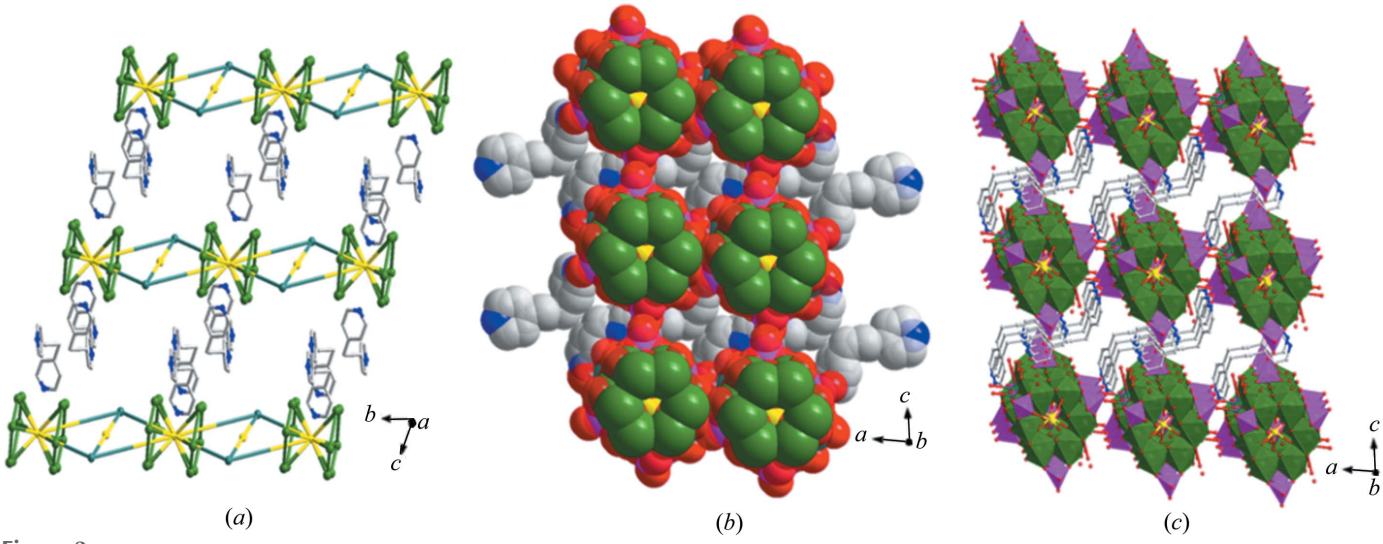

Figure 3
(*a*) A simplified diagram showing the 2D structure in **1** in the *bc* plane. (*b*) A space-filling view showing the 3D stacked structure of polyanions and bpp cations in **1**. (*c*) A mixed polyhedral and ball-and-stick view showing the packing arrangement in **1**. All solvent water molecules and H atoms have been omitted for clarity.

3.2. Structure analysis

X-ray single-crystal diffraction analysis revealed that hybrids **1–3** contained hourglass-type $\{Fe[P_4Mo_6O_{31}]_2\}^{22-}$ anionic clusters (see Fig. 1), protonated organic counter-cations and water molecules. The basic $[P_4Mo_6O_{31}]^{12-}$ building unit with C_3 symmetry is composed of four $\{PO_4\}$ tetrahedra and six $\{MoO_6\}$ octahedra interconnected in corner- and edge-sharing mode. The six Mo atoms [Mo—O = 1.666 (2)–2.329 (4) Å] are located in the same plane with alternating short (average 2.59 Å) and long Mo···Mo distances (average 3.51 Å). The central phosphate group bridges the ring internally through three μ_3-O atoms, and the other three phosphate groups externally link three long Mo···Mo contacts through two μ_2-O donors (Yu *et al.*, 2011). The P—O bond lengths are in the range 1.506 (2)–1.597 (4) Å and the O—P—O angles are 103.30 (12)–114.3 (3)°. The central transition-metal Fe ion connects two $\{P_4Mo_6\}$ units *via* six μ_3-O atoms between short Mo···Mo contacts to form the hourglass-type $\{Fe[P_4Mo_6]_2\}$ moiety. The bond valence sums

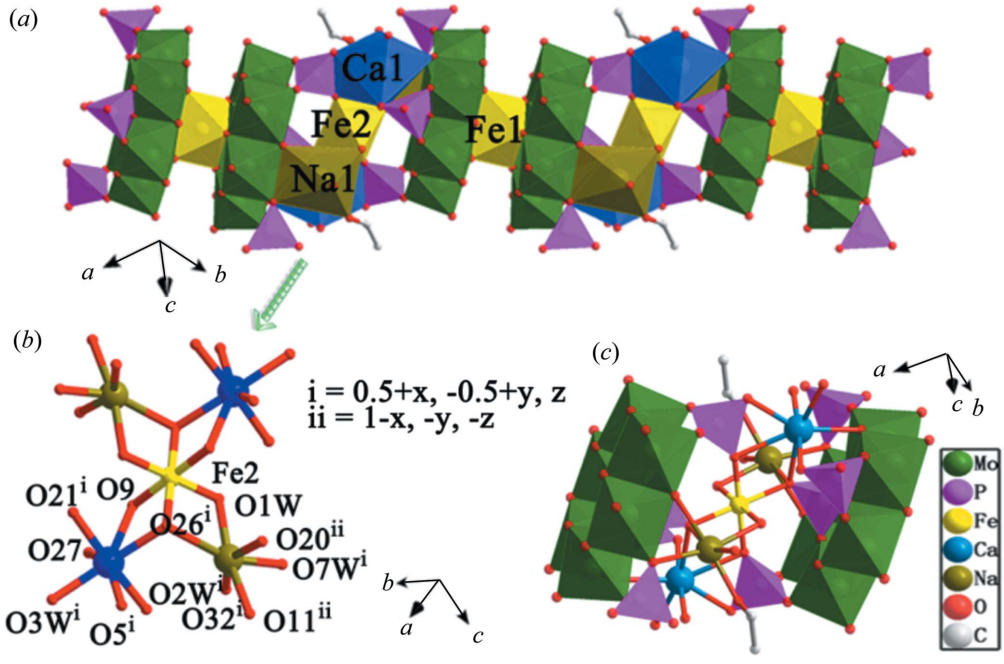

Figure 4
(*a*) Polyhedral representation showing the connection between $\{Fe(P_4Mo_6)_2\}$ units and $\{FeCa_2Na_2\}$ linkers in **2**. (*b*) The pentanuclear fragment of $\{FeCa_2Na_2\}$ in **2**, presenting the coordination environments of the metal centres. (*c*) The connection mode of the $\{FeCa_2Na_2\}$ fragment between two adjacent $\{P_4Mo_6\}$ units.

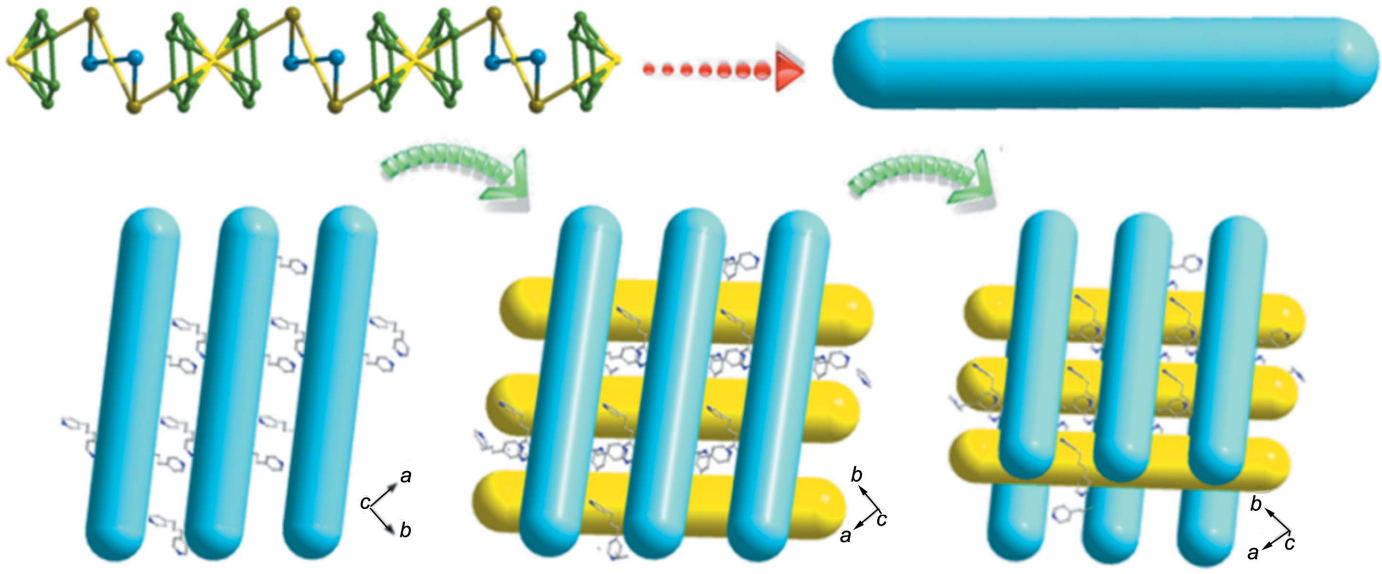

Figure 5
Schematic views showing the packing mode of the inorganic and organic moieties in **2**.

(BVSs) of hybrids **1–3** show that all the Mo and P atoms are in the +5 valence state and the Fe atoms are in the +2 valence state (Table S4 in the supporting information).

Hybrid **1** crystallizes in the triclinic space group $P\overline{1}$ and is composed of an $\{Fe[Mo_6O_{12}(OH)_3(H_2PO_4)(HPO_4)(PO_4)_2]_2\}^{10-}$ polyoxoanion, a protonated $[H_2bpp]^{2+}$ cation, $\{M(H_2O)_x\}^{2+}$ (M = Fe or Sr) subunits and water molecules. There are two types of six-coordinated Fe atoms in this structure, labelled as Fe1 and Fe2. The Fe1—O bond lengths are 2.165 (7), 2.178 (7) and 2.183 (7) Å (× 2), and the Fe2—O bond lengths are

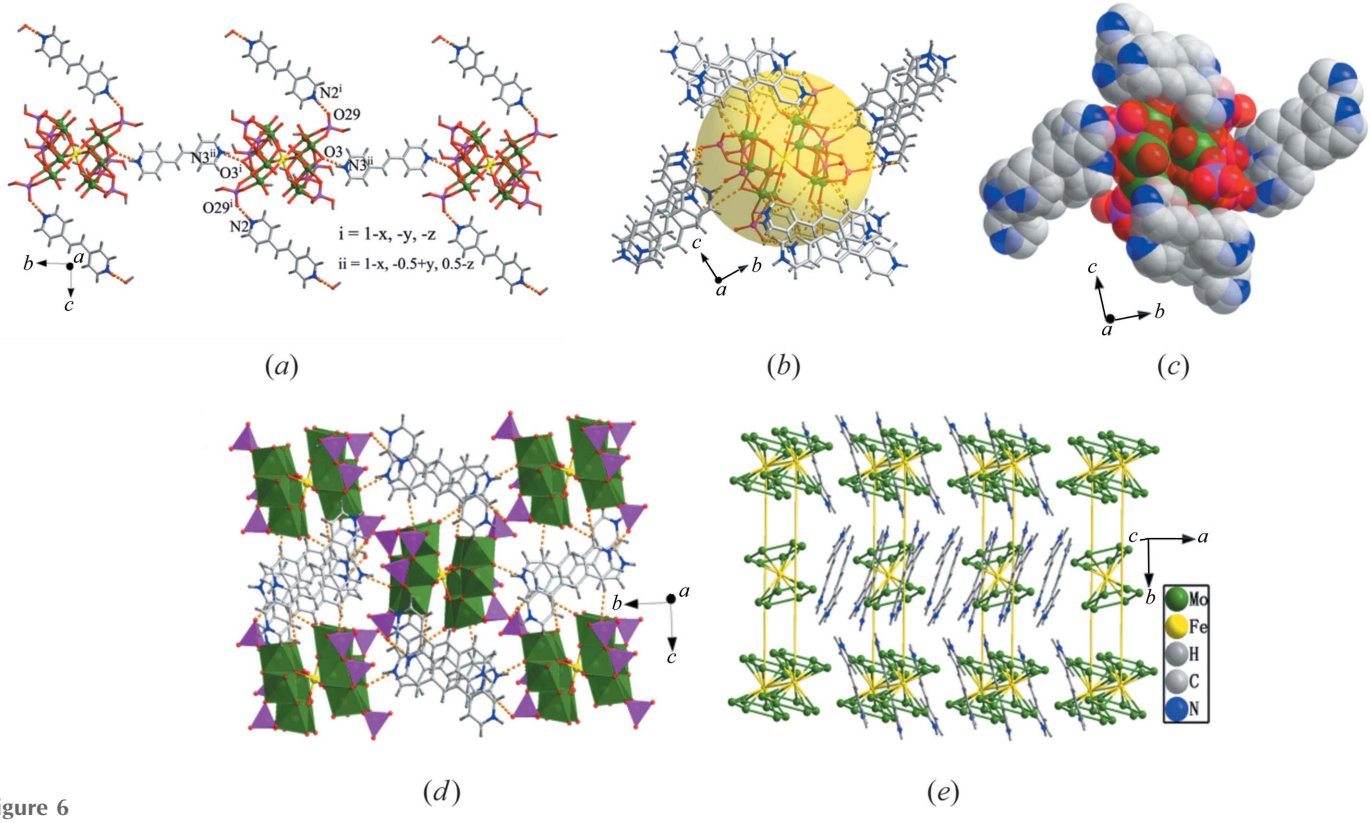

Figure 6
(*a*) A view showing the N—H···O interactions among polyanionic clusters and organic cations. (*b*) The 'core–shell' inclusive structure model of hybrid **3**, showing the C—H···O and N—H···O hydrogen-bonding interactions (dashed lines) among bpe and polyanionic clusters. (*c*) A space-filling representation of the organic counter-cationic bpe around one polyanionic cluster. (*d*) The 2D inorganic–organic grid in **3**. (*e*) The 3D topology structure of **3**.

Table 2
Peak potential data (mV) for each peak of hybrids **1–3** at a sweep speed of 140 mV s^{-1}.

Scan rate 140 mV s^{-1}	E_a/E_c (I)/mV $E_{1/2}$, ΔE	E_a/E_c (II)/mV $E_{1/2}$, ΔE	E_a/E_c (III)/mV $E_{1/2}$, ΔE	E_a/E_c (IV)/mV
Hybrid **1**	11/−26	271/240	424/380	−122
	−8, 37	256, 31	402, 44	
Hybrid **2**	30/−21	277/234	439/386	−121
	5, 51	256, 43	413, 53	
Hybrid **3**	26/−4	253/220	412/348	−122
	11, 30	237, 33	380, 64	

2.089 (6), 2.104 (8) and 2.157 (8) Å (× 2). As shown in Fig. 2(*a*), Fe1 serves as the central metal of the hourglass-like $\{Fe1(P_4Mo_6)_2\}$ cluster, while Fe2 acts as a bridging atom linking adjacent $\{Fe1(P_4Mo_6)_2\}$ subunits into a one-dimensional (1D) inorganic structure. Meanwhile, two alkali-earth-metal Sr atoms and Fe2 form a trinuclear cationic $\{Sr_2Fe(H_2O)_9\}^{6+}$ fragment which further stabilizes the chain-like structure. In the trinuclear unit, the coordination environment of the Fe2 atom involves two coordinated water molecules (O1*W*) and four phosphate O atoms from two $\{Fe(P_4Mo_6)_2\}$ clusters. The Sr centre exhibits an eight-coordinated environment with three coordinated water molecules (O2*W*, O3*W* and O9*W*) and five O atoms derived from two $\{Fe(P_4Mo_6)_2\}$ clusters (Figs. 2*b* and 2*c*). The Sr1—O bond lengths range from 2.433 (18) to 3.087 (8) Å. In the *bc* plane, adjacent inorganic chains are parallel to each other (Fig. 3). In the packing arrangement of the crystal, the organic counter-cations are packed between the 1D inorganic chains. The polyanions and bpp cations interact through C—H···O and N—H···O hydrogen-bonding interactions to form a three-dimensional (3D) supramolecular structure (Table S5 in the supporting information).

Hybrid **2** crystallizes in the monoclinic space group *C*2/*c*, in which the basic unit is composed of an $\{Fe[Mo_6O_{12}(OH)_3(H_2PO_4)(HPO_4)(PO_4)_2]_2\}^{10-}$ polyoxoanion, an $[Na(H_2O)(OC_2H_5)]$ unit, two protonated $[H_2bpp]^{2+}$ cations, three $\{M(H_2O)_2\}^{2+}$ (M = Fe or Ca) subunits and four crystal water molecules. Similarly, there are two kinds of Fe atoms in **2**. The Fe1—O bond lengths are 2.157 (4), 2.198 (4) and 2.254 (4) Å (× 2), and the Fe2—O bond lengths are 2.065 (4), 2.133 (4) and 2.189 (5) Å (× 2). In contrast, the Fe2 atom, together with two Ca and two Na atoms, forms an edge-shared pentanuclear $\{FeCa_2Na_2\}$ bridging unit (Fig. 4*a*). In the pentanuclear unit (Figs. 4*b* and 4*c*), the Fe2 atom occupies the centre and shows an octahedral coordination geometry with two coordinated water molecules (O1*W* and its symmetry-related congener), and four phosphates (μ_3-O9 and μ_3-O26, and their symmetrical equivalent positions) derived from two $\{Fe(P_4Mo_6)_2\}$ clusters. Ca1 adopts a seven-coordinated environment which consists of two water molecules (O2*W* and O3*W*), two bridging oxygen donors (O9 and O26) and three phosphate O atoms derived from adjacent $\{Fe(P_4Mo_6)_2\}$ clusters. Na1 presents a hexacoordination environment with one terminal coordination water molecule (O7*W*), one bridging water molecule (O1*W*), one bridging μ_3-O atom (O26 and O32) and two phosphate O atoms from two adjacent $\{Fe(P_4Mo_6)_2\}$ clusters. Therefore, the $\{Fe(P_4Mo_6)_2\}$ clusters are bridged through pentanuclear $\{FeCa_2Na_2\}$ units into a 1D chain-like structure. In the packing arrangement, adjacent inorganic chains are parallel to each other and form a two-dimensional (2D) supramolecular layer. However, these chains in adjacent layers extend in different directions (Fig. 5). At the same time, the hydrogen-bonding interactions between the organic bpp counter-cations and the inorganic chains form the 3D structure of hybrid **2** (Table S6 in the supporting information).

Hybrid **3** crystallizes in the monoclinic space group $P2_1/c$ and is composed of the $\{Fe[Mo_6O_{12}(OH)_3(HPO_4)_3(H_2PO_4)]_2\}^{6-}$ polyoxoanion, a protonated $[H_2bpe]^{2+}$ cation and crystal water molecules. Each isolated hourglass-like $\{Fe(P_4Mo_6)_2\}$ cluster is linked by the organic bpe counter-cation through N—H···O hydrogen bonding into a 1D hybrid structure (see Fig. 6*a*). There is only one type of Fe centre present in the polyanionic cluster. The $\{FeO_6\}$ octahedron shares its six O-atom donors with 12 $\{MoO_6\}$ octahedra from two $\{P_4Mo_6\}$ subunits. The Fe—O bond lengths are 2.1401 (18), 2.1751 (18) and 2.1857 (18) Å (× 2). Figs. 6(*b*)/(*c*) clearly illustrate an approximate 'inorganic core–organic shell' structure based on a multiple-point C—H···O and N—H···O hydrogen-bonding network. As shown in Fig. 6(*d*), the upper and lower inorganic clusters in adjacent 1D chains are arranged in an interleaved manner, so that 2D reticular supramolecular layers are formed. Organic counter-cations and water molecules closely surround the anionic clusters *via* O—H···O, C—H···O and N—H···O hydrogen-bonding interactions (Table S7 in the supporting information), resulting in the formation of a 3D supramolecular structure (Fig. 6*e*).

3.3. FT–IR, EDS, XRD and TG

The IR spectra of hybrids **1–3** at 4000–400 cm^{-1} (Fig. S2 in the supporting information) were measured. Although the structures of **1–3** are slightly different, the kinds of chemical bonds are similar. The basic peak positions are almost coincident in their IR spectra. The characteristic absorption peak of the ν(Mo—O—Mo) stretching vibration is located at 600∼750 cm^{-1}, and the characteristic absorption peak at 950 cm^{-1} is due to a ν(Mo═O) stretching vibration. The antisymmetric vibrations of ν_{as}(P—O) are in the vicinity of 1033∼1178 cm^{-1}. The two groups of characteristic absorption peaks appearing around 1500 cm^{-1} are the stretching vibration of C═C and C═N bonds, which are consistent with the organic part in the three hybrids. In addition, the peaks at 3247∼3440 cm^{-1} belong to the stretching vibrations of ν(O—H), ν(C—H) and ν(N—H). A comprehensive analysis on IR of the three hybrids shows that they are consistent with the crystal structure analyses. The IR spectra of the hybrids before and after catalysis reaction were also measured. It can be seen from Fig. 7 that the positions and intensities of the main vibration peaks basically remain intact, indicating that there is no obvious change in the skeleton of the hybrids after the catalysis reaction.

The EDS results showed that the molar ratio of P to Mo was 4:6, which further verified the correctness of the structural

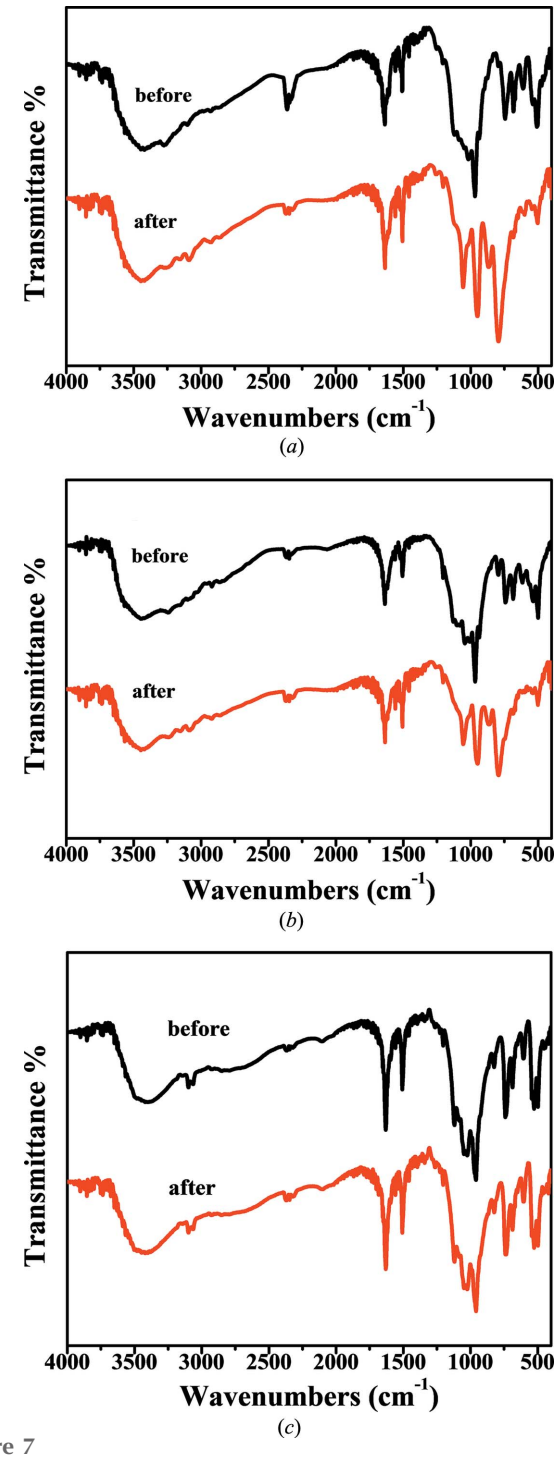

Figure 7
IR spectra of hybrids (*a*) **1**, (*b*) **2** and (*c*) **3** before and after the catalytic experiments.

analysis of hybrids **1–3** (Fig. S3 in the supporting information). The EDS elemental analysis of the crystals after the catalytic reaction revealed that the main elements exist in the POM (Fig. S4 in the supporting information). Powder X-ray diffraction data were tested in the $2\theta = 0$ to 50° range (Fig. S5 in the supporting information). It can be seen that hybrids **1–3** have strong diffraction peaks in the range 5∼10°. The experimental XRD patterns and simulated patterns from the single-crystal diffraction data are roughly the same, further supporting the results of crystal structure analysis. The XRD spectra of the hybrids before and after the catalysis reaction were also measured. The positions of the main vibration peaks basically remain intact, indicating that there is no obvious change in the skeleton of the hybrids after the catalysis reaction. Thermogravimetric analyses of hybrids **1–3** were carried out under an N_2 atmosphere from 20 to 800 °C. The TG curves exhibit two weight-loss steps between 25 and 788 °C, showing that the main structures are stable below 550 °C. As shown in Fig. S6 (see supporting information), the 14.57% weight loss of hybrid **1** is due to the loss of lattice water and bpp molecules in the temperature range 29–750 °C (theoretical value: 14.67%). The TG–DSC curves of **2** show that the weight loss from 36 to 550 °C is *ca* 14.76% and is equivalent to the loss of lattice water and organic components (theoretical value: 14.49%). Similarly, for hybrid **3**, the overall weight loss is *ca* 22.78% from 25 up to 788 °C, attributed to the loss of crystal water and organic components (theoretical value: 22.05%).

3.4. Electrochemical characterization

Cyclic voltammograms of hybrids **1–3** in 1 *M* H_2SO_4 solution at different sweep rates (20, 50, 80, 110 and 140 mV s^{-1}) were measured. The three hybrids present three pairs of bi-electronically reversible redox peaks. As shown in Table 2, three pairs of ideally reversible redox peaks (I–I′, II–II′ and III–III′) with corresponding mid-point potentials [$E_{1/2} = (E_{pa} + E_{pc})/2$, scan rate 140 mV s^{-1}] were observed at −8, 256 and 402 mV for **1**-CPE, at 5, 256 and 413 mV for **2**-CPE, and at 11, 237 and 380 mV for **3**-CPE. Differences in the potentials of hybrids **1–3** may be due to different metal species and chemical environments (Wang *et al.*, 2013). Obviously, as the scan rates increase, there is only a slight change in the peak potentials of anode and cathode, indicating that the redox reaction is almost ideally reversible and not related to ion diffusion in solution. As can be seen from the insets in Fig. 8, the peak currents are directly proportional to the scan rates, illustrating that this redox process is surface-controlled.

As is known, POMs have been exploited extensively in electrocatalytic reduction (Papaconstantinou *et al.*, 1993). Fig. 9 shows cyclic voltammograms for the electrocatalytic reduction of dichromate by **1**(**2–3**)-CPE. After the addition of potassium dichromate, the catalytic wave of **1** and **2** mainly appears on the first, second and fourth reduction waves (peaks I, II and IV). The catalytic waves of **3** all appear on each reduction peak. The results indicate that hybrids **1** and **2** were electrocatalytically active toward the reduction of Cr^{VI}, while hybrid **3** was almost inactive.

3.5. Catalytic experiments

The ideal reversible redox potential and abundant exposed O atoms in polyanionic clusters imply that hybrids **1–3** might be explored as electron-transfer catalysts in redox processes. Here, they are evaluated as low-cost and environmentally friendly catalysts for the removal of Cr^{VI} ions from waste-

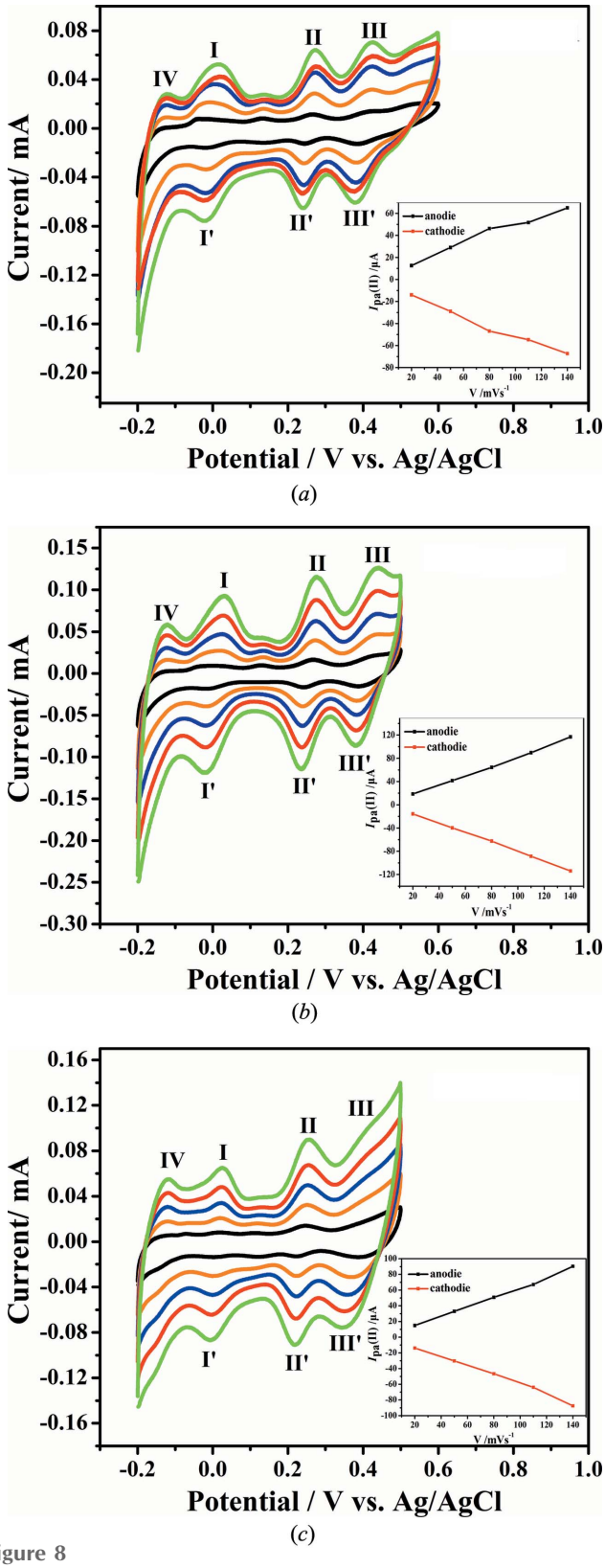

Figure 8
Cyclic voltammograms of hybrids (*a*) **1**, (*b*) **2** and (*c*) **3** with different sweep rates (20, 50, 80, 110 and 140 mV s^{-1}) in 1 *M* H_2SO_4 solution. The insets are plots of peak current of peak (II–II′) *versus* scan rate.

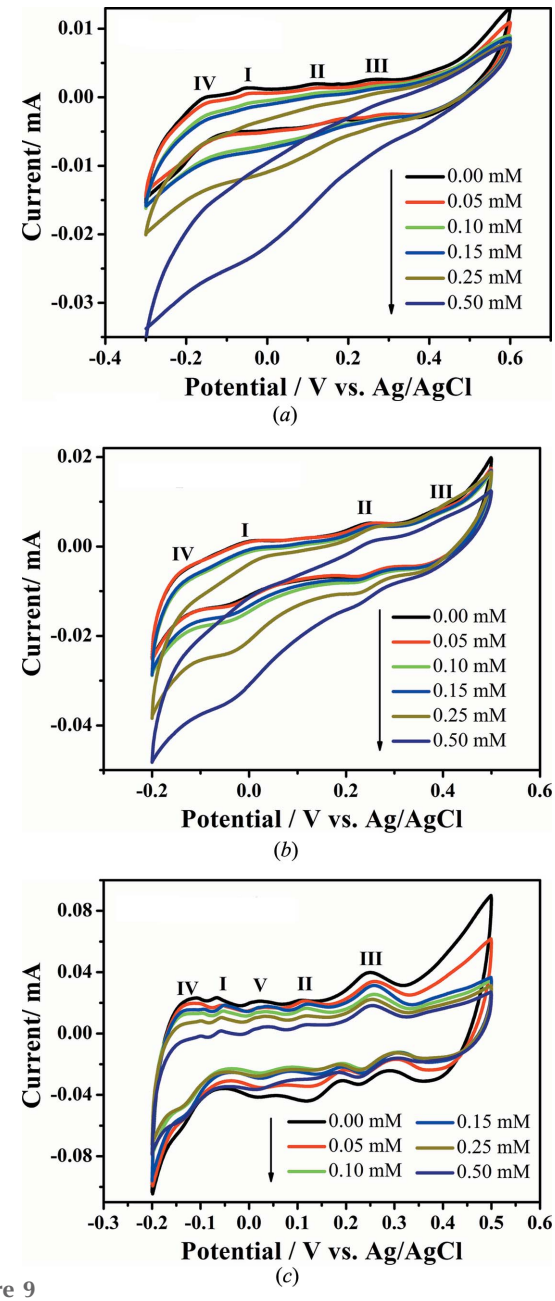

Figure 9
Cyclic voltammograms of (*a*) **1**-CPE, (*b*) **2**-CPE and (*c*) **3**-CPE in 1 *M* H_2SO_4 containing different concentrations of $K_2Cr_2O_7$, *i.e.* 0.00, 0.05, 0.10, 0.15, 0.25 and 0.50 m*M*; scan rate: 50 mV s^{-1}.

water. Among them, FA is used as a reducing agent because it does not cause secondary pollution during the reaction. As can be seen from Figs. 10(*a*) and 10(*b*), when the amount of catalyst is 20 mg, hybrids **1** and **2** were remarkably effective for the reduction of Cr^{VI}. The characteristic absorption peaks of Cr^{VI} ions at 348 nm distinctly decreased with increasing reaction time. When the reaction temperature is 75 °C, the reduction percentage of Cr^{VI} can reach more than 95% in 180 min. However, when hybrid **3** was used as a catalyst, accompanied by a decrease in the absorbance of Cr^{VI} at 348 nm, the peak around 310 nm gradually became apparent (Fig. 10*c*). One reason is that bpe-containing **3** is more easily dissolved in solution in the presence of FA. In order to confirm the above hypothesis, we tested the UV spectrum of free bpe

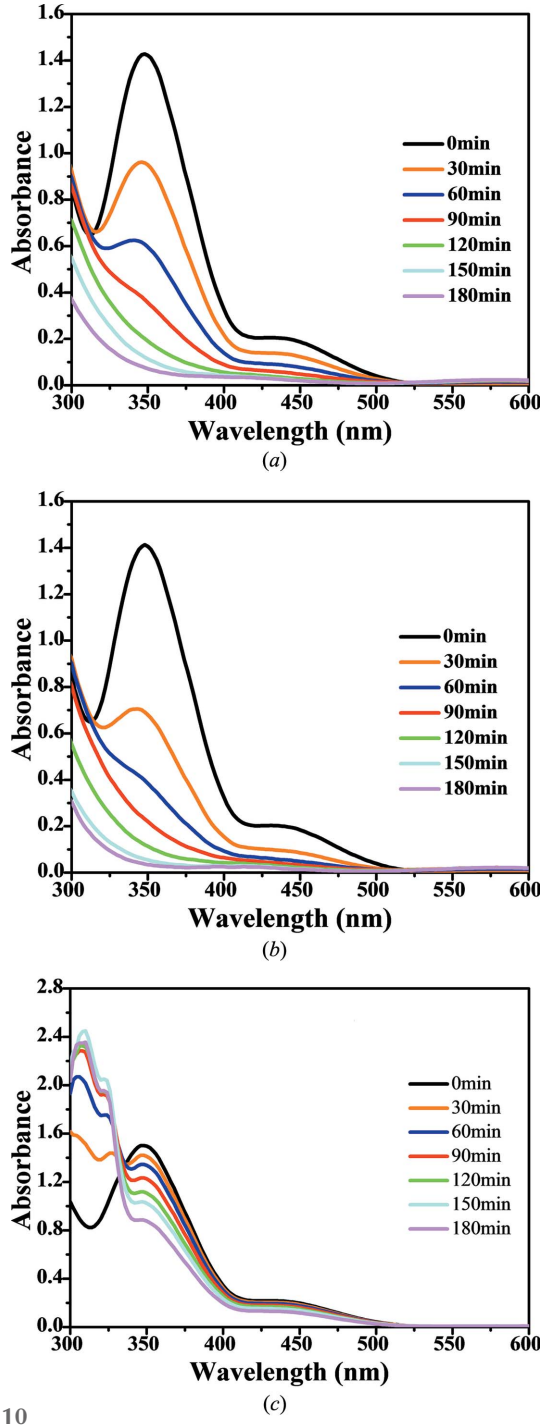

Figure 10
Successive UV–Vis absorption spectra for aqueous solutions of the catalytic reduction of Cr^{VI} using FA as reducing agent at 75 °C in the presence of hybrids (*a*) **1**, (*b*) **2** and (*c*) **3**.

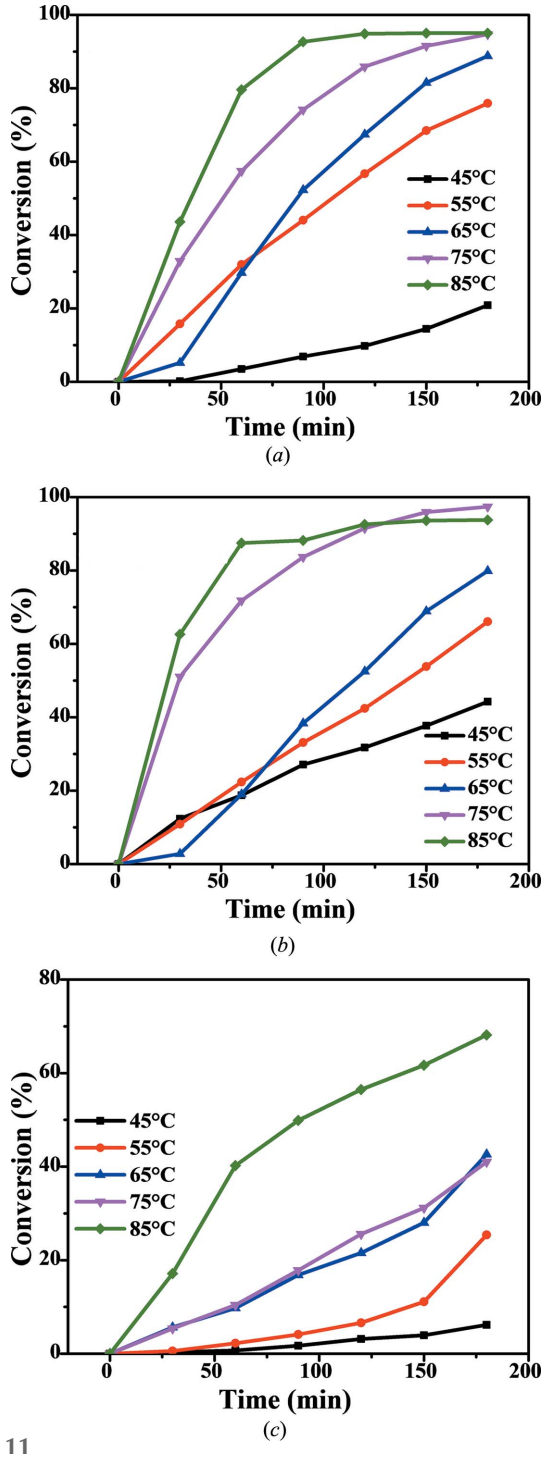

Figure 11
Plots of the conversion (%) of Cr^{VI} *versus* time in the presence of hybrids (*a*) **1**, (*b*) **2** and (*c*) **3** at different temperatures.

in FA-containing solution. There was a strong characteristic absorption peak at 310 nm, which provided the theoretical support for this presupposition (Fig. S7*a* in the supporting information). As a blank experiment, free bpe was also used as a catalyst for this system and it is found that it did not have any activity for Cr^{VI}–FA redox reduction (Fig. S7*b*).

According to the Arrhenius relationship, there is a certain relationship between the rate constant and temperature. In order to explore this relationship and find the best reaction conditions, it is necessary to make parallel experiments by changing the temperature. As shown in Fig. 11, the temperature is very important for the catalytic process and can accelerate the redox reaction. It is also found that the increase of reduction efficiency catalyzed by **1–3** is not always linear with reaction temperature. At lower temperatures, the reaction rate is slow, basically in line with the Arrhenius formula.

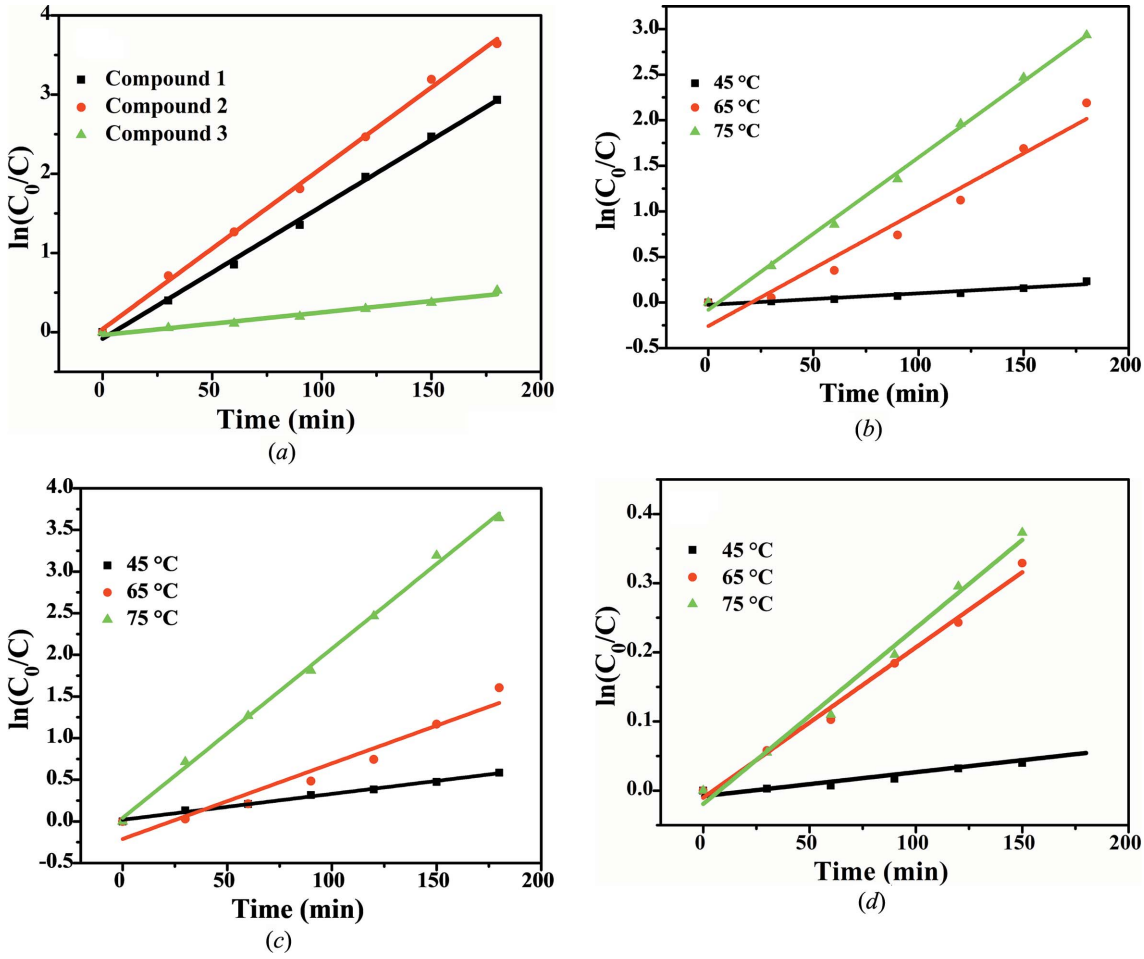

Figure 12
(*a*) Pseudo-first-order plots of $-\ln(C_0/C)$ (absorbance at 348 nm) against time for Cr^{VI} reduction at 75 °C. The rate constants k are determined at different temperatures with (*b*) **1**, (*c*) **2** and (*d*) **3** as catalysts, and the calculated activation energies are 27.4, 78.9 and 15.8 kJ mol^{-1}.

When the temperature rises to a certain critical value, the reaction rate increases rapidly at the initial reaction stage, but level off at long-term high temperature. The reason may be due to the fact that the higher temperature will certainly go against the surface adsorption capacity of solid catalyst.

The reduction progress of $Cr_2O_7^{2-}$ follows pseudo-first-order kinetics in the presence of excess FA. Based on the above experimental results, the reduction reactions catalyzed by hybrids **1–3** were discussed in detail. The linear relationship between $-\ln(C_0/C)$ and reaction time (min) for this system is shown in Fig. 12(*a*). The apparent rate constants K_{app} for this reaction were calculated to be 1.67×10^{-2} (standard error: 3.94×10^{-4}) for **1**, 2.03×10^{-2} (standard error: 4.30×10^{-4}) for **2** and 2.86×10^{-3} min^{-1} (standard error: 2.10×10^{-4}) for **3**. In that sense, the K_{app} constant of hybrid **2** is better than the other two samples. It should be pointed out that these K_{app} constants are of the same order of magnitude compared to noble metals Pd and Pt nanoparticles (NPs) as catalysts (Yang *et al.*, 2014). However, these hybrid materials are inexpensive and easy to prepare, and, more importantly, their structural design and optimization can be performed. In addition, as shown in Fig. 12(*b*), the reaction rate constants of **1** were determined at 45, 55 and 65 °C, and the activation energy was calculated to be 27.4 kJ mol^{-1} according to the Arrhenius equation. Similarly, the activation energy for hybrid **2** was 78.9 kJ mol^{-1} and for hybrid **3** was 15.8 kJ mol^{-1}. As shown in Table 3, the TON and TOF of the catalytic reaction system are further calculated according to the formula TON = $n(Cr^{VI})/n$(catalyst) and TOF = $n(Cr^{VI})/n$(catalyst) $\times$ t (Maeda *et al.*, 2005). Higher TON and TOF values were obtained when hybrid **2** was used as catalyst, which indicated that this hybrid was an ideal candidate for the catalytic reaction of Cr^{VI} reduction. These results clearly demonstrate that the catalysis process is determined by kinetic and thermodynamic characteristics.

Our group has previously reported an example of a $\{P_4Mo_6\}$-based compound, *i.e.* $(H_2bpp)_6\{Fe[Mo_6O_{12}(OH)_3(HPO_4)_2(H_2PO_4)_2]_2\}_2\cdot 11H_2O$ (Wang *et al*, 2017). In this compound, the hourglass-like polyanionic clusters exist in two kinds of zero-dimensional clusters, labelled as Fe1-$\{P_4Mo_6\}_2$ and Fe2-$\{P_4Mo_6\}_2$. Catalytic experiments showed that the reduction percentage of Cr^{VI} can reach 83% within 180 min at 55 °C. Compared with hybrids **1** and **2** which consist of 1D chains linked by M (M = Fe, Sr and Na, Ca) bonds in the current work, the reduction rates were 76 and 66% under the same conditions, respectively. Through structural comparisons,

Table 3
Catalytic performance of catalysts **1**–**3** for the reduction of Cr^{VI} to Cr^{III} at 75 °C within 180 min.

Hybrid	$n(K_2Cr_2O_7)$ (10^{-5} mol)	n(catalyst) (10^{-6} mol)	Conversion (%)	TON[a]	TOF[b] (10^{-4} s^{-1})
1	2.2	5.98	94.68	6.97	6.45
2	2.2	6.13	97.38	6.99	6.47
3	2.2	6.33	41.01	2.85	2.64

Notes: (*a*) TON = 2 × moles of $K_2Cr_2O_7$ × conversion/moles of catalyst; (*b*) TOF = 2 × moles of $K_2Cr_2O_7$ × conversion/[moles of catalyst × time (180 × 60 s)].

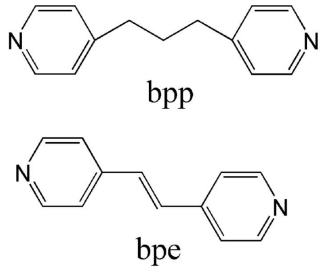

(*a*)

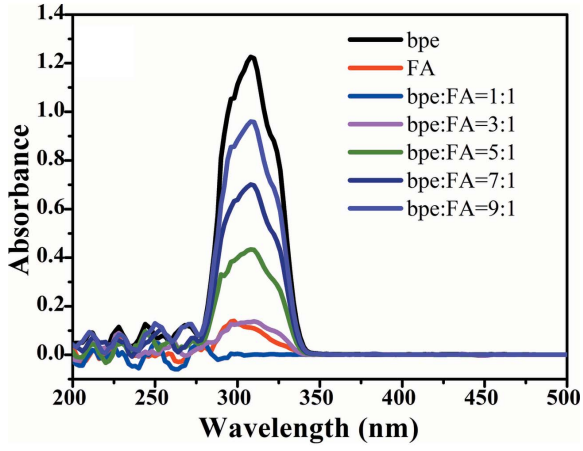

(*b*)

Figure 13
(*a*) Structural diagrams of bpp and bpe. (*b*) Successive UV–Vis absorption spectra for bpe, FA, bpe and FA (volume ratio).

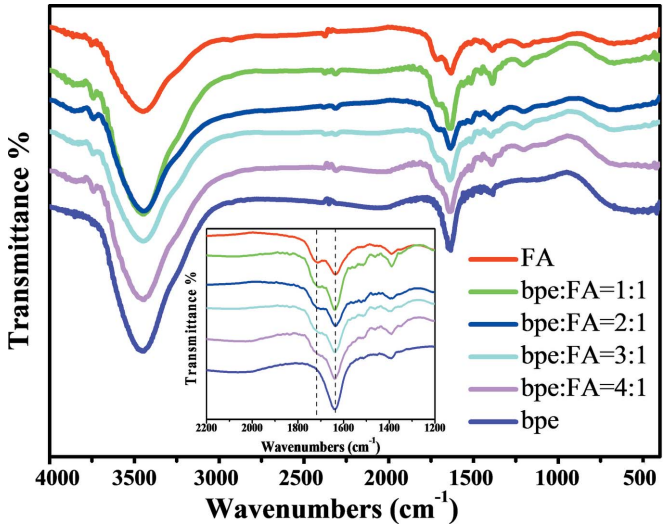

Figure 14
IR spectra of bpe, FA and bpe/FA (volume ratio).

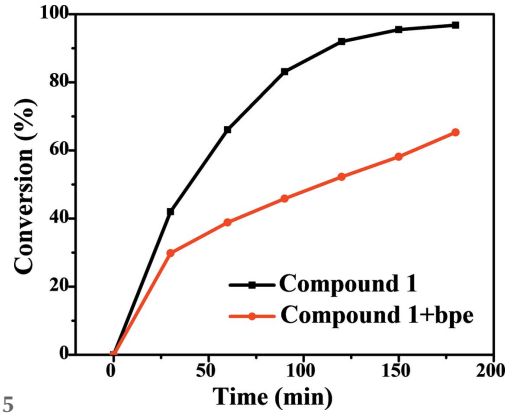

Figure 15
Plots of the conversion (%) of Cr^{VI} *versus* time using hybrid **1** as catalyst in the presence/absence of bpe.

it is found that low-dimensional structures are more conducive to the catalytic process. In the covalent 1D structure, some of the surface-active oxygen sites are coordinated by the bridging metal units, resulting in a decrease in the activity of the catalyst. However, the 1D structure can be retained at a higher reaction temperature, resulting in a catalytic activity that can

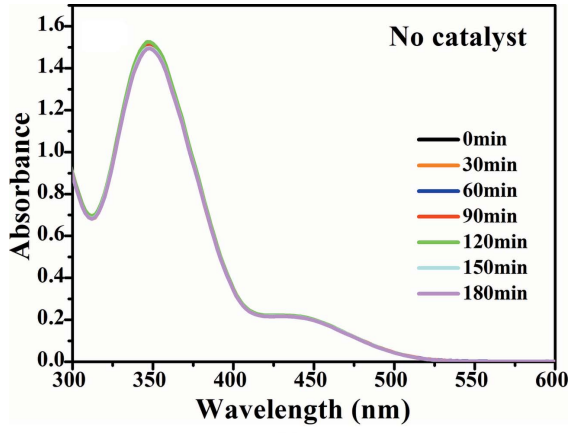

(*a*)

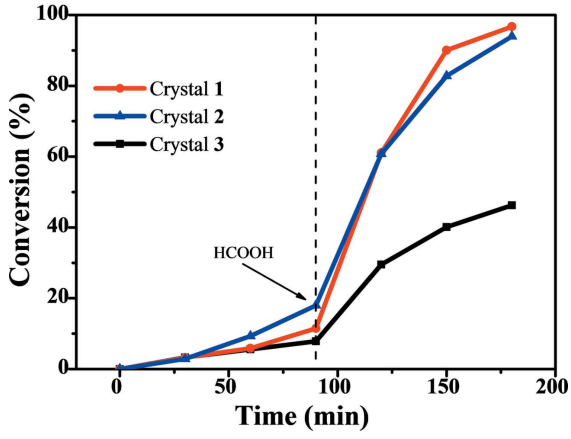

(*b*)

Figure 16
(*a*) The blank experiment showing the successive UV–Vis absorption spectra of a $Cr_2O_7^{2-}$ aqueous solution reacting with FA at 75 °C. (*b*) The control experiments prove that the hybrids **1**–**3** are catalysts rather than a reductant in the $K_2Cr_2O_7$–FA system. Experiments were carried out at 75 °C, with the FA reducing agent absent for the first 90 min.

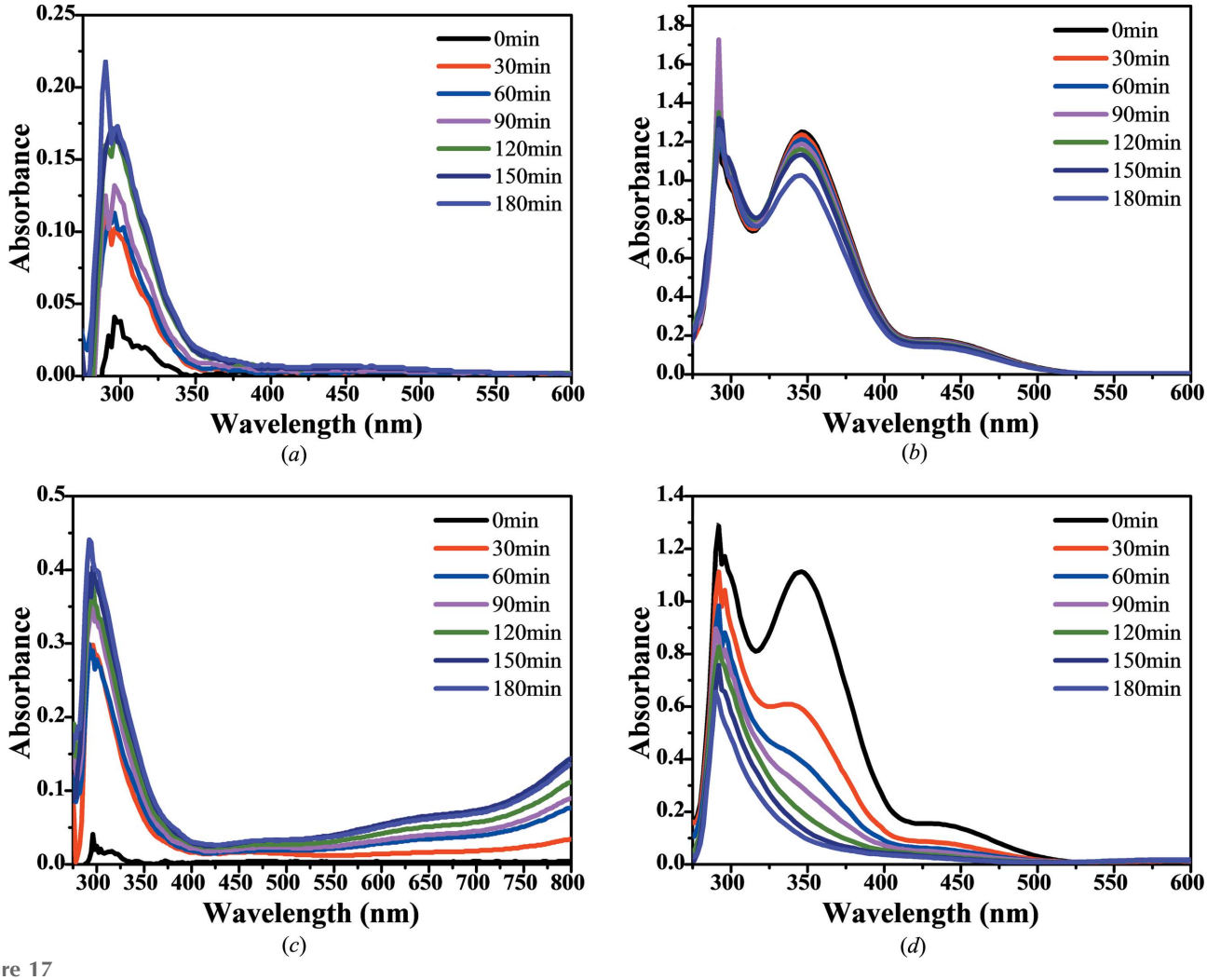

Figure 17
Successive UV–Vis absorption spectra of crystal **2** reacting with an FA-diluted solution at 25 °C in the presence of (*a*) the blank and (*b*) potassium dichromate. (*c*)/(*d*) The same as for parts (*a*) and (*b*), except that the temperature was 75 °C.

be fully maintained. Within 180 min, the reduction efficiency of Cr^{VI} can reach more than 95%. Simultaneously, it was found that hybrid **3** with bpe as the organic moiety exhibited a poor catalytic activity for the catalytic reaction of Cr^{VI} reduction. The main structural difference between bpe and bpp is the presence of a double bond in bpe (Fig. 13*a*). FA is the only carboxylic acid that can undergo an addition reaction with olefins. Therefore, one can suppose that the reaction of bpe with FA under certain conditions leads to a decrease of catalytic efficiency in the current system. As shown in Fig. 13(*b*), bpe and FA alone have absorption peaks around 310 and 290 nm, respectively. When a particular concentration of bpe and FA are mixed in a volume ratio of 1:1, the two characteristic absorption peaks fully disappear, indicating that the two substances have reacted. The absorption peaks at 310 nm gradually become more and more evident with increasing bpe ratio. In addition, the IR spectra were recorded to test this reaction between bpe and FA. With increasing bpe, the C═O absorption peaks of FA at 1717 cm^{-1} disappeared slowly (Fig. 14), illustrating that the C═O group of FA had been destroyed. For further comparison, as shown in Fig. 15, bpe was purposely added to the reaction system with hybrid **1** as catalyst. The catalytic performance for Cr^{VI} reduction was significantly reduced, indicating that bpe does inhibit the reaction.

3.6. Discussion of the catalytic mechanism

To experimentally verify that the reaction observed is truly a catalytic process, a blank experiment was designed and performed. As can be seen from Fig. 16(*a*), pure FA has no effect on the reduction of Cr^{VI} when the catalyst is absent. It is obvious that the characteristic peak intensity of Cr^{VI} at 348 nm remains almost constant at 75 °C for a long period of 180 min. Furthermore, the absorbance of solutions initially containing $K_2Cr_2O_7$ was monitored as a function of time in the presence or absence of FA and hybrids **1** and **2** at 75 °C. As shown in Fig. 16(*b*), the absorbance of Cr^{VI} decreases slightly in the first 90 min when the catalyst is present but the FA is absent. This may be due to the physical adsorption of the solid catalysts. When FA is added at 90 min, the Cr^{VI} absorbance decreases rapidly and the reduction rate reaches 95% within

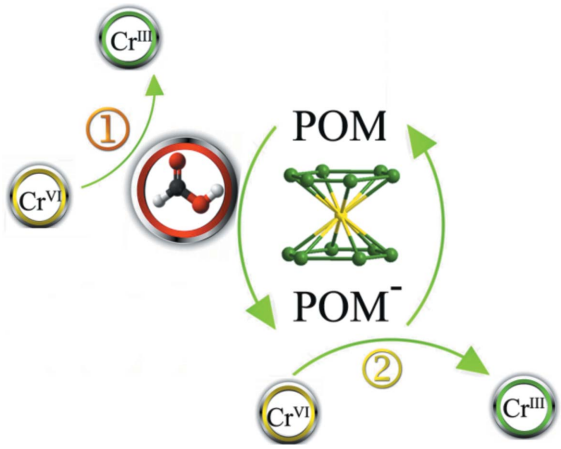

Figure 18
The proposed mechanism for the POM-mediated reduction of Cr^{VI} and FA, showing (1) the possible route at low temperature and (2) the possible route at high temperature.

the following 90 min due to the catalysis of the POM. We conducted another control experiment as follows: hybrid **2** and FA were mixed and stirred at 25 °C for 180 min, then potassium dichromate solution was added, and the reaction was continued for 180 min. The Cr^{VI} reduction rate was 18% (Figs. 17*a* and 17*b*). When the same reaction was repeated at 75 °C, it was found that the solution turned slightly blue, indicating that the pure POM reacts with FA to produce POM^-. The UV–Vis absorbance of POM^- between 450 and 800 nm increasing as a function of time is shown in Fig. 17(*c*), which indicates the production of POM^- increased with time. When the potassium dichromate solution was added, the blue (POM^-) disappeared quickly and the Cr^{VI} was reduced by 91% within 180 min (Fig. 17*d*). This proves that POM^- is the active intermediate to reduce Cr^{VI} to Cr^{III}.

Based on an analysis of the above experimental results, we propose a reaction mechanism for Cr^{VI} and FA (Fig. 18). The overall catalytic reaction is described using steps (1) and (2). The whole reaction mechanism is mainly considered from two aspects. It has been discussed earlier that FA alone does not have a reducing activity on Cr^{VI}. At low temperatures, the physical adsorption of the solid crystals and the surface catalysis reaction of Cr^{VI}–FA are predominant. When POM exists as a catalyst, it can lower markedly the activation energy of the reactions and accelerate the electron transfer of Cr^{VI}–FA (equation 1). When the temperature rises, the reaction mechanism is mainly that FA reduces the POM, and the product POM^- further reduces Cr^{VI} to Cr^{III} (equations 2 and 3).

$$FA + 2POM \rightarrow 2POM^- + CO_2 + 2H^+ \quad (2)$$

$$6POM^- + Cr_2O_7^{2-} + 14H^+ \rightarrow 6POM + 2Cr^{3+}\ 7H_2O \quad (3)$$

4. Conclusions

In summary, three new $\{FeP_4Mo_6\}$-based phosphomolybdate hybrids were synthesized and characterized by changing the metal and organic species under hydrothermal conditions. These completely reduced polyanionic clusters exhibit the desired ideally reversible redox properties. Hybrids **1** and **2** have good catalytic activity for the Cr^{VI}–FA system under 75 °C. Within 180 min, the reduction efficiency for Cr^{VI} can reach more than 95%. This is of great significance for the reduction of the highly toxic heavy metal ion Cr^{VI} in the environment. Based on the summary of previous research results, it is also found that the catalytic activity of the bpe–$\{P_4Mo_6\}$ hybrid was not satisfactory. Some facts can be stated: (i) as the temperature rises, the solubility of the three hybrids in the reaction solution continuously increases, resulting in a heterogeneous and homogeneously catalyzed multiple reaction; (ii) the extended structures of the metal–oxygen clusters are related to the catalytic properties of **1–3**, with the result that the catalytic activity can be fully maintained at a higher reaction temperature; (iii) the bpp-containing hybrids **1** and **2** have better activity. Meanwhile, we are working to explore the mechanism that affects the catalytic activity of crystals, although this is expected to be a complex undertaking.

Funding information

Funding for this research was provided by: National Natural Science Foundation of China (grant No. 21871076); Natural Science Foundation of Hebei Province (grant Nos. B2016205051 and B2015205116).

References

Bruker (2008). *SMART*, *SAINT* and *SADABS*. Bruker AXS Inc., Madison, Wisconsin, USA.
Chang, W. J., Jiang, Y. C. S., Wang, L. & Lii, K. H. (2006). *Inorg. Chem.* **45**, 6586–6588.
Chen, X. Q., Lin, S., Chen, L. J., Chen, X. H., Liu, C. L., Chen, J. B. & Yang, L. Y. (2007). *Inorg. Chem. Commun.* **10**, 1285–1288.
Dolbecq, A., Dumas, E., Mayer, C. R. & Mialane, P. (2010). *Chem. Rev.* **110**, 6009–6048.
Fu, Z. Y., Zeng, Y., Liu, X. L., Song, D. S., Liao, S. J. & Dai, J. (2012). *Chem. Commun.* **48**, 6154–6156.
Gkika, E., Troupis, A., Hiskia, A. & Papaconstantinou, E. (2006). *Appl. Catal. B*, **62**, 28–34.
Gong, K. N., Liu, Y. P., Wang, W. J., Fang, T., Zhao, C., Han, Z. G. & Zhai, X. L. (2015*a*). *Inorg. Chem.* **32**, 5351–5356.
Gong, K. N., Wang, W. J., Yan, J. S. & Han, Z. G. (2015*b*). *Mater. Chem. A*, **3**, 6019–6027.
Han, J. W. & Hill, C. L. (2007). *J. Am. Chem. Soc.* **129**, 15094–15095.
Han, F. X. X., Sridhar, M. B. B., Monts, D. L. & Su, Y. (2004). *New Phytol.* **162**, 189–199.
Hao, Z. M., Dong, Q. S., Zhang, L., Zhang, Y. & Luo, F. (2010). *CrystEngComm*, **12**, 977–982.
He, X. L., Liu, Y. P., Gong, K. N., Han, Z. G. & Zhai, X. L. (2015). *Inorg. Chem.* **54**, 1215–1217.
Huang, R., Liu, F., Li, Y., Yuan, M., Wang, E., De, G., Hu, C., Hu, N. & Jia, H. (2003). *Inorg. Chim. Acta*, **349**, 85–90.
Liang, R. W., Chen, R., Jing, F. F., Qin, N. & Wu, L. (2015). *Dalton Trans.* **44**, 18227–18236.
Liang, M., Su, R. X., Qi, W., Zhang, Y., Huang, R. L., Yu, Y. J., Wang, L. B. & He, Z. M. (2014). *Ind. Eng. Chem. Res.* **53**, 13635–13643.
Lin, B. Z., Liu, X. Z., Xu, B. H., Wang, Q. Q. & Xiao, Z. J. (2008). *Solid State Sci.* **10**, 1517–1524.
Linos, A., Petralias, A., Christophi, C. A., Christoforidou, E., Kouroutou, P., Stoltidis, M., Veloudaki, A., Tzala, E., Makris, K. C. & Karagas, M. R. (2011). *Environ. Health*, **10**, 50.

Maeda, K., Takata, T., Hara, M., Saito, N., Inoue, Y., Kobayashi, H. & Domen, K. (2005). *J. Am. Chem. Soc.* **127**, 8286–8287.
Miras, H. N., Vilà-Nadal, L. & Cronin, L. (2014). *Chem. Soc. Rev.* **43**, 5679–5699.
Omole, M. A., K'Owino, I. O. & Sadik, O. A. (2007). *Appl. Catal. B*, **76**, 158–167.
Papaconstantinou, E., Ioannidis, A., Hiskia, A., Argitis, P., Dimoticali, D. & Korres, S. (1993). *Mol. Eng.* **3**, 231–239.
Shao, F. Q., Feng, J. J., Lin, X. X., Jiang, L. Y. & Wang, A. J. (2017). *Appl. Catal. B*, **208**, 128–134.
Sheldrick, G. M. (2008). *Acta Cryst.* A**64**, 112–122.
Sheldrick, G. M. (2015). *Acta Cryst.* C**71**, 3–8.
Streb, C., Ritchie, C., Long, D. L., Kögerler, P. & Cronin, L. (2007). *Angew. Chem. Int. Ed.* **46**, 7579–7582.
Walsh, J. J., Bond, A. M., Forster, R. J. & Keyes, T. E. (2016). *Coord. Chem. Rev.* **306**, 217–234.
Wang, X. L., Cao, J. J., Liu, G. C., Lin, H. Y. & Tian, A. X. (2013). *Inorg. Chem.* **15**, 551–559.
Wang, X. X., Wang, J. J., Geng, Z. K., Qian, Z. & Han, Z. G. (2017). *Dalton Trans.* **46**, 7917–7925.
Yang, C. X., Meldon, J. H., Lee, B. & Yi, H. (2014). *Catal. Today*, **233**, 108–116.
Yu, K., Chen, W. L., Zhou, B. B., Li, Y. G., Yu, Y., Su, Z. H., Gao, S. & Chen, Y. (2011). *CrystEngComm*, **13**, 3417–3424.
Yu, K., Zhou, B. B., Yu, Y., Su, Z. H., Wang, C. M., Wang, C. X., Gao, S. & Chen, Y. (2012). *Inorg. Chim. Acta*, **384**, 8–17.
Zhang, D. Y., Li, X., Tan, H. Q., Zhang, G. Q., Zhao, Z., Shi, H. F., Zhang, L. T., Yu, W. X. & Sun, Z. C. (2014). *RSC Adv.* **4**, 44322–44326.
Zhang, X., Xu, J. Q., Yu, J. H., Lu, J., Xu, Y., Chen, Y., Wang, T. G., Yu, X. Y., Yang, Q. F. & Hou, Q. (2007*a*). *J. Solid State Chem.* **180**, 1949–1956.
Zhang, H., Yu, K., Li, J. S., Wang, C. M., Lv, J. H., Chen, Z. Y., Cai, H. H. & Zhou, B. B. (2015). *RSC Adv.* **5**, 3552–3559.
Zhang, L. J., Zhou, Y. S., Li, X. Q. & Li, Y. H. (2007*b*). *J. Cluster Sci.* **18**, 921–933.

supporting information

Acta Cryst. (2018). C**74**, 1310-1324 [https://doi.org/10.1107/S2053229618013025]

Crystal structures of hybrid completely reduced phosphomolybdates and catalytic performance applied as molecular catalysts for the reduction of chromium(VI)

Xuerui Tian, Xing Xin, Yuanzhe Gao, Dandan Dai, Jinjin Huang and Zhangang Han

Computing details

For all structures, data collection: *SMART* (Bruker, 2008); cell refinement: *SMART* (Bruker, 2008); data reduction: *SAINT* (Bruker, 2008); program(s) used to solve structure: *SHELXTL* (Sheldrick, 2008); program(s) used to refine structure: *SHELXL2014* (Sheldrick, 2015); molecular graphics: *SHELXTL* (Sheldrick, 2008); software used to prepare material for publication: *SHELXTL* (Sheldrick, 2008).

(1)

Crystal data

$(C_{13}H_{16}N_2)_2[Fe(H_2O)][Sr(H_2O)_4]_2\{Fe[Mo_6O_{12}(OH)_3(H_2PO_4)(HPO_4)(PO_4)_2]_2\}\cdot 5H_2O$
M_r = 3338.82
Triclinic, $P\overline{1}$
a = 11.385 (3) Å
b = 14.121 (3) Å
c = 15.126 (4) Å
α = 69.259 (3)°
β = 82.422 (4)°
γ = 88.086 (4)°
V = 2254.0 (9) Å^3
Z = 1
F(000) = 1612
D_x = 2.460 Mg m^{-3}
Mo $K\alpha$ radiation, λ = 0.71073 Å
Cell parameters from 6029 reflections
θ = 2.4–28.3°
μ = 3.35 mm^{-1}
T = 296 K
Block, brown
0.17 × 0.15 × 0.13 mm

Data collection

Bruker SMART CCD area detector diffractometer
phi and ω scans
Absorption correction: multi-scan (SADABS; Bruker, 2008)
T_{min} = 0.571, T_{max} = 0.647
10357 measured reflections
7715 independent reflections
5705 reflections with $I > 2\sigma(I)$
R_{int} = 0.033
θ_{max} = 25.0°, θ_{min} = 2.2°
$h = -13 \rightarrow 10$
$k = -16 \rightarrow 16$
$l = -17 \rightarrow 17$

Refinement

Refinement on F^2
Least-squares matrix: full
$R[F^2 > 2\sigma(F^2)]$ = 0.057
$wR(F^2)$ = 0.161
S = 1.05
7715 reflections
616 parameters
0 restraints
Hydrogen site location: inferred from neighbouring sites
H-atom parameters constrained

$w = 1/[\sigma^2(F_o^2) + (0.0682P)^2 + 32.5759P]$
where $P = (F_o^2 + 2F_c^2)/3$
$(\Delta/\sigma)_{max} = 0.001$
$\Delta\rho_{max} = 2.59$ e Å^{-3}
$\Delta\rho_{min} = -1.40$ e Å^{-3}

Special details

Geometry. All esds (except the esd in the dihedral angle between two l.s. planes) are estimated using the full covariance matrix. The cell esds are taken into account individually in the estimation of esds in distances, angles and torsion angles; correlations between esds in cell parameters are only used when they are defined by crystal symmetry. An approximate (isotropic) treatment of cell esds is used for estimating esds involving l.s. planes.

Fractional atomic coordinates and isotropic or equivalent isotropic displacement parameters (Å²)

	x	*y*	*z*	U_{iso}*/U_{eq}	Occ. (<1)
Mo1	0.57784 (9)	0.13710 (6)	0.16185 (6)	0.0200 (2)	
Mo2	0.74318 (8)	0.20453 (6)	−0.06481 (6)	0.0198 (2)	
Mo3	0.78967 (8)	−0.14855 (6)	0.01976 (6)	0.0194 (2)	
Mo4	0.66655 (9)	−0.19228 (6)	0.18635 (6)	0.0205 (2)	
Mo5	0.64028 (9)	0.22227 (7)	−0.21242 (6)	0.0227 (2)	
Mo6	0.34944 (9)	0.11409 (7)	0.18114 (6)	0.0204 (2)	
Sr1	0.77683 (11)	0.56098 (8)	0.09982 (9)	0.0339 (3)	
Fe1	0.5000	0.0000	0.0000	0.0185 (5)	
Fe2	0.5000	0.5000	0.0000	0.0211 (5)	
P1	0.5384 (2)	0.71460 (19)	0.04041 (18)	0.0174 (6)	
P2	0.7434 (2)	0.34275 (19)	0.0705 (2)	0.0201 (6)	
P3	0.1238 (3)	0.2705 (2)	0.1310 (2)	0.0243 (6)	
P4	0.5250 (3)	−0.3822 (2)	0.3651 (2)	0.0285 (7)	
O1	0.6345 (6)	0.1121 (5)	−0.0875 (5)	0.0171 (15)	
O2	0.6509 (6)	−0.0831 (5)	0.0641 (5)	0.0211 (16)	
O3	0.4805 (6)	0.0532 (5)	0.1189 (5)	0.0206 (16)	
O4	0.5719 (6)	0.2448 (5)	0.0079 (5)	0.0193 (15)	
O5	0.5016 (6)	−0.1465 (5)	0.2334 (5)	0.0225 (16)	
O6	0.7649 (6)	−0.0528 (5)	−0.1177 (5)	0.0210 (16)	
O7	0.5576 (7)	0.6035 (5)	0.0559 (5)	0.0231 (16)	
O8	0.7217 (6)	0.1034 (5)	0.0775 (5)	0.0204 (16)	
O9	0.9025 (7)	−0.0820 (6)	0.0299 (6)	0.0324 (19)	
O10	0.7738 (6)	−0.2722 (5)	0.1303 (5)	0.0229 (16)	
O11	0.4486 (7)	0.2185 (5)	0.1901 (5)	0.0240 (16)	
O12	0.6863 (7)	0.2525 (5)	0.1548 (5)	0.0255 (17)	
O13	0.6476 (6)	−0.2233 (5)	−0.0251 (5)	0.0192 (15)	
O14	0.8773 (7)	0.1639 (6)	−0.0958 (6)	0.0332 (19)	
O15	0.1768 (8)	0.3823 (6)	0.0850 (6)	0.037 (2)	
O16	0.6076 (7)	0.0573 (6)	0.2677 (5)	0.0306 (18)	
O17	0.8002 (7)	0.3080 (5)	−0.0102 (5)	0.0236 (16)	
O18	0.5277 (6)	0.7343 (5)	0.1357 (5)	0.0212 (16)	
O19	0.6330 (7)	−0.3228 (6)	0.3013 (5)	0.0313 (19)	
O20	0.1132 (7)	0.2385 (6)	0.0460 (5)	0.0278 (18)	
O21	0.7126 (7)	0.3202 (5)	−0.1729 (5)	0.0270 (17)	
O22	0.8461 (7)	0.3845 (5)	0.1067 (6)	0.0289 (18)	
O23	0.6614 (7)	0.4316 (5)	0.0392 (6)	0.0294 (18)	

O24	0.2097 (7)	0.2058 (6)	0.1964 (5)	0.0276 (17)	
O25	0.7476 (8)	0.1840 (6)	−0.2791 (6)	0.036 (2)	
O26	0.0044 (7)	0.2743 (6)	0.1863 (6)	0.0327 (19)	
O27	0.7487 (8)	−0.1362 (6)	0.2373 (5)	0.034 (2)	
O28	0.3255 (8)	0.0279 (6)	0.2908 (5)	0.034 (2)	
O29	0.4114 (8)	−0.3429 (6)	0.3230 (6)	0.037 (2)	
O30	0.5208 (9)	−0.3648 (6)	0.4611 (6)	0.048 (3)	
H30	0.4636	−0.3954	0.4978	0.071*	
O31	0.5377 (9)	−0.4943 (6)	0.3817 (6)	0.041 (2)	
C1	0.9973 (15)	0.8774 (18)	0.2727 (16)	0.077 (6)	
H1	1.0307	0.8189	0.2662	0.092*	
C2	0.9599 (17)	0.8808 (17)	0.3610 (13)	0.078 (6)	
H2	0.9713	0.8249	0.4147	0.094*	
C3	0.9053 (17)	0.9652 (16)	0.3726 (14)	0.073 (5)	
C4	0.8930 (16)	1.0440 (14)	0.2890 (14)	0.069 (5)	
H4	0.8543	1.1018	0.2926	0.082*	
C5	0.9350 (15)	1.0415 (14)	0.2009 (12)	0.064 (5)	
H5	0.9279	1.0967	0.1457	0.077*	
C6	0.8547 (19)	0.9660 (17)	0.4675 (14)	0.085 (6)	
H6A	0.8726	1.0307	0.4719	0.103*	
H6B	0.8920	0.9137	0.5160	0.103*	
C7	0.717 (2)	0.9477 (16)	0.4880 (13)	0.089 (7)	
H7A	0.6891	0.9522	0.5498	0.107*	
H7B	0.6800	1.0015	0.4406	0.107*	
C8	0.677 (2)	0.8479 (16)	0.4874 (16)	0.095 (7)	
H8A	0.6973	0.8459	0.4238	0.114*	
H8B	0.7190	0.7941	0.5304	0.114*	
C9	0.385 (3)	0.7544 (14)	0.6339 (13)	0.091 (8)	
H9	0.3545	0.7203	0.6972	0.109*	
C10	0.506 (2)	0.7815 (16)	0.6066 (13)	0.085 (6)	
H10	0.5576	0.7661	0.6528	0.102*	
C11	0.5478 (19)	0.8285 (13)	0.5158 (11)	0.065 (5)	
C12	0.4692 (19)	0.8551 (12)	0.4482 (11)	0.066 (5)	
H12	0.4966	0.8919	0.3848	0.079*	
C13	0.355 (2)	0.8283 (12)	0.4732 (12)	0.077 (6)	
H13	0.3036	0.8433	0.4270	0.092*	
N1	0.9860 (11)	0.9569 (13)	0.1979 (10)	0.062 (4)	
H1A	1.0133	0.9545	0.1430	0.075*	
N2	0.3145 (16)	0.7804 (11)	0.5638 (10)	0.080 (5)	
H2A	0.2403	0.7651	0.5789	0.095*	
O1W	0.4017 (9)	0.4128 (6)	0.1351 (6)	0.041 (2)	
O2W	0.9998 (9)	0.5614 (9)	0.1097 (9)	0.070 (3)	
O3W	0.7289 (17)	0.4716 (14)	0.2704 (12)	0.039 (4)	0.5
O4W	0.3427 (15)	0.4794 (11)	0.2759 (11)	0.105 (5)	
O5W	0.9230 (19)	0.268 (2)	0.3702 (13)	0.169 (10)	
O6W	0.833 (2)	0.622 (2)	0.420 (2)	0.105 (10)	0.5
O7W	0.199 (4)	0.599 (3)	0.473 (3)	0.165 (18)	0.5
O8W	0.886 (5)	0.615 (3)	0.596 (3)	0.174 (18)	0.5

O9W	0.821 (4)	0.513 (4)	0.282 (2)	0.17 (2)	0.5
O3W′	0.614 (2)	0.4526 (18)	0.2350 (16)	0.079 (8)	0.5

Atomic displacement parameters (Å²)

	U^{11}	U^{22}	U^{33}	U^{12}	U^{13}	U^{23}
Mo1	0.0321 (5)	0.0110 (4)	0.0181 (5)	0.0005 (4)	−0.0053 (4)	−0.0060 (4)
Mo2	0.0266 (5)	0.0113 (4)	0.0226 (5)	−0.0001 (4)	−0.0026 (4)	−0.0075 (4)
Mo3	0.0269 (5)	0.0117 (4)	0.0205 (5)	0.0000 (4)	−0.0043 (4)	−0.0062 (4)
Mo4	0.0340 (6)	0.0106 (4)	0.0168 (5)	−0.0007 (4)	−0.0049 (4)	−0.0040 (4)
Mo5	0.0329 (6)	0.0151 (5)	0.0182 (5)	−0.0029 (4)	−0.0015 (4)	−0.0039 (4)
Mo6	0.0312 (5)	0.0129 (4)	0.0178 (5)	0.0003 (4)	−0.0025 (4)	−0.0064 (4)
Sr1	0.0405 (7)	0.0183 (6)	0.0494 (7)	0.0048 (5)	−0.0110 (6)	−0.0183 (5)
Fe1	0.0292 (12)	0.0109 (10)	0.0163 (10)	0.0003 (8)	−0.0041 (9)	−0.0056 (8)
Fe2	0.0290 (12)	0.0103 (10)	0.0269 (12)	0.0016 (9)	−0.0086 (9)	−0.0083 (9)
P1	0.0259 (15)	0.0096 (12)	0.0169 (13)	0.0004 (10)	−0.0036 (11)	−0.0047 (10)
P2	0.0268 (15)	0.0105 (13)	0.0261 (15)	0.0010 (11)	−0.0064 (12)	−0.0095 (11)
P3	0.0281 (16)	0.0192 (14)	0.0278 (16)	0.0034 (12)	−0.0021 (12)	−0.0117 (12)
P4	0.052 (2)	0.0132 (14)	0.0174 (14)	−0.0007 (13)	−0.0052 (13)	−0.0010 (11)
O1	0.028 (4)	0.009 (3)	0.016 (4)	−0.002 (3)	−0.007 (3)	−0.004 (3)
O2	0.032 (4)	0.015 (4)	0.017 (4)	−0.001 (3)	0.001 (3)	−0.008 (3)
O3	0.025 (4)	0.012 (3)	0.027 (4)	0.003 (3)	−0.001 (3)	−0.010 (3)
O4	0.025 (4)	0.013 (4)	0.021 (4)	0.002 (3)	−0.004 (3)	−0.007 (3)
O5	0.028 (4)	0.018 (4)	0.023 (4)	0.001 (3)	−0.001 (3)	−0.011 (3)
O6	0.031 (4)	0.009 (3)	0.020 (4)	−0.001 (3)	−0.007 (3)	−0.001 (3)
O7	0.032 (4)	0.010 (4)	0.030 (4)	−0.002 (3)	−0.004 (3)	−0.011 (3)
O8	0.034 (4)	0.009 (3)	0.021 (4)	0.009 (3)	−0.011 (3)	−0.007 (3)
O9	0.034 (5)	0.027 (4)	0.038 (5)	−0.006 (4)	−0.009 (4)	−0.011 (4)
O10	0.027 (4)	0.017 (4)	0.027 (4)	−0.001 (3)	−0.009 (3)	−0.008 (3)
O11	0.039 (5)	0.016 (4)	0.021 (4)	0.004 (3)	−0.007 (3)	−0.011 (3)
O12	0.040 (5)	0.019 (4)	0.024 (4)	−0.003 (3)	−0.005 (3)	−0.014 (3)
O13	0.020 (4)	0.018 (4)	0.019 (4)	−0.001 (3)	−0.003 (3)	−0.007 (3)
O14	0.032 (5)	0.035 (5)	0.037 (5)	0.012 (4)	−0.010 (4)	−0.018 (4)
O15	0.050 (6)	0.025 (4)	0.035 (5)	−0.007 (4)	0.000 (4)	−0.010 (4)
O16	0.047 (5)	0.019 (4)	0.026 (4)	0.008 (4)	−0.009 (4)	−0.007 (3)
O17	0.031 (4)	0.016 (4)	0.027 (4)	−0.002 (3)	−0.005 (3)	−0.012 (3)
O18	0.035 (4)	0.009 (3)	0.019 (4)	−0.003 (3)	−0.002 (3)	−0.006 (3)
O19	0.042 (5)	0.021 (4)	0.020 (4)	−0.005 (4)	−0.003 (4)	0.006 (3)
O20	0.026 (4)	0.033 (4)	0.029 (4)	0.008 (3)	−0.007 (3)	−0.016 (4)
O21	0.045 (5)	0.013 (4)	0.020 (4)	−0.003 (3)	−0.006 (3)	−0.002 (3)
O22	0.035 (5)	0.018 (4)	0.042 (5)	0.007 (3)	−0.013 (4)	−0.019 (4)
O23	0.042 (5)	0.013 (4)	0.039 (5)	0.004 (3)	−0.006 (4)	−0.015 (3)
O24	0.036 (5)	0.026 (4)	0.021 (4)	0.005 (3)	0.000 (3)	−0.010 (3)
O25	0.048 (5)	0.032 (5)	0.031 (5)	−0.001 (4)	−0.004 (4)	−0.016 (4)
O26	0.031 (5)	0.034 (5)	0.035 (5)	0.008 (4)	−0.003 (4)	−0.017 (4)
O27	0.055 (6)	0.025 (4)	0.025 (4)	0.000 (4)	−0.011 (4)	−0.008 (4)
O28	0.052 (5)	0.027 (4)	0.020 (4)	−0.004 (4)	−0.001 (4)	−0.006 (4)
O29	0.043 (5)	0.029 (5)	0.025 (4)	−0.006 (4)	−0.003 (4)	0.006 (4)

O30	0.091 (8)	0.025 (5)	0.025 (5)	−0.013 (5)	0.000 (5)	−0.008 (4)
O31	0.071 (7)	0.014 (4)	0.031 (5)	−0.001 (4)	0.005 (4)	−0.004 (4)
C1	0.043 (10)	0.111 (17)	0.096 (15)	0.012 (10)	−0.022 (10)	−0.058 (14)
C2	0.081 (13)	0.108 (16)	0.050 (10)	0.033 (12)	−0.029 (9)	−0.028 (11)
C3	0.081 (13)	0.092 (15)	0.068 (12)	0.001 (11)	−0.010 (10)	−0.054 (12)
C4	0.066 (11)	0.069 (12)	0.082 (13)	−0.019 (9)	0.011 (10)	−0.047 (11)
C5	0.066 (11)	0.070 (12)	0.062 (11)	−0.032 (9)	0.021 (9)	−0.036 (9)
C6	0.090 (16)	0.099 (16)	0.079 (14)	−0.013 (12)	−0.013 (11)	−0.042 (12)
C7	0.14 (2)	0.089 (15)	0.048 (10)	0.021 (14)	−0.004 (11)	−0.045 (11)
C8	0.13 (2)	0.077 (14)	0.092 (15)	0.020 (13)	0.000 (14)	−0.053 (13)
C9	0.19 (3)	0.048 (11)	0.033 (10)	0.014 (14)	−0.019 (13)	−0.014 (8)
C10	0.14 (2)	0.091 (15)	0.039 (11)	0.008 (14)	−0.013 (11)	−0.038 (10)
C11	0.108 (15)	0.055 (10)	0.034 (9)	0.006 (10)	−0.006 (9)	−0.021 (8)
C12	0.121 (17)	0.043 (9)	0.026 (8)	0.001 (10)	−0.001 (9)	−0.007 (7)
C13	0.14 (2)	0.045 (10)	0.036 (10)	−0.005 (11)	0.007 (11)	−0.011 (8)
N1	0.048 (8)	0.096 (12)	0.055 (9)	−0.016 (8)	0.002 (7)	−0.041 (9)
N2	0.120 (14)	0.057 (9)	0.056 (10)	−0.011 (9)	0.002 (9)	−0.018 (8)
O1W	0.070 (7)	0.015 (4)	0.034 (5)	0.004 (4)	−0.004 (4)	−0.004 (4)
O2W	0.047 (7)	0.061 (7)	0.085 (8)	−0.019 (5)	−0.005 (6)	−0.003 (6)
O3W	0.044 (12)	0.042 (11)	0.029 (10)	0.008 (9)	−0.010 (9)	−0.009 (8)
O4W	0.151 (15)	0.077 (10)	0.099 (11)	−0.010 (9)	−0.019 (10)	−0.044 (9)
O5W	0.169 (19)	0.26 (3)	0.100 (13)	−0.095 (18)	0.037 (12)	−0.100 (16)
O6W	0.066 (18)	0.10 (2)	0.15 (3)	0.015 (15)	−0.051 (18)	−0.03 (2)
O7W	0.15 (3)	0.10 (3)	0.17 (4)	−0.04 (2)	0.06 (3)	0.02 (3)
O8W	0.26 (6)	0.12 (3)	0.15 (4)	0.00 (3)	−0.03 (4)	−0.05 (3)
O9W	0.18 (4)	0.25 (5)	0.047 (18)	0.12 (4)	−0.04 (2)	−0.04 (2)
O3W′	0.12 (2)	0.072 (16)	0.062 (15)	0.047 (15)	−0.029 (14)	−0.039 (13)

Geometric parameters (Å, º)

Mo1—O16	1.669 (7)	P1—O7	1.515 (7)
Mo1—O11	1.933 (7)	P1—O4^{iii}	1.528 (7)
Mo1—O3	1.969 (7)	P1—O18	1.551 (7)
Mo1—O12	2.041 (7)	P1—O13^{iv}	1.559 (7)
Mo1—O8	2.088 (7)	P2—O23	1.513 (8)
Mo1—O4	2.294 (7)	P2—O17	1.531 (7)
Mo1—Mo6	2.5965 (15)	P2—O12	1.536 (8)
Mo2—O14	1.680 (8)	P2—O22	1.566 (8)
Mo2—O21	1.919 (7)	P3—O26	1.509 (8)
Mo2—O1	1.972 (6)	P3—O24	1.526 (8)
Mo2—O17	2.073 (7)	P3—O20	1.526 (8)
Mo2—O8	2.107 (7)	P3—O15	1.586 (8)
Mo2—O4	2.267 (7)	P3—Sr1^{iii}	3.519 (3)
Mo2—Mo5	2.5874 (14)	P4—O29	1.517 (9)
Mo3—O9	1.671 (8)	P4—O31	1.517 (8)
Mo3—O10	1.937 (7)	P4—O19	1.526 (8)
Mo3—O2	1.965 (7)	P4—O30	1.551 (8)
Mo3—O20^{i}	2.083 (7)	O4—P1^{iii}	1.528 (7)

Mo3—O6	2.090 (7)	O5—Mo5^{i}	2.085 (7)
Mo3—O13	2.259 (7)	O6—Mo6^{i}	2.088 (7)
Mo3—Mo4	2.5922 (13)	O10—Sr1^{ii}	2.555 (7)
Mo3—Sr1^{ii}	3.8453 (16)	O13—P1^{ii}	1.559 (7)
Mo4—O27	1.663 (8)	O13—Mo6^{i}	2.314 (7)
Mo4—O10	1.948 (7)	O15—Sr1^{iii}	2.605 (8)
Mo4—O2	1.970 (7)	O18—Mo4^{iv}	2.270 (7)
Mo4—O19	2.042 (7)	O18—Mo5^{iii}	2.285 (7)
Mo4—O5	2.084 (7)	O20—Mo3^{i}	2.083 (7)
Mo4—O18^{ii}	2.270 (7)	O20—Sr1^{iii}	3.087 (8)
Mo5—O25	1.679 (8)	O29—Mo5^{i}	2.055 (8)
Mo5—O21	1.933 (7)	O30—H30	0.8200
Mo5—O1	1.972 (6)	C1—N1	1.30 (2)
Mo5—O29^{i}	2.055 (8)	C1—C2	1.36 (2)
Mo5—O5^{i}	2.085 (7)	C1—H1	0.9300
Mo5—O18^{iii}	2.285 (7)	C2—C3	1.38 (3)
Mo6—O28	1.667 (8)	C2—H2	0.9300
Mo6—O11	1.940 (7)	C3—C4	1.38 (3)
Mo6—O3	1.992 (7)	C3—C6	1.48 (2)
Mo6—O24	2.059 (7)	C4—C5	1.37 (2)
Mo6—O6^{i}	2.088 (7)	C4—H4	0.9300
Mo6—O13^{i}	2.314 (7)	C5—N1	1.32 (2)
Sr1—O3W	2.433 (18)	C5—H5	0.9300
Sr1—O10^{iv}	2.555 (7)	C6—C7	1.57 (3)
Sr1—O22	2.559 (7)	C6—H6A	0.9700
Sr1—O2W	2.563 (11)	C6—H6B	0.9700
Sr1—O15^{iii}	2.605 (8)	C7—C8	1.50 (3)
Sr1—O3W′	2.64 (3)	C7—H7A	0.9700
Sr1—O7	2.662 (8)	C7—H7B	0.9700
Sr1—O9W	2.70 (3)	C8—C11	1.48 (3)
Sr1—O23	2.751 (7)	C8—H8A	0.9700
Sr1—O20^{iii}	3.087 (8)	C8—H8B	0.9700
Sr1—P2	3.306 (3)	C9—N2	1.35 (2)
Sr1—P1	3.428 (3)	C9—C10	1.42 (3)
Fe1—O3	2.165 (7)	C9—H9	0.9300
Fe1—O3^{i}	2.165 (7)	C10—C11	1.32 (2)
Fe1—O1^{i}	2.178 (7)	C10—H10	0.9300
Fe1—O1	2.178 (7)	C11—C12	1.39 (2)
Fe1—O2^{i}	2.183 (7)	C12—C13	1.34 (3)
Fe1—O2	2.183 (7)	C12—H12	0.9300
Fe2—O7^{iii}	2.089 (6)	C13—N2	1.32 (2)
Fe2—O7	2.089 (7)	C13—H13	0.9300
Fe2—O23	2.104 (8)	N1—H1A	0.8600
Fe2—O23^{iii}	2.104 (8)	N2—H2A	0.8600
Fe2—O1W	2.157 (8)	O3W—O9W	1.28 (5)
Fe2—O1W^{iii}	2.157 (8)	O3W—O3W′	1.55 (3)

O16—Mo1—O11	105.3 (3)	O7—Sr1—P2	87.04 (15)

O16—Mo1—O3	102.8 (3)	O9W—Sr1—P2	105.7 (11)
O11—Mo1—O3	95.6 (3)	O23—Sr1—P2	26.99 (16)
O16—Mo1—O12	96.7 (3)	O20^{iii}—Sr1—P2	128.75 (15)
O11—Mo1—O12	86.0 (3)	O3W—Sr1—P1	103.7 (5)
O3—Mo1—O12	159.3 (3)	O10^{iv}—Sr1—P1	62.70 (17)
O16—Mo1—O8	98.1 (3)	O22—Sr1—P1	138.91 (18)
O11—Mo1—O8	155.2 (3)	O2W—Sr1—P1	143.6 (3)
O3—Mo1—O8	86.9 (3)	O15^{iii}—Sr1—P1	81.5 (2)
O12—Mo1—O8	83.2 (3)	O3W′—Sr1—P1	80.9 (5)
O16—Mo1—O4	169.9 (3)	O7—Sr1—P1	24.99 (14)
O11—Mo1—O4	83.4 (3)	O9W—Sr1—P1	115.2 (8)
O3—Mo1—O4	81.0 (3)	O23—Sr1—P1	84.77 (17)
O12—Mo1—O4	78.7 (3)	O20^{iii}—Sr1—P1	75.76 (15)
O8—Mo1—O4	72.6 (2)	P2—Sr1—P1	111.53 (7)
O16—Mo1—Mo6	100.5 (3)	O3—Fe1—O3^{i}	180.0
O11—Mo1—Mo6	48.0 (2)	O3—Fe1—O1^{i}	84.6 (2)
O3—Mo1—Mo6	49.4 (2)	O3^{i}—Fe1—O1^{i}	95.4 (2)
O12—Mo1—Mo6	133.7 (2)	O3—Fe1—O1	95.4 (2)
O8—Mo1—Mo6	135.29 (19)	O3^{i}—Fe1—O1	84.6 (2)
O4—Mo1—Mo6	89.11 (18)	O1^{i}—Fe1—O1	180.0
O14—Mo2—O21	105.4 (4)	O3—Fe1—O2^{i}	95.1 (3)
O14—Mo2—O1	102.7 (3)	O3^{i}—Fe1—O2^{i}	84.9 (3)
O21—Mo2—O1	95.3 (3)	O1^{i}—Fe1—O2^{i}	83.8 (3)
O14—Mo2—O17	97.5 (3)	O1—Fe1—O2^{i}	96.2 (3)
O21—Mo2—O17	85.9 (3)	O3—Fe1—O2	84.9 (3)
O1—Mo2—O17	158.5 (3)	O3^{i}—Fe1—O2	95.1 (3)
O14—Mo2—O8	96.2 (3)	O1^{i}—Fe1—O2	96.2 (3)
O21—Mo2—O8	157.6 (3)	O1—Fe1—O2	83.8 (3)
O1—Mo2—O8	85.4 (3)	O2^{i}—Fe1—O2	180.0
O17—Mo2—O8	85.5 (3)	O7^{iii}—Fe2—O7	180.0 (3)
O14—Mo2—O4	168.2 (3)	O7^{iii}—Fe2—O23	98.3 (3)
O21—Mo2—O4	85.1 (3)	O7—Fe2—O23	81.7 (3)
O1—Mo2—O4	81.2 (3)	O7^{iii}—Fe2—O23^{iii}	81.7 (3)
O17—Mo2—O4	77.6 (3)	O7—Fe2—O23^{iii}	98.3 (3)
O8—Mo2—O4	72.8 (3)	O23—Fe2—O23^{iii}	180.0
O14—Mo2—Mo5	100.8 (3)	O7^{iii}—Fe2—O1W	88.1 (3)
O21—Mo2—Mo5	48.0 (2)	O7—Fe2—O1W	91.9 (3)
O1—Mo2—Mo5	48.99 (19)	O23—Fe2—O1W	93.1 (3)
O17—Mo2—Mo5	133.5 (2)	O23^{iii}—Fe2—O1W	86.9 (3)
O8—Mo2—Mo5	133.7 (2)	O7^{iii}—Fe2—O1W^{iii}	91.9 (3)
O4—Mo2—Mo5	90.15 (18)	O7—Fe2—O1W^{iii}	88.1 (3)
O9—Mo3—O10	107.2 (3)	O23—Fe2—O1W^{iii}	86.9 (3)
O9—Mo3—O2	102.5 (3)	O23^{iii}—Fe2—O1W^{iii}	93.1 (3)
O10—Mo3—O2	95.3 (3)	O1W—Fe2—O1W^{iii}	180.0
O9—Mo3—O20^{i}	98.1 (4)	O7—P1—O4^{iii}	112.4 (4)
O10—Mo3—O20^{i}	83.9 (3)	O7—P1—O18	111.4 (4)
O2—Mo3—O20^{i}	158.6 (3)	O4^{iii}—P1—O18	108.7 (4)
O9—Mo3—O6	95.5 (3)	O7—P1—O13^{iv}	108.8 (4)

O10—Mo3—O6	156.3 (3)	O4^{iii}—P1—O13^{iv}	107.9 (4)
O2—Mo3—O6	86.2 (3)	O18—P1—O13^{iv}	107.5 (4)
O20^{i}—Mo3—O6	86.2 (3)	O7—P1—Sr1	47.9 (3)
O9—Mo3—O13	168.7 (3)	O4^{iii}—P1—Sr1	157.2 (3)
O10—Mo3—O13	82.7 (3)	O18—P1—Sr1	91.3 (3)
O2—Mo3—O13	81.5 (3)	O13^{iv}—P1—Sr1	74.7 (3)
O20^{i}—Mo3—O13	77.1 (3)	O23—P2—O17	114.1 (4)
O6—Mo3—O13	74.1 (3)	O23—P2—O12	113.3 (5)
O9—Mo3—Mo4	101.5 (3)	O17—P2—O12	110.6 (4)
O10—Mo3—Mo4	48.3 (2)	O23—P2—O22	104.1 (4)
O2—Mo3—Mo4	48.9 (2)	O17—P2—O22	107.0 (4)
O20^{i}—Mo3—Mo4	131.8 (2)	O12—P2—O22	107.1 (4)
O6—Mo3—Mo4	134.3 (2)	O23—P2—Sr1	55.6 (3)
O13—Mo3—Mo4	89.17 (17)	O17—P2—Sr1	128.9 (3)
O9—Mo3—Sr1^{ii}	124.7 (3)	O12—P2—Sr1	119.2 (3)
O10—Mo3—Sr1^{ii}	36.3 (2)	O22—P2—Sr1	48.7 (3)
O2—Mo3—Sr1^{ii}	116.6 (2)	O26—P3—O24	111.1 (4)
O20^{i}—Mo3—Sr1^{ii}	53.2 (2)	O26—P3—O20	111.8 (5)
O6—Mo3—Sr1^{ii}	123.18 (18)	O24—P3—O20	113.1 (4)
O13—Mo3—Sr1^{ii}	60.64 (18)	O26—P3—O15	108.1 (5)
Mo4—Mo3—Sr1^{ii}	79.68 (3)	O24—P3—O15	107.8 (5)
O27—Mo4—O10	106.7 (4)	O20—P3—O15	104.5 (5)
O27—Mo4—O2	101.8 (3)	O26—P3—Sr1^{iii}	125.0 (3)
O10—Mo4—O2	94.8 (3)	O24—P3—Sr1^{iii}	121.7 (3)
O27—Mo4—O19	96.5 (3)	O20—P3—Sr1^{iii}	61.2 (3)
O10—Mo4—O19	86.2 (3)	O15—P3—Sr1^{iii}	43.4 (3)
O2—Mo4—O19	160.5 (3)	O29—P4—O31	110.4 (5)
O27—Mo4—O5	97.5 (4)	O29—P4—O19	111.3 (4)
O10—Mo4—O5	155.1 (3)	O31—P4—O19	110.6 (5)
O2—Mo4—O5	85.5 (3)	O29—P4—O30	108.6 (5)
O19—Mo4—O5	85.5 (3)	O31—P4—O30	109.7 (5)
O27—Mo4—O18^{ii}	169.9 (3)	O19—P4—O30	106.1 (5)
O10—Mo4—O18^{ii}	82.5 (3)	Mo5—O1—Mo2	82.0 (2)
O2—Mo4—O18^{ii}	81.1 (3)	Mo5—O1—Fe1	133.7 (3)
O19—Mo4—O18^{ii}	79.7 (3)	Mo2—O1—Fe1	135.7 (3)
O5—Mo4—O18^{ii}	72.9 (3)	Mo3—O2—Mo4	82.4 (3)
O27—Mo4—Mo3	100.6 (3)	Mo3—O2—Fe1	135.2 (3)
O10—Mo4—Mo3	48.0 (2)	Mo4—O2—Fe1	133.4 (4)
O2—Mo4—Mo3	48.7 (2)	Mo1—O3—Mo6	81.9 (2)
O19—Mo4—Mo3	134.0 (2)	Mo1—O3—Fe1	134.8 (4)
O5—Mo4—Mo3	133.2 (2)	Mo6—O3—Fe1	134.9 (4)
O18^{ii}—Mo4—Mo3	88.69 (18)	P1^{iii}—O4—Mo2	125.1 (4)
O25—Mo5—O21	106.5 (4)	P1^{iii}—O4—Mo1	127.2 (4)
O25—Mo5—O1	102.2 (4)	Mo2—O4—Mo1	100.6 (3)
O21—Mo5—O1	94.9 (3)	Mo4—O5—Mo5^{i}	113.5 (3)
O25—Mo5—O29^{i}	95.9 (4)	Mo6^{i}—O6—Mo3	113.1 (3)
O21—Mo5—O29^{i}	87.1 (3)	P1—O7—Fe2	136.1 (5)
O1—Mo5—O29^{i}	160.4 (3)	P1—O7—Sr1	107.1 (4)

O25—Mo5—O5^{i}	97.9 (3)	Fe2—O7—Sr1	110.3 (3)
O21—Mo5—O5^{i}	154.8 (3)	Mo1—O8—Mo2	113.5 (3)
O1—Mo5—O5^{i}	85.6 (3)	Mo3—O10—Mo4	83.7 (3)
O29^{i}—Mo5—O5^{i}	84.5 (3)	Mo3—O10—Sr1^{ii}	117.1 (3)
O25—Mo5—O18^{iii}	170.1 (3)	Mo4—O10—Sr1^{ii}	139.9 (3)
O21—Mo5—O18^{iii}	82.6 (3)	Mo1—O11—Mo6	84.2 (3)
O1—Mo5—O18^{iii}	80.4 (3)	P2—O12—Mo1	132.1 (4)
O29^{i}—Mo5—O18^{iii}	80.5 (3)	P1^{ii}—O13—Mo3	126.5 (4)
O5^{i}—Mo5—O18^{iii}	72.6 (3)	P1^{ii}—O13—Mo6^{i}	126.2 (4)
O25—Mo5—Mo2	101.3 (3)	Mo3—O13—Mo6^{i}	99.3 (3)
O21—Mo5—Mo2	47.6 (2)	P3—O15—Sr1^{iii}	111.9 (4)
O1—Mo5—Mo2	49.01 (19)	P2—O17—Mo2	131.3 (4)
O29^{i}—Mo5—Mo2	134.4 (2)	P1—O18—Mo4^{iv}	126.7 (4)
O5^{i}—Mo5—Mo2	133.4 (2)	P1—O18—Mo5^{iii}	126.4 (4)
O18^{iii}—Mo5—Mo2	87.72 (18)	Mo4^{iv}—O18—Mo5^{iii}	99.9 (3)
O28—Mo6—O11	105.9 (3)	P4—O19—Mo4	137.6 (5)
O28—Mo6—O3	102.4 (4)	P3—O20—Mo3^{i}	135.7 (5)
O11—Mo6—O3	94.7 (3)	P3—O20—Sr1^{iii}	93.2 (4)
O28—Mo6—O24	96.7 (4)	Mo3^{i}—O20—Sr1^{iii}	94.1 (3)
O11—Mo6—O24	85.6 (3)	Mo2—O21—Mo5	84.4 (3)
O3—Mo6—O24	160.0 (3)	P2—O22—Sr1	103.9 (4)
O28—Mo6—O6^{i}	97.7 (3)	P2—O23—Fe2	154.2 (5)
O11—Mo6—O6^{i}	155.4 (3)	P2—O23—Sr1	97.4 (4)
O3—Mo6—O6^{i}	86.5 (3)	Fe2—O23—Sr1	106.7 (3)
O24—Mo6—O6^{i}	85.1 (3)	P3—O24—Mo6	134.9 (4)
O28—Mo6—O13^{i}	170.1 (3)	P4—O29—Mo5^{i}	137.7 (5)
O11—Mo6—O13^{i}	83.0 (3)	P4—O30—H30	109.5
O3—Mo6—O13^{i}	80.5 (3)	N1—C1—C2	119.3 (19)
O24—Mo6—O13^{i}	79.6 (3)	N1—C1—H1	120.4
O6^{i}—Mo6—O13^{i}	72.9 (2)	C2—C1—H1	120.4
O28—Mo6—Mo1	100.7 (3)	C1—C2—C3	121.5 (19)
O11—Mo6—Mo1	47.8 (2)	C1—C2—H2	119.2
O3—Mo6—Mo1	48.6 (2)	C3—C2—H2	119.2
O24—Mo6—Mo1	133.1 (2)	C4—C3—C2	114.8 (16)
O6^{i}—Mo6—Mo1	134.2 (2)	C4—C3—C6	123.2 (19)
O13^{i}—Mo6—Mo1	88.38 (17)	C2—C3—C6	122 (2)
O3W—Sr1—O10^{iv}	89.1 (5)	C5—C4—C3	123.3 (18)
O3W—Sr1—O22	81.4 (5)	C5—C4—H4	118.4
O10^{iv}—Sr1—O22	157.9 (2)	C3—C4—H4	118.4
O3W—Sr1—O2W	93.0 (5)	N1—C5—C4	117.0 (18)
O10^{iv}—Sr1—O2W	85.9 (3)	N1—C5—H5	121.5
O22—Sr1—O2W	74.9 (3)	C4—C5—H5	121.5
O3W—Sr1—O15^{iii}	167.5 (5)	C3—C6—C7	112.8 (15)
O10^{iv}—Sr1—O15^{iii}	103.4 (2)	C3—C6—H6A	109.0
O22—Sr1—O15^{iii}	87.2 (3)	C7—C6—H6A	109.0
O2W—Sr1—O15^{iii}	89.1 (3)	C3—C6—H6B	109.0
O3W—Sr1—O3W′	35.3 (7)	C7—C6—H6B	109.0
O10^{iv}—Sr1—O3W′	102.1 (5)	H6A—C6—H6B	107.8

O22—Sr1—O3W′	81.4 (5)	C8—C7—C6	114.8 (17)
O2W—Sr1—O3W′	126.1 (6)	C8—C7—H7A	108.6
O15^{iii}—Sr1—O3W′	137.7 (6)	C6—C7—H7A	108.6
O3W—Sr1—O7	98.6 (5)	C8—C7—H7B	108.6
O10^{iv}—Sr1—O7	86.7 (2)	C6—C7—H7B	108.6
O22—Sr1—O7	114.3 (2)	H7A—C7—H7B	107.5
O2W—Sr1—O7	166.1 (3)	C11—C8—C7	113.7 (16)
O15^{iii}—Sr1—O7	81.3 (3)	C11—C8—H8A	108.8
O3W′—Sr1—O7	67.1 (5)	C7—C8—H8A	108.8
O3W—Sr1—O9W	28.2 (11)	C11—C8—H8B	108.8
O10^{iv}—Sr1—O9W	74.1 (11)	C7—C8—H8B	108.8
O22—Sr1—O9W	88.6 (10)	H8A—C8—H8B	107.7
O2W—Sr1—O9W	68.5 (10)	N2—C9—C10	117.1 (18)
O15^{iii}—Sr1—O9W	157.5 (10)	N2—C9—H9	121.5
O3W′—Sr1—O9W	63.1 (13)	C10—C9—H9	121.5
O7—Sr1—O9W	120.4 (9)	C11—C10—C9	120 (2)
O3W—Sr1—O23	97.7 (5)	C11—C10—H10	119.8
O10^{iv}—Sr1—O23	147.4 (2)	C9—C10—H10	119.8
O22—Sr1—O23	54.3 (2)	C10—C11—C12	119 (2)
O2W—Sr1—O23	125.2 (3)	C10—C11—C8	120 (2)
O15^{iii}—Sr1—O23	71.2 (2)	C12—C11—C8	121.1 (17)
O3W′—Sr1—O23	69.1 (5)	C13—C12—C11	120.8 (16)
O7—Sr1—O23	60.8 (2)	C13—C12—H12	119.6
O9W—Sr1—O23	122.9 (12)	C11—C12—H12	119.6
O3W—Sr1—O20^{iii}	141.7 (5)	N2—C13—C12	120 (2)
O10^{iv}—Sr1—O20^{iii}	56.0 (2)	N2—C13—H13	120.2
O22—Sr1—O20^{iii}	124.6 (2)	C12—C13—H13	120.2
O2W—Sr1—O20^{iii}	71.3 (3)	C1—N1—C5	124.1 (16)
O15^{iii}—Sr1—O20^{iii}	50.3 (2)	C1—N1—H1A	118.0
O3W′—Sr1—O20^{iii}	153.5 (5)	C5—N1—H1A	118.0
O7—Sr1—O20^{iii}	94.8 (2)	C13—N2—C9	123 (2)
O9W—Sr1—O20^{iii}	116.7 (13)	C13—N2—H2A	118.5
O23—Sr1—O20^{iii}	120.1 (2)	C9—N2—H2A	118.5
O3W—Sr1—P2	87.8 (4)	O9W—O3W—O3W′	163 (3)
O10^{iv}—Sr1—P2	172.53 (18)	O9W—O3W—Sr1	87.7 (17)
O22—Sr1—P2	27.39 (18)	O3W′—O3W—Sr1	79.5 (12)
O2W—Sr1—P2	101.1 (3)	O3W—O9W—Sr1	64.1 (15)
O15^{iii}—Sr1—P2	79.70 (18)	O3W—O3W′—Sr1	65.2 (12)
O3W′—Sr1—P2	71.6 (5)		

Symmetry codes: (i) $-x+1, -y, -z$; (ii) $x, y-1, z$; (iii) $-x+1, -y+1, -z$; (iv) $x, y+1, z$.

(2)

Crystal data

$(C_{13}H_{16}N_2)_2[Na(H_2O)(C_2H_5O)][Fe(H_2O)_2][Ca(H_2O)_2]2\ \{Fe[Mo_6O_{12}(OH)_3(H_2PO_4)(HPO_4)(PO_4)_2]_2\}\cdot 4H_2O$	Monoclinic, $C2/c$
M_r = 3260.77	a = 21.317 (7) Å
	b = 18.533 (6) Å
	c = 22.838 (8) Å

β = 95.130 (5)°
V = 8986 (5) Å^3
Z = 4
F(000) = 6340
D_x = 2.410 Mg m^{-3}
Mo $K\alpha$ radiation, λ = 0.71073 Å

Cell parameters from 9260 reflections
θ = 2.4–27.9°
μ = 2.31 mm^{-1}
T = 296 K
Block, red
0.19 × 0.17 × 0.15 mm

Data collection

Bruker SMART CCD area detector diffractometer
phi and ω scans
Absorption correction: multi-scan (SADABS; Bruker, 2008)
T_{min} = 0.652, T_{max} = 0.708
19982 measured reflections

7781 independent reflections
7629 reflections with $I > 2\sigma(I)$
R_{int} = 0.022
θ_{max} = 25.0°, θ_{min} = 1.8°
h = −25→19
k = −22→21
l = −27→26

Refinement

Refinement on F^2
Least-squares matrix: full
$R[F^2 > 2\sigma(F^2)]$ = 0.038
$wR(F^2)$ = 0.111
S = 1.06
7781 reflections
616 parameters
3 restraints

Hydrogen site location: mixed
H atoms treated by a mixture of independent and constrained refinement
$w = 1/[\sigma^2(F_o^2) + (0.0626P)^2 + 126.1618P]$ where $P = (F_o^2 + 2F_c^2)/3$
$(\Delta/\sigma)_{max}$ = 0.001
$\Delta\rho_{max}$ = 1.89 e Å^{-3}
$\Delta\rho_{min}$ = −0.73 e Å^{-3}

Special details

Geometry. All esds (except the esd in the dihedral angle between two l.s. planes) are estimated using the full covariance matrix. The cell esds are taken into account individually in the estimation of esds in distances, angles and torsion angles; correlations between esds in cell parameters are only used when they are defined by crystal symmetry. An approximate (isotropic) treatment of cell esds is used for estimating esds involving l.s. planes.

Fractional atomic coordinates and isotropic or equivalent isotropic displacement parameters (Å^2)

	x	y	z	U_{iso}*/U_{eq}	Occ. (<1)
Mo1	0.19573 (2)	0.39849 (2)	−0.11379 (2)	0.01551 (12)	
Mo2	0.27126 (2)	0.40320 (2)	0.11744 (2)	0.01539 (12)	
Mo3	0.42188 (2)	0.26408 (2)	−0.03694 (2)	0.01558 (12)	
Mo4	0.29055 (2)	0.45615 (2)	0.01341 (2)	0.01544 (12)	
Mo5	0.34973 (2)	0.22651 (3)	−0.13064 (2)	0.01646 (13)	
Mo6	0.10529 (2)	0.30434 (2)	−0.10468 (2)	0.01554 (12)	
P1	0.53381 (7)	0.17840 (8)	0.04940 (7)	0.0195 (3)	
P2	0.31143 (8)	0.10455 (8)	−0.23305 (7)	0.0210 (3)	
P3	0.21097 (7)	0.57394 (8)	−0.07794 (7)	0.0199 (3)	
P4	0.13500 (7)	0.40689 (7)	0.02340 (6)	0.0139 (3)	
Fe1	0.2500	0.2500	0.0000	0.0159 (2)	
Ca1	0.15813 (7)	0.58587 (7)	0.05502 (6)	0.0315 (3)	
Fe2	0.5000	0.0000	0.0000	0.0200 (3)	
Na1	0.0495 (4)	0.4277 (5)	0.1438 (4)	0.080 (3)	0.5
O1	0.32807 (18)	0.2655 (2)	−0.05262 (17)	0.0166 (8)	
O2	0.16924 (18)	0.3796 (2)	0.08254 (16)	0.0167 (8)	

O3	0.28649 (18)	0.3540 (2)	0.04133 (17)	0.0180 (8)	
O4	0.40033 (18)	0.15799 (19)	0.00802 (16)	0.0152 (8)	
O5	0.25154 (19)	0.4983 (2)	0.08050 (17)	0.0192 (8)	
O6	0.19656 (18)	0.3004 (2)	−0.07602 (17)	0.0170 (8)	
O7	0.24688 (18)	0.3000 (2)	0.14807 (17)	0.0185 (8)	
H7	0.2723	0.2715	0.1308	0.08 (3)*	
O8	0.3684 (2)	0.4748 (2)	0.02342 (19)	0.0261 (9)	
O9	0.5332 (2)	0.0995 (2)	0.0293 (2)	0.0294 (10)	
O10	0.28819 (18)	0.4119 (2)	−0.07210 (17)	0.0195 (8)	
H10A	0.3094	0.3638	−0.0698	0.05 (3)*	
O11	0.3616 (2)	0.1532 (2)	−0.19819 (18)	0.0267 (9)	
O12	0.1036 (2)	0.2613 (2)	−0.17037 (19)	0.0263 (9)	
O13	0.18622 (18)	0.4329 (2)	−0.01728 (17)	0.0175 (8)	
O14	0.2680 (2)	0.1448 (3)	−0.27817 (19)	0.0324 (11)	
O15	0.09462 (19)	0.2099 (2)	−0.05261 (17)	0.0188 (8)	
H15	0.1323	0.1823	−0.0539	0.04 (2)*	
O16	0.51120 (19)	0.2321 (2)	−0.00166 (19)	0.0216 (9)	
O17	0.2755 (2)	0.0595 (2)	−0.18823 (18)	0.0230 (9)	
O18	0.10380 (19)	0.4076 (2)	−0.12222 (18)	0.0194 (8)	
O19	0.49130 (18)	0.1899 (2)	0.10094 (18)	0.0212 (9)	
O20	0.43748 (19)	0.2043 (2)	−0.10470 (18)	0.0216 (9)	
O21	0.1524 (2)	0.5974 (2)	−0.0495 (2)	0.0306 (10)	
O22	0.1966 (2)	0.5119 (2)	−0.12379 (18)	0.0217 (9)	
O23	0.2157 (2)	0.3800 (2)	−0.18266 (19)	0.0273 (10)	
O24	0.4429 (2)	0.3496 (2)	−0.0541 (2)	0.0273 (10)	
O25	0.2632 (2)	0.5515 (2)	−0.02999 (19)	0.0247 (9)	
O26	0.09176 (19)	0.4695 (2)	0.03649 (18)	0.0213 (9)	
O27	0.6021 (2)	0.1967 (2)	0.0708 (2)	0.0307 (10)	
O28	0.3512 (2)	0.3035 (2)	−0.17078 (19)	0.0297 (10)	
O29	0.2387 (2)	0.6384 (2)	−0.1122 (2)	0.0351 (11)	
H29	0.2482	0.6715	−0.0893	0.053*	
O30	0.3454 (2)	0.4097 (2)	0.1503 (2)	0.0281 (10)	
O31	0.3528 (2)	0.0478 (3)	−0.2656 (2)	0.0314 (10)	
H31	0.3294	0.0189	−0.2839	0.047*	
O32	0.0345 (15)	0.5075 (16)	0.2160 (14)	0.30 (2)	0.5
C1	0.0997 (6)	0.7473 (6)	0.8591 (6)	0.088 (4)	
H1	0.0931	0.6981	0.8535	0.105*	
C2	0.1292 (6)	0.7873 (5)	0.8177 (5)	0.068 (3)	
H2	0.1434	0.7651	0.7849	0.082*	
C3	0.1368 (4)	0.8611 (4)	0.8265 (3)	0.0391 (17)	
C4	0.1143 (5)	0.8925 (6)	0.8757 (4)	0.059 (2)	
H4	0.1183	0.9420	0.8816	0.070*	
C5	0.0864 (5)	0.8513 (8)	0.9156 (5)	0.071 (3)	
H5	0.0712	0.8725	0.9484	0.086*	
C6	0.1672 (4)	0.9087 (4)	0.7830 (3)	0.0351 (16)	
H6A	0.1912	0.8787	0.7582	0.042*	
H6B	0.1963	0.9416	0.8043	0.042*	
C7	0.1181 (4)	0.9525 (4)	0.7440 (3)	0.0413 (18)	

H7A	0.0879	0.9195	0.7242	0.050*	
H7B	0.0955	0.9838	0.7688	0.050*	
C8	0.1476 (4)	0.9984 (4)	0.6978 (4)	0.046 (2)	
H8A	0.1811	1.0278	0.7169	0.055*	
H8B	0.1658	0.9671	0.6698	0.055*	
C9	0.0381 (9)	1.1565 (7)	0.6595 (6)	0.131 (7)	
H9	0.0287	1.2015	0.6745	0.158*	
C10	0.0864 (8)	1.1140 (6)	0.6870 (6)	0.106 (6)	
H10	0.1103	1.1316	0.7201	0.127*	
C11	0.0991 (4)	1.0466 (4)	0.6657 (4)	0.0402 (18)	
C12	0.0640 (5)	1.0244 (5)	0.6146 (5)	0.068 (3)	
H12	0.0717	0.9797	0.5981	0.082*	
C13	0.0179 (5)	1.0687 (6)	0.5885 (5)	0.075 (3)	
H13	−0.0050	1.0539	0.5539	0.090*	
C14	0.0582 (17)	0.657 (2)	0.2133 (11)	0.135 (16)	0.5
H14A	0.0331	0.6787	0.2414	0.202*	0.5
H14B	0.0549	0.6850	0.1779	0.202*	0.5
H14C	0.1014	0.6551	0.2293	0.202*	0.5
C15	0.0345 (12)	0.581 (2)	0.1997 (15)	0.117 (14)	0.5
H15A	−0.0105	0.5895	0.1950	0.141*	0.5
H15B	0.0461	0.5758	0.1597	0.141*	0.5
N1	0.0810 (4)	0.7798 (6)	0.9069 (4)	0.077 (3)	
H1A	0.0649	0.7540	0.9330	0.092*	
N2	0.0057 (4)	1.1307 (5)	0.6111 (4)	0.074 (3)	
H2A	−0.0245	1.1563	0.5944	0.089*	
O1W	0.4586 (2)	−0.0251 (3)	0.0820 (2)	0.0318 (10)	
H1WA	0.4407	0.0201	0.0964	0.23 (10)*	
H1WB	0.4226	−0.0522	0.0693	0.21 (9)*	
O2W	0.1567 (5)	0.5737 (5)	0.1587 (3)	0.105 (4)	
O3W	0.2425 (3)	0.6755 (4)	0.0632 (5)	0.091 (3)	
O4W	0.8391 (6)	0.8120 (6)	0.4735 (5)	0.136 (5)	
O6W	0.8065 (7)	0.2744 (6)	0.7882 (6)	0.147 (5)	
O7W	−0.0088 (13)	0.3830 (17)	0.2048 (14)	0.30 (2)	0.5

Atomic displacement parameters (Å²)

	U^{11}	U^{22}	U^{33}	U^{12}	U^{13}	U^{23}
Mo1	0.0199 (2)	0.0132 (2)	0.0129 (2)	0.00124 (18)	−0.00156 (18)	0.00079 (17)
Mo2	0.0193 (2)	0.0137 (2)	0.0125 (2)	0.00214 (18)	−0.00284 (18)	−0.00088 (17)
Mo3	0.0181 (2)	0.0118 (2)	0.0164 (3)	0.00086 (18)	−0.00142 (18)	0.00031 (17)
Mo4	0.0185 (2)	0.0127 (2)	0.0145 (3)	0.00104 (18)	−0.00167 (18)	0.00037 (17)
Mo5	0.0218 (3)	0.0142 (2)	0.0130 (3)	0.00137 (18)	−0.00041 (18)	0.00031 (18)
Mo6	0.0179 (2)	0.0131 (2)	0.0149 (3)	0.00159 (18)	−0.00281 (18)	−0.00085 (17)
P1	0.0181 (7)	0.0160 (7)	0.0238 (8)	0.0023 (6)	−0.0020 (6)	0.0014 (6)
P2	0.0282 (8)	0.0217 (8)	0.0126 (7)	0.0024 (6)	0.0000 (6)	−0.0036 (6)
P3	0.0270 (8)	0.0130 (7)	0.0191 (8)	−0.0007 (6)	−0.0007 (6)	0.0038 (6)
P4	0.0180 (7)	0.0101 (6)	0.0128 (7)	0.0019 (5)	−0.0023 (5)	−0.0005 (5)
Fe1	0.0182 (5)	0.0144 (5)	0.0147 (6)	0.0025 (4)	−0.0014 (4)	0.0008 (4)

Ca1	0.0365 (7)	0.0246 (7)	0.0319 (8)	0.0064 (6)	−0.0057 (6)	−0.0026 (5)
Fe2	0.0178 (6)	0.0155 (6)	0.0258 (6)	0.0026 (4)	−0.0025 (5)	−0.0010 (5)
Na1	0.070 (5)	0.076 (6)	0.087 (6)	0.035 (5)	−0.036 (5)	−0.011 (5)
O1	0.020 (2)	0.0144 (19)	0.015 (2)	0.0029 (15)	−0.0018 (15)	−0.0012 (15)
O2	0.022 (2)	0.0153 (19)	0.012 (2)	0.0016 (16)	−0.0019 (15)	0.0003 (15)
O3	0.022 (2)	0.017 (2)	0.014 (2)	0.0024 (16)	−0.0018 (15)	−0.0001 (15)
O4	0.0205 (19)	0.0099 (17)	0.0146 (19)	−0.0018 (15)	−0.0025 (15)	−0.0021 (14)
O5	0.024 (2)	0.0153 (19)	0.017 (2)	0.0029 (16)	−0.0019 (16)	−0.0028 (15)
O6	0.020 (2)	0.0147 (19)	0.015 (2)	0.0032 (15)	−0.0011 (15)	−0.0009 (15)
O7	0.020 (2)	0.017 (2)	0.019 (2)	0.0030 (16)	−0.0006 (16)	0.0014 (16)
O8	0.025 (2)	0.026 (2)	0.027 (2)	−0.0002 (18)	−0.0005 (18)	0.0031 (18)
O9	0.033 (2)	0.018 (2)	0.037 (3)	0.0074 (18)	0.002 (2)	−0.0014 (18)
O10	0.021 (2)	0.019 (2)	0.018 (2)	0.0019 (16)	0.0019 (16)	0.0013 (16)
O11	0.035 (2)	0.028 (2)	0.017 (2)	−0.0029 (19)	0.0048 (18)	−0.0097 (18)
O12	0.030 (2)	0.030 (2)	0.018 (2)	0.0002 (19)	−0.0030 (17)	−0.0081 (18)
O13	0.021 (2)	0.0149 (19)	0.016 (2)	−0.0005 (16)	−0.0011 (15)	0.0011 (15)
O14	0.045 (3)	0.034 (3)	0.017 (2)	0.011 (2)	−0.0021 (19)	−0.0012 (19)
O15	0.024 (2)	0.0135 (19)	0.019 (2)	0.0014 (16)	0.0008 (16)	−0.0012 (15)
O16	0.020 (2)	0.020 (2)	0.025 (2)	−0.0015 (16)	−0.0008 (17)	0.0048 (17)
O17	0.030 (2)	0.021 (2)	0.016 (2)	0.0008 (17)	−0.0039 (17)	−0.0066 (16)
O18	0.021 (2)	0.0159 (19)	0.020 (2)	0.0013 (16)	−0.0045 (16)	0.0023 (16)
O19	0.0165 (19)	0.024 (2)	0.022 (2)	0.0009 (16)	−0.0039 (16)	0.0018 (17)
O20	0.022 (2)	0.024 (2)	0.019 (2)	0.0009 (17)	0.0013 (16)	−0.0025 (17)
O21	0.032 (2)	0.028 (2)	0.031 (3)	0.0083 (19)	0.004 (2)	−0.0011 (19)
O22	0.031 (2)	0.015 (2)	0.018 (2)	−0.0043 (17)	−0.0046 (17)	0.0038 (16)
O23	0.035 (2)	0.027 (2)	0.019 (2)	−0.0029 (19)	−0.0002 (18)	−0.0015 (18)
O24	0.032 (2)	0.018 (2)	0.031 (2)	−0.0024 (18)	−0.0021 (19)	0.0013 (18)
O25	0.033 (2)	0.015 (2)	0.025 (2)	−0.0012 (17)	−0.0054 (18)	0.0034 (17)
O26	0.024 (2)	0.017 (2)	0.022 (2)	0.0062 (17)	−0.0027 (17)	−0.0014 (16)
O27	0.021 (2)	0.032 (2)	0.038 (3)	0.0011 (19)	−0.0059 (19)	0.004 (2)
O28	0.044 (3)	0.022 (2)	0.022 (2)	0.002 (2)	−0.0010 (19)	0.0079 (18)
O29	0.056 (3)	0.022 (2)	0.026 (3)	−0.014 (2)	−0.004 (2)	0.0035 (19)
O30	0.027 (2)	0.030 (2)	0.026 (2)	0.0020 (19)	−0.0077 (18)	−0.0012 (18)
O31	0.035 (3)	0.033 (3)	0.026 (2)	0.007 (2)	0.0016 (19)	−0.013 (2)
O32	0.18 (2)	0.28 (3)	0.40 (5)	0.15 (2)	−0.11 (3)	−0.16 (3)
C1	0.116 (10)	0.044 (6)	0.110 (10)	0.000 (6)	0.050 (8)	0.024 (6)
C2	0.103 (8)	0.039 (5)	0.068 (7)	−0.003 (5)	0.031 (6)	0.004 (4)
C3	0.040 (4)	0.044 (4)	0.033 (4)	0.009 (3)	0.002 (3)	0.003 (3)
C4	0.064 (6)	0.069 (6)	0.046 (5)	0.000 (5)	0.019 (4)	−0.007 (4)
C5	0.051 (6)	0.117 (10)	0.046 (6)	0.012 (6)	0.012 (4)	0.000 (6)
C6	0.040 (4)	0.029 (4)	0.036 (4)	−0.003 (3)	−0.002 (3)	0.001 (3)
C7	0.047 (4)	0.037 (4)	0.038 (4)	0.008 (3)	−0.006 (3)	−0.005 (3)
C8	0.039 (4)	0.041 (4)	0.057 (5)	0.009 (3)	−0.006 (4)	0.017 (4)
C9	0.23 (2)	0.075 (9)	0.078 (9)	0.093 (11)	−0.048 (11)	−0.011 (7)
C10	0.173 (15)	0.060 (7)	0.072 (8)	0.049 (8)	−0.055 (9)	−0.017 (6)
C11	0.041 (4)	0.036 (4)	0.042 (4)	0.006 (3)	−0.005 (3)	0.012 (3)
C12	0.083 (7)	0.047 (5)	0.069 (7)	0.023 (5)	−0.025 (5)	−0.012 (5)
C13	0.079 (7)	0.065 (7)	0.074 (7)	0.004 (6)	−0.031 (6)	0.010 (6)

C14	0.18 (3)	0.17 (3)	0.046 (15)	0.09 (3)	−0.056 (18)	−0.045 (18)
C15	0.058 (14)	0.18 (3)	0.12 (2)	0.046 (19)	0.022 (15)	0.09 (3)
N1	0.059 (5)	0.111 (8)	0.066 (6)	0.029 (5)	0.029 (4)	0.050 (6)
N2	0.083 (6)	0.069 (6)	0.067 (6)	0.046 (5)	−0.010 (5)	0.026 (5)
O1W	0.032 (2)	0.028 (2)	0.034 (3)	0.002 (2)	−0.004 (2)	−0.004 (2)
O2W	0.146 (8)	0.128 (7)	0.041 (4)	0.098 (7)	0.015 (4)	0.026 (4)
O3W	0.048 (4)	0.057 (4)	0.162 (9)	0.005 (3)	−0.023 (5)	−0.026 (5)
O4W	0.156 (10)	0.120 (8)	0.122 (8)	0.094 (8)	−0.050 (7)	−0.033 (7)
O6W	0.220 (14)	0.075 (7)	0.142 (10)	−0.042 (8)	−0.012 (9)	0.001 (7)
O7W	0.18 (2)	0.28 (3)	0.40 (5)	0.15 (2)	−0.11 (3)	−0.16 (3)

Geometric parameters (Å, º)

Mo1—O23	1.700 (4)	Fe2—O9	2.065 (4)
Mo1—O18	1.959 (4)	Fe2—O9^{iv}	2.065 (4)
Mo1—O6	2.011 (4)	Fe2—O26^{i}	2.133 (4)
Mo1—O22	2.114 (4)	Fe2—O26^{ii}	2.133 (4)
Mo1—O10	2.125 (4)	Fe2—O1W	2.189 (5)
Mo1—O13	2.321 (4)	Fe2—O1W^{iv}	2.189 (5)
Mo1—Mo6	2.6222 (9)	Na1—O7W	2.12 (2)
Mo2—O30	1.691 (4)	Na1—O32	2.260 (18)
Mo2—O5	1.983 (4)	Na1—O1W^{iii}	2.454 (8)
Mo2—O3	2.014 (4)	Na1—O20^{i}	2.628 (10)
Mo2—O17^{i}	2.092 (4)	Na1—O11^{i}	2.639 (9)
Mo2—O7	2.117 (4)	Na1—O26	2.794 (12)
Mo2—O2	2.290 (4)	Na1—Mo5^{i}	3.604 (8)
Mo2—Mo4	2.6363 (10)	O2—Mo5^{i}	2.306 (4)
Mo3—O24	1.703 (4)	O4—P4^{i}	1.559 (4)
Mo3—O20	1.956 (4)	O4—Mo6^{i}	2.329 (4)
Mo3—O1	2.000 (4)	O7—Mo5^{i}	2.120 (4)
Mo3—O16	2.086 (4)	O7—H7	0.8753
Mo3—O15^{i}	2.160 (4)	O9—Ca1^{ii}	2.688 (5)
Mo3—O4	2.284 (4)	O10—H10A	0.9987
Mo3—Mo5	2.6155 (9)	O11—Na1^{i}	2.639 (9)
Mo4—O8	1.690 (4)	O15—Mo3^{i}	2.160 (4)
Mo4—O5	1.969 (4)	O15—H15	0.9561
Mo4—O3	2.001 (4)	O17—Mo2^{i}	2.092 (4)
Mo4—O25	2.084 (4)	O19—Mo6^{i}	2.071 (4)
Mo4—O10	2.115 (4)	O20—Na1^{i}	2.628 (10)
Mo4—O13	2.312 (4)	O26—Fe2^{iii}	2.133 (4)
Mo5—O28	1.698 (4)	O27—Ca1^{ii}	2.420 (5)
Mo5—O20	1.955 (4)	O29—H29	0.8200
Mo5—O1	2.014 (4)	O31—H31	0.8200
Mo5—O11	2.088 (4)	O32—C15	1.404 (19)
Mo5—O7^{i}	2.120 (4)	C1—N1	1.339 (16)
Mo5—O2^{i}	2.306 (4)	C1—C2	1.393 (14)
Mo5—Na1^{i}	3.604 (8)	C1—H1	0.9300
Mo6—O12	1.697 (4)	C2—C3	1.390 (12)

Mo6—O18	1.954 (4)	C2—H2	0.9300
Mo6—O6	1.998 (4)	C3—C4	1.389 (11)
Mo6—O19^{i}	2.071 (4)	C3—C6	1.516 (10)
Mo6—O15	2.139 (4)	C4—C5	1.365 (15)
Mo6—O4^{i}	2.329 (4)	C4—H4	0.9300
P1—O9	1.532 (4)	C5—N1	1.343 (15)
P1—O27	1.531 (4)	C5—H5	0.9300
P1—O19	1.563 (4)	C6—C7	1.543 (10)
P1—O16	1.575 (4)	C6—H6A	0.9700
P1—Ca1^{ii}	3.149 (2)	C6—H6B	0.9700
P2—O14	1.517 (5)	C7—C8	1.533 (11)
P2—O11	1.561 (4)	C7—H7A	0.9700
P2—O17	1.572 (5)	C7—H7B	0.9700
P2—O31	1.597 (4)	C8—C11	1.506 (10)
P3—O21	1.521 (5)	C8—H8A	0.9700
P3—O25	1.547 (4)	C8—H8B	0.9700
P3—O22	1.567 (4)	C9—N2	1.339 (17)
P3—O29	1.572 (5)	C9—C10	1.399 (16)
P3—Ca1	3.339 (2)	C9—H9	0.9300
P4—O26	1.528 (4)	C10—C11	1.377 (14)
P4—O4^{i}	1.559 (4)	C10—H10	0.9300
P4—O2	1.561 (4)	C11—C12	1.391 (12)
P4—O13	1.572 (4)	C12—C13	1.375 (13)
P4—Ca1	3.421 (2)	C12—H12	0.9300
Fe1—O1	2.157 (4)	C13—N2	1.296 (14)
Fe1—O1^{i}	2.157 (4)	C13—H13	0.9300
Fe1—O6	2.198 (4)	C14—C15	1.53 (4)
Fe1—O6^{i}	2.198 (4)	C14—H14A	0.9600
Fe1—O3^{i}	2.254 (4)	C14—H14B	0.9600
Fe1—O3	2.254 (4)	C14—H14C	0.9600
Ca1—O2W	2.381 (7)	C15—H15A	0.9700
Ca1—O21	2.388 (5)	C15—H15B	0.9700
Ca1—O27^{iii}	2.420 (5)	N1—H1A	0.8600
Ca1—O3W	2.443 (7)	N2—H2A	0.8600
Ca1—O26	2.593 (4)	O1W—Na1^{ii}	2.454 (9)
Ca1—O5	2.594 (4)	O1W—H1WA	0.9884
Ca1—O9^{iii}	2.688 (5)	O1W—H1WB	0.9428
Ca1—P1^{iii}	3.149 (2)		

O23—Mo1—O18	104.88 (19)	O3W—Ca1—O5	82.1 (2)
O23—Mo1—O6	102.81 (19)	O26—Ca1—O5	85.01 (13)
O18—Mo1—O6	95.18 (16)	O2W—Ca1—O9^{iii}	97.3 (3)
O23—Mo1—O22	95.43 (19)	O21—Ca1—O9^{iii}	79.17 (16)
O18—Mo1—O22	85.54 (16)	O27^{iii}—Ca1—O9^{iii}	57.29 (14)
O6—Mo1—O22	160.87 (16)	O3W—Ca1—O9^{iii}	131.4 (2)
O23—Mo1—O10	98.02 (19)	O26—Ca1—O9^{iii}	61.77 (13)
O18—Mo1—O10	155.98 (16)	O5—Ca1—O9^{iii}	146.49 (14)
O6—Mo1—O10	86.62 (15)	O2W—Ca1—P1^{iii}	90.39 (18)

O22—Mo1—O10	85.17 (15)	O21—Ca1—P1^{iii}	86.74 (12)
O23—Mo1—O13	169.78 (18)	O27^{iii}—Ca1—P1^{iii}	28.22 (11)
O18—Mo1—O13	84.16 (15)	O3W—Ca1—P1^{iii}	104.13 (17)
O6—Mo1—O13	80.76 (14)	O26—Ca1—P1^{iii}	90.08 (10)
O22—Mo1—O13	80.30 (15)	O5—Ca1—P1^{iii}	167.41 (11)
O10—Mo1—O13	72.47 (14)	O9^{iii}—Ca1—P1^{iii}	29.08 (9)
O23—Mo1—Mo6	100.70 (15)	O2W—Ca1—P3	158.9 (2)
O18—Mo1—Mo6	47.85 (11)	O21—Ca1—P3	24.27 (11)
O6—Mo1—Mo6	48.93 (11)	O27^{iii}—Ca1—P3	113.76 (13)
O22—Mo1—Mo6	133.13 (12)	O3W—Ca1—P3	79.0 (2)
O10—Mo1—Mo6	134.51 (11)	O26—Ca1—P3	91.15 (10)
O13—Mo1—Mo6	88.88 (10)	O5—Ca1—P3	81.26 (10)
O30—Mo2—O5	106.22 (19)	O9^{iii}—Ca1—P3	102.45 (12)
O30—Mo2—O3	101.47 (19)	P1^{iii}—Ca1—P3	110.49 (6)
O5—Mo2—O3	94.56 (16)	O2W—Ca1—P4	96.0 (3)
O30—Mo2—O17^{i}	97.14 (19)	O21—Ca1—P4	83.24 (12)
O5—Mo2—O17^{i}	86.41 (16)	O27^{iii}—Ca1—P4	142.26 (12)
O3—Mo2—O17^{i}	160.27 (16)	O3W—Ca1—P4	140.04 (18)
O30—Mo2—O7	99.50 (19)	O26—Ca1—P4	24.90 (9)
O5—Mo2—O7	153.47 (16)	O5—Ca1—P4	62.23 (9)
O3—Mo2—O7	86.54 (16)	O9^{iii}—Ca1—P4	85.63 (10)
O17^{i}—Mo2—O7	83.98 (16)	P1^{iii}—Ca1—P4	114.48 (6)
O30—Mo2—O2	171.12 (18)	P3—Ca1—P4	78.33 (5)
O5—Mo2—O2	82.14 (15)	O9—Fe2—O9^{iv}	180.0
O3—Mo2—O2	80.49 (15)	O9—Fe2—O26^{i}	99.53 (16)
O17^{i}—Mo2—O2	80.13 (15)	O9^{iv}—Fe2—O26^{i}	80.47 (16)
O7—Mo2—O2	71.88 (14)	O9—Fe2—O26^{ii}	80.47 (16)
O30—Mo2—Mo4	99.12 (16)	O9^{iv}—Fe2—O26^{ii}	99.53 (16)
O5—Mo2—Mo4	47.93 (11)	O26^{i}—Fe2—O26^{ii}	180.0 (3)
O3—Mo2—Mo4	48.76 (11)	O9—Fe2—O1W	93.73 (18)
O17^{i}—Mo2—Mo4	134.19 (12)	O9^{iv}—Fe2—O1W	86.27 (18)
O7—Mo2—Mo4	134.16 (11)	O26^{i}—Fe2—O1W	87.98 (17)
O2—Mo2—Mo4	88.70 (10)	O26^{ii}—Fe2—O1W	92.02 (17)
O24—Mo3—O20	106.2 (2)	O9—Fe2—O1W^{iv}	86.27 (18)
O24—Mo3—O1	103.04 (18)	O9^{iv}—Fe2—O1W^{iv}	93.73 (18)
O20—Mo3—O1	95.96 (16)	O26^{i}—Fe2—O1W^{iv}	92.02 (17)
O24—Mo3—O16	95.98 (18)	O26^{ii}—Fe2—O1W^{iv}	87.98 (17)
O20—Mo3—O16	86.01 (17)	O1W—Fe2—O1W^{iv}	180.00 (11)
O1—Mo3—O16	159.45 (15)	O7W—Na1—O32	69.3 (14)
O24—Mo3—O15^{i}	94.49 (19)	O7W—Na1—O1W^{iii}	92.2 (9)
O20—Mo3—O15^{i}	158.28 (16)	O32—Na1—O1W^{iii}	91.8 (9)
O1—Mo3—O15^{i}	85.52 (15)	O7W—Na1—O20^{i}	86.8 (10)
O16—Mo3—O15^{i}	85.30 (16)	O32—Na1—O20^{i}	152.1 (11)
O24—Mo3—O4	166.58 (18)	O1W^{iii}—Na1—O20^{i}	103.8 (3)
O20—Mo3—O4	85.60 (16)	O7W—Na1—O11^{i}	84.7 (8)
O1—Mo3—O4	81.60 (14)	O32—Na1—O11^{i}	99.8 (9)
O16—Mo3—O4	78.16 (14)	O1W^{iii}—Na1—O11^{i}	166.0 (4)
O15^{i}—Mo3—O4	73.15 (14)	O20^{i}—Na1—O11^{i}	62.5 (2)

O24—Mo3—Mo5	101.96 (15)	O7W—Na1—O26	160.0 (10)
O20—Mo3—Mo5	48.01 (12)	O32—Na1—O26	122.5 (11)
O1—Mo3—Mo5	49.58 (11)	O1W^{iii}—Na1—O26	72.3 (3)
O16—Mo3—Mo5	133.61 (12)	O20^{i}—Na1—O26	84.7 (3)
O15^{i}—Mo3—Mo5	134.46 (11)	O11^{i}—Na1—O26	107.2 (4)
O4—Mo3—Mo5	90.66 (9)	O7W—Na1—Mo5^{i}	97.7 (9)
O8—Mo4—O5	106.93 (19)	O32—Na1—Mo5^{i}	134.8 (9)
O8—Mo4—O3	102.73 (18)	O1W^{iii}—Na1—Mo5^{i}	132.9 (3)
O5—Mo4—O3	95.41 (16)	O20^{i}—Na1—Mo5^{i}	31.94 (13)
O8—Mo4—O25	96.93 (19)	O11^{i}—Na1—Mo5^{i}	34.94 (13)
O5—Mo4—O25	85.05 (17)	O26—Na1—Mo5^{i}	84.6 (2)
O3—Mo4—O25	159.25 (16)	Mo3—O1—Mo5	81.32 (14)
O8—Mo4—O10	98.41 (19)	Mo3—O1—Fe1	135.01 (19)
O5—Mo4—O10	153.60 (16)	Mo5—O1—Fe1	133.96 (19)
O3—Mo4—O10	85.93 (16)	P4—O2—Mo2	126.5 (2)
O25—Mo4—O10	84.67 (16)	P4—O2—Mo5^{i}	126.9 (2)
O8—Mo4—O13	170.14 (18)	Mo2—O2—Mo5^{i}	101.46 (14)
O5—Mo4—O13	81.26 (15)	Mo4—O3—Mo2	82.06 (15)
O3—Mo4—O13	81.54 (14)	Mo4—O3—Fe1	134.30 (19)
O25—Mo4—O13	78.02 (15)	Mo2—O3—Fe1	132.22 (19)
O10—Mo4—O13	72.84 (14)	P4^{i}—O4—Mo3	124.4 (2)
O8—Mo4—Mo2	100.64 (15)	P4^{i}—O4—Mo6^{i}	127.1 (2)
O5—Mo4—Mo2	48.38 (12)	Mo3—O4—Mo6^{i}	101.39 (14)
O3—Mo4—Mo2	49.18 (11)	Mo4—O5—Mo2	83.68 (15)
O25—Mo4—Mo2	133.21 (12)	Mo4—O5—Ca1	116.29 (17)
O10—Mo4—Mo2	134.03 (11)	Mo2—O5—Ca1	141.3 (2)
O13—Mo4—Mo2	88.89 (10)	Mo6—O6—Mo1	81.71 (14)
O28—Mo5—O20	106.1 (2)	Mo6—O6—Fe1	134.0 (2)
O28—Mo5—O1	101.12 (19)	Mo1—O6—Fe1	135.01 (19)
O20—Mo5—O1	95.53 (16)	Mo2—O7—Mo5^{i}	114.23 (17)
O28—Mo5—O11	98.0 (2)	Mo2—O7—H7	102.4
O20—Mo5—O11	84.92 (17)	Mo5^{i}—O7—H7	114.0
O1—Mo5—O11	159.96 (17)	P1—O9—Fe2	160.5 (3)
O28—Mo5—O7^{i}	99.11 (19)	P1—O9—Ca1^{ii}	92.4 (2)
O20—Mo5—O7^{i}	153.54 (16)	Fe2—O9—Ca1^{ii}	106.91 (17)
O1—Mo5—O7^{i}	87.33 (16)	Mo4—O10—Mo1	113.79 (18)
O11—Mo5—O7^{i}	83.68 (16)	Mo4—O10—H10A	108.9
O28—Mo5—O2^{i}	170.58 (19)	Mo1—O10—H10A	108.4
O20—Mo5—O2^{i}	83.10 (16)	P2—O11—Mo5	129.1 (3)
O1—Mo5—O2^{i}	79.68 (14)	P2—O11—Na1^{i}	110.0 (3)
O11—Mo5—O2^{i}	80.49 (16)	Mo5—O11—Na1^{i}	98.7 (3)
O7^{i}—Mo5—O2^{i}	71.51 (14)	P4—O13—Mo4	125.3 (2)
O28—Mo5—Mo3	100.37 (16)	P4—O13—Mo1	127.0 (2)
O20—Mo5—Mo3	48.04 (12)	Mo4—O13—Mo1	100.13 (15)
O1—Mo5—Mo3	49.10 (11)	Mo6—O15—Mo3^{i}	112.22 (17)
O11—Mo5—Mo3	132.59 (13)	Mo6—O15—H15	106.9
O7^{i}—Mo5—Mo3	134.87 (11)	Mo3^{i}—O15—H15	110.9
O2^{i}—Mo5—Mo3	87.29 (10)	P1—O16—Mo3	132.4 (2)

O28—Mo5—Na1^{i}	125.6 (2)	P2—O17—Mo2^{i}	128.4 (2)
O20—Mo5—Na1^{i}	45.33 (18)	Mo6—O18—Mo1	84.15 (15)
O1—Mo5—Na1^{i}	122.93 (19)	P1—O19—Mo6^{i}	133.1 (2)
O11—Mo5—Na1^{i}	46.38 (19)	Mo3—O20—Mo5	83.95 (16)
O7^{i}—Mo5—Na1^{i}	112.13 (19)	Mo3—O20—Na1^{i}	145.8 (3)
O2^{i}—Mo5—Na1^{i}	59.6 (2)	Mo5—O20—Na1^{i}	102.7 (2)
Mo3—Mo5—Na1^{i}	88.17 (13)	P3—O21—Ca1	115.5 (3)
O12—Mo6—O18	106.3 (2)	P3—O22—Mo1	131.3 (2)
O12—Mo6—O6	102.46 (18)	P3—O25—Mo4	135.9 (3)
O18—Mo6—O6	95.74 (16)	P4—O26—Fe2^{iii}	132.3 (2)
O12—Mo6—O19^{i}	96.78 (19)	P4—O26—Ca1	109.5 (2)
O18—Mo6—O19^{i}	87.72 (16)	Fe2^{iii}—O26—Ca1	108.14 (16)
O6—Mo6—O19^{i}	158.58 (16)	P4—O26—Na1	102.0 (3)
O12—Mo6—O15	96.41 (19)	Fe2^{iii}—O26—Na1	93.4 (2)
O18—Mo6—O15	156.08 (16)	Ca1—O26—Na1	107.5 (2)
O6—Mo6—O15	86.39 (15)	P1—O27—Ca1^{ii}	103.4 (2)
O19^{i}—Mo6—O15	82.16 (16)	P3—O29—H29	109.5
O12—Mo6—O4^{i}	168.62 (18)	P2—O31—H31	109.5
O18—Mo6—O4^{i}	84.23 (15)	C15—O32—Na1	116 (3)
O6—Mo6—O4^{i}	80.29 (14)	N1—C1—C2	119.9 (10)
O19^{i}—Mo6—O4^{i}	79.04 (15)	N1—C1—H1	120.0
O15—Mo6—O4^{i}	72.62 (14)	C2—C1—H1	120.0
O12—Mo6—Mo1	101.58 (15)	C1—C2—C3	118.7 (10)
O18—Mo6—Mo1	48.00 (12)	C1—C2—H2	120.7
O6—Mo6—Mo1	49.36 (11)	C3—C2—H2	120.7
O19^{i}—Mo6—Mo1	135.21 (12)	C4—C3—C2	119.0 (8)
O15—Mo6—Mo1	134.74 (11)	C4—C3—C6	119.1 (8)
O4^{i}—Mo6—Mo1	88.63 (9)	C2—C3—C6	121.9 (7)
O9—P1—O27	106.9 (3)	C5—C4—C3	120.6 (10)
O9—P1—O19	111.5 (3)	C5—C4—H4	119.7
O27—P1—O19	109.1 (3)	C3—C4—H4	119.7
O9—P1—O16	112.7 (3)	N1—C5—C4	119.3 (10)
O27—P1—O16	108.4 (2)	N1—C5—H5	120.3
O19—P1—O16	108.2 (2)	C4—C5—H5	120.3
O9—P1—Ca1^{ii}	58.50 (18)	C3—C6—C7	112.1 (6)
O27—P1—Ca1^{ii}	48.36 (18)	C3—C6—H6A	109.2
O19—P1—Ca1^{ii}	125.87 (16)	C7—C6—H6A	109.2
O16—P1—Ca1^{ii}	125.09 (17)	C3—C6—H6B	109.2
O14—P2—O11	114.3 (3)	C7—C6—H6B	109.2
O14—P2—O17	113.6 (3)	H6A—C6—H6B	107.9
O11—P2—O17	109.0 (2)	C8—C7—C6	113.0 (6)
O14—P2—O31	109.6 (3)	C8—C7—H7A	109.0
O11—P2—O31	103.7 (3)	C6—C7—H7A	109.0
O17—P2—O31	105.9 (2)	C8—C7—H7B	109.0
O21—P3—O25	109.9 (3)	C6—C7—H7B	109.0
O21—P3—O22	112.1 (3)	H7A—C7—H7B	107.8
O25—P3—O22	111.2 (2)	C11—C8—C7	111.1 (7)
O21—P3—O29	110.8 (3)	C11—C8—H8A	109.4

O25—P3—O29	106.2 (3)	C7—C8—H8A	109.4
O22—P3—O29	106.6 (2)	C11—C8—H8B	109.4
O21—P3—Ca1	40.20 (18)	C7—C8—H8B	109.4
O25—P3—Ca1	69.74 (18)	H8A—C8—H8B	108.0
O22—P3—Ca1	126.48 (17)	N2—C9—C10	118.4 (11)
O29—P3—Ca1	125.06 (19)	N2—C9—H9	120.8
O26—P4—O4^{i}	113.6 (2)	C10—C9—H9	120.8
O26—P4—O2	108.7 (2)	C11—C10—C9	120.7 (11)
O4^{i}—P4—O2	108.5 (2)	C11—C10—H10	119.7
O26—P4—O13	110.2 (2)	C9—C10—H10	119.7
O4^{i}—P4—O13	107.3 (2)	C10—C11—C12	117.2 (8)
O2—P4—O13	108.4 (2)	C10—C11—C8	120.9 (8)
O26—P4—Ca1	45.61 (16)	C12—C11—C8	121.9 (8)
O4^{i}—P4—Ca1	154.08 (16)	C13—C12—C11	119.8 (9)
O2—P4—Ca1	94.81 (15)	C13—C12—H12	120.1
O13—P4—Ca1	74.47 (15)	C11—C12—H12	120.1
O1—Fe1—O1^{i}	180.00 (11)	N2—C13—C12	121.1 (10)
O1—Fe1—O6	82.79 (14)	N2—C13—H13	119.4
O1^{i}—Fe1—O6	97.21 (14)	C12—C13—H13	119.4
O1—Fe1—O6^{i}	97.21 (14)	C15—C14—H14A	109.5
O1^{i}—Fe1—O6^{i}	82.79 (14)	C15—C14—H14B	109.5
O6—Fe1—O6^{i}	180.0	H14A—C14—H14B	109.5
O1—Fe1—O3^{i}	97.77 (14)	C15—C14—H14C	109.5
O1^{i}—Fe1—O3^{i}	82.23 (14)	H14A—C14—H14C	109.5
O6—Fe1—O3^{i}	84.14 (14)	H14B—C14—H14C	109.5
O6^{i}—Fe1—O3^{i}	95.86 (14)	O32—C15—C14	148 (3)
O1—Fe1—O3	82.23 (14)	O32—C15—H15A	99.8
O1^{i}—Fe1—O3	97.77 (14)	C14—C15—H15A	99.8
O6—Fe1—O3	95.86 (14)	O32—C15—H15B	99.8
O6^{i}—Fe1—O3	84.14 (14)	C14—C15—H15B	99.8
O3^{i}—Fe1—O3	180.0	H15A—C15—H15B	104.1
O2W—Ca1—O21	176.4 (3)	C1—N1—C5	122.4 (9)
O2W—Ca1—O27^{iii}	83.2 (2)	C1—N1—H1A	118.8
O21—Ca1—O27^{iii}	95.23 (16)	C5—N1—H1A	118.8
O2W—Ca1—O3W	93.6 (4)	C13—N2—C9	122.6 (9)
O21—Ca1—O3W	89.3 (3)	C13—N2—H2A	118.7
O27^{iii}—Ca1—O3W	77.4 (2)	C9—N2—H2A	118.7
O2W—Ca1—O26	91.6 (3)	Fe2—O1W—Na1^{ii}	102.1 (3)
O21—Ca1—O26	86.16 (15)	Fe2—O1W—H1WA	107.7
O27^{iii}—Ca1—O26	117.44 (15)	Na1^{ii}—O1W—H1WA	114.8
O3W—Ca1—O26	164.8 (2)	Fe2—O1W—H1WB	103.3
O2W—Ca1—O5	78.2 (2)	Na1^{ii}—O1W—H1WB	124.5
O21—Ca1—O5	104.45 (15)	H1WA—O1W—H1WB	103.0
O27^{iii}—Ca1—O5	151.29 (15)		

Symmetry codes: (i) $-x+1/2, -y+1/2, -z$; (ii) $x+1/2, y-1/2, z$; (iii) $x-1/2, y+1/2, z$; (iv) $-x+1, -y, -z$.

(3)

Crystal data

$(C_{12}H_{14}N_2)_3\{Fe[Mo_6O_{12}(OH)_3(HPO_4)_3(H_2PO_4)]_2\}\cdot 8H_2O$
M_r = 3159.85
Monoclinic, $P2_1/c$
a = 11.8121 (9) Å
b = 22.6484 (16) Å
c = 16.0089 (12) Å
β = 98.701 (1)°
V = 4233.5 (5) Å^3
Z = 2
$F(000)$ = 3072
D_x = 2.479 Mg m^{-3}
Mo $K\alpha$ radiation, λ = 0.71073 Å
Cell parameters from 9201 reflections
θ = 2.2–28.3°
μ = 2.15 mm^{-1}
T = 296 K
Block, brown
0.19 × 0.15 × 0.13 mm

Data collection

Bruker SMART CCD area detector diffractometer
phi and ω scans
Absorption correction: multi-scan (SADABS; Bruker, 2008)
T_{min} = 0.685, T_{max} = 0.756
20768 measured reflections
7432 independent reflections
7075 reflections with $I > 2\sigma(I)$
R_{int} = 0.018
θ_{max} = 25.0°, θ_{min} = 2.0°
$h = -14 \rightarrow 11$
$k = -22 \rightarrow 26$
$l = -19 \rightarrow 18$

Refinement

Refinement on F^2
Least-squares matrix: full
$R[F^2 > 2\sigma(F^2)]$ = 0.020
$wR(F^2)$ = 0.050
S = 1.07
7432 reflections
628 parameters
0 restraints
Hydrogen site location: mixed
H atoms treated by a mixture of independent and constrained refinement
$w = 1/[\sigma^2(F_o^2) + (0.0214P)^2 + 6.4728P]$ where $P = (F_o^2 + 2F_c^2)/3$
$(\Delta/\sigma)_{max}$ = 0.001
$\Delta\rho_{max}$ = 0.72 e Å^{-3}
$\Delta\rho_{min}$ = −0.59 e Å^{-3}

Special details

Geometry. All esds (except the esd in the dihedral angle between two l.s. planes) are estimated using the full covariance matrix. The cell esds are taken into account individually in the estimation of esds in distances, angles and torsion angles; correlations between esds in cell parameters are only used when they are defined by crystal symmetry. An approximate (isotropic) treatment of cell esds is used for estimating esds involving l.s. planes.

Fractional atomic coordinates and isotropic or equivalent isotropic displacement parameters (Å^2)

	x	y	z	U_{iso}*/U_{eq}	Occ. (<1)
Mo1	0.29173 (2)	0.10155 (2)	−0.13897 (2)	0.01548 (6)	
Mo2	0.58422 (2)	0.13730 (2)	−0.11323 (2)	0.01578 (6)	
Mo3	0.70667 (2)	0.12867 (2)	0.03583 (2)	0.01592 (6)	
Mo4	0.36395 (2)	0.05522 (2)	0.18837 (2)	0.01419 (6)	
Mo5	0.57919 (2)	0.08259 (2)	0.20924 (2)	0.01492 (6)	
Mo6	0.19815 (2)	0.06670 (2)	−0.01213 (2)	0.01551 (6)	
Fe1	0.5000	0.0000	0.0000	0.01291 (11)	
P1	0.42471 (6)	0.15907 (3)	0.04509 (4)	0.01395 (14)	
P2	0.76911 (6)	0.18718 (3)	0.22285 (5)	0.01953 (15)	
P3	0.10178 (6)	0.10738 (3)	0.16149 (5)	0.02016 (15)	
P4	0.38953 (7)	0.22009 (3)	−0.22689 (5)	0.02158 (16)	

O1	0.60533 (17)	0.07110 (8)	−0.03128 (11)	0.0166 (4)
O2	0.44798 (16)	0.12122 (8)	0.24506 (11)	0.0176 (4)
O3	0.65325 (17)	0.19655 (8)	−0.03302 (12)	0.0200 (4)
O4	0.18549 (17)	0.13936 (8)	−0.07578 (12)	0.0197 (4)
O5	0.45048 (17)	0.08830 (8)	−0.18085 (12)	0.0182 (4)
H5A	0.4662	0.0513	−0.1770	0.038 (10)*
O6	0.54235 (16)	0.14502 (8)	0.09499 (11)	0.0168 (4)
O7	0.36566 (18)	0.00329 (9)	0.26305 (12)	0.0249 (4)
O8	0.25157 (16)	0.01367 (8)	0.09375 (11)	0.0176 (4)
H8A	0.2830	−0.0170	0.0786	0.068 (15)*
O9	0.33550 (16)	0.11885 (8)	0.07558 (11)	0.0161 (4)
O10	0.71037 (17)	0.07104 (8)	0.13729 (12)	0.0183 (4)
H10A	0.7109	0.0339	0.1179	0.045 (11)*
O11	0.33592 (16)	0.03812 (8)	−0.05589 (11)	0.0161 (4)
O12	0.48878 (16)	0.02874 (8)	0.12813 (11)	0.0158 (4)
O13	0.22022 (17)	0.09800 (9)	0.21252 (12)	0.0218 (4)
O14	0.42692 (16)	0.14955 (8)	−0.04916 (11)	0.0157 (4)
O15	0.21073 (18)	0.06543 (9)	−0.21747 (13)	0.0254 (5)
O16	0.68317 (18)	0.12247 (9)	−0.17452 (13)	0.0263 (5)
O17	0.75679 (18)	0.19221 (9)	0.12701 (12)	0.0233 (4)
O18	0.09570 (18)	0.02219 (9)	−0.06138 (13)	0.0265 (5)
O19	0.29620 (18)	0.18141 (8)	−0.19907 (13)	0.0246 (4)
O20	0.50802 (18)	0.20688 (9)	−0.17904 (13)	0.0259 (5)
O21	0.83426 (18)	0.11294 (9)	0.00918 (14)	0.0283 (5)
O22	0.10384 (17)	0.10971 (9)	0.06682 (12)	0.0241 (4)
O23	0.39470 (19)	0.22459 (8)	0.05370 (12)	0.0234 (4)
H23A	0.4022	0.2399	0.1041	0.079 (16)*
O24	0.62769 (18)	0.03663 (9)	0.28820 (13)	0.0254 (5)
O25	0.66925 (17)	0.15631 (8)	0.25386 (12)	0.0221 (4)
O26	0.8794 (2)	0.15572 (11)	0.26037 (14)	0.0359 (6)
H26A	0.9508	0.1581	0.2328	0.080 (16)*
O27	0.04978 (19)	0.16256 (9)	0.19178 (14)	0.0308 (5)
O28	0.0280 (2)	0.05302 (11)	0.18183 (17)	0.0348 (6)
H28A	−0.003 (5)	0.039 (2)	0.148 (3)	0.08 (2)*
O29	0.3885 (2)	0.21579 (10)	−0.32086 (13)	0.0373 (6)
O30	0.7742 (2)	0.25196 (9)	0.25497 (15)	0.0336 (5)
H30A	0.7986	0.2535	0.3096	0.066 (14)*
O31	0.3561 (2)	0.28356 (9)	−0.20143 (15)	0.0329 (5)
H31A	0.3975	0.3168	−0.2193	0.072 (15)*
C1	1.0091 (4)	0.1796 (2)	0.6889 (3)	0.0648 (13)
H1	1.0439	0.2131	0.6709	0.078*
C2	0.9653 (5)	0.1387 (2)	0.6319 (3)	0.0672 (13)
H2	0.9691	0.1443	0.5748	0.081*
C3	0.9147 (4)	0.08854 (19)	0.6581 (3)	0.0539 (11)
C4	0.9078 (4)	0.08310 (17)	0.7443 (3)	0.0528 (11)
H4	0.8724	0.0503	0.7640	0.063*
C5	0.9535 (3)	0.12643 (17)	0.7999 (3)	0.0483 (10)
H5	0.9494	0.1232	0.8573	0.058*

C6	0.8704 (4)	0.0440 (2)	0.5939 (3)	0.0588 (12)	
H6	0.8670	0.0545	0.5374	0.071*	
C7	0.8362 (4)	−0.00794 (18)	0.6101 (3)	0.0528 (10)	
H7	0.8374	−0.0184	0.6664	0.063*	
C8	0.7371 (5)	−0.0840 (2)	0.4031 (3)	0.0615 (13)	
H8	0.7255	−0.0762	0.3454	0.074*	
C9	0.7789 (5)	−0.04090 (19)	0.4583 (3)	0.0610 (12)	
H9	0.7967	−0.0040	0.4384	0.073*	
C10	0.7949 (3)	−0.05206 (17)	0.5448 (2)	0.0440 (9)	
C11	0.7658 (4)	−0.10720 (17)	0.5711 (2)	0.0507 (11)	
H11	0.7737	−0.1158	0.6285	0.061*	
C12	0.7254 (4)	−0.14922 (18)	0.5132 (2)	0.0500 (10)	
H12	0.7067	−0.1865	0.5314	0.060*	
C13	0.3812 (4)	0.83311 (15)	0.3958 (3)	0.0448 (9)	
H13	0.3577	0.8131	0.3454	0.054*	
C14	0.4127 (3)	0.89124 (14)	0.3946 (2)	0.0395 (9)	
H14	0.4109	0.9107	0.3433	0.047*	
C15	0.4473 (3)	0.92112 (13)	0.4698 (2)	0.0302 (7)	
C16	0.4495 (4)	0.89016 (16)	0.5444 (2)	0.0426 (9)	
H16	0.4731	0.9088	0.5958	0.051*	
C17	0.4170 (4)	0.83217 (16)	0.5429 (3)	0.0472 (10)	
H17	0.4178	0.8114	0.5932	0.057*	
C18	0.4830 (3)	0.98314 (14)	0.4669 (2)	0.0336 (8)	
H18	0.4814	1.0001	0.4139	0.040*	
N1	1.0032 (3)	0.17258 (14)	0.7703 (2)	0.0496 (9)	
H1A	1.0333	0.2052	0.8034	0.058 (13)*	
N2	0.7125 (3)	−0.13723 (14)	0.43059 (19)	0.0454 (8)	
H2A	0.6661	−0.1654	0.3885	0.092 (17)*	
N3	0.3842 (3)	0.80562 (12)	0.4690 (2)	0.0413 (8)	
H3A	0.3691	0.7656	0.4755	0.076 (15)*	
O1W	0.1208 (3)	0.23304 (12)	0.34121 (19)	0.0513 (7)	
H1WA	0.1011	0.2006	0.3049	0.12 (2)*	
H1WB	0.1996	0.2395	0.3271	0.17 (3)*	
O2W	0.8433 (3)	0.25122 (15)	0.91727 (18)	0.0652 (9)	
H2WA	0.9111	0.2461	0.9452	0.071 (16)*	
H2WB	0.7915	0.2301	0.9423	0.11 (2)*	
O3W	0.0547 (3)	0.23455 (15)	0.0109 (2)	0.0785 (10)	
H3WA	0.0755	0.2027	0.0352	0.118*	
H3WB	0.0716	0.2493	−0.0345	0.118*	
O4W	0.8772 (12)	0.1106 (5)	0.4230 (6)	0.145 (5)	0.5
H4WA	0.8205	0.1294	0.4446	0.217*	
H4WB	0.9402	0.1311	0.4414	0.217*	
O5W	0.9039 (10)	0.0537 (8)	0.3586 (12)	0.226 (10)	0.5

Atomic displacement parameters (Å^2)

	U^{11}	U^{22}	U^{33}	U^{12}	U^{13}	U^{23}
Mo1	0.02102 (13)	0.01320 (11)	0.01198 (11)	0.00036 (9)	0.00167 (9)	0.00130 (8)

Mo2	0.02169 (13)	0.01310 (11)	0.01328 (12)	−0.00064 (9)	0.00506 (9)	0.00043 (9)
Mo3	0.01905 (13)	0.01403 (11)	0.01505 (12)	−0.00090 (9)	0.00379 (9)	−0.00111 (9)
Mo4	0.01798 (13)	0.01363 (11)	0.01139 (11)	0.00042 (9)	0.00361 (9)	−0.00018 (8)
Mo5	0.01785 (13)	0.01473 (11)	0.01218 (11)	0.00060 (9)	0.00223 (9)	−0.00128 (9)
Mo6	0.01761 (13)	0.01603 (12)	0.01291 (12)	0.00089 (9)	0.00237 (9)	0.00018 (9)
Fe1	0.0174 (3)	0.0111 (2)	0.0106 (2)	0.0005 (2)	0.0033 (2)	−0.00001 (19)
P1	0.0192 (4)	0.0112 (3)	0.0117 (3)	0.0014 (3)	0.0029 (3)	−0.0001 (2)
P2	0.0197 (4)	0.0199 (4)	0.0188 (4)	−0.0018 (3)	0.0024 (3)	−0.0046 (3)
P3	0.0185 (4)	0.0232 (4)	0.0199 (4)	0.0017 (3)	0.0064 (3)	−0.0024 (3)
P4	0.0333 (4)	0.0149 (3)	0.0162 (4)	0.0000 (3)	0.0024 (3)	0.0055 (3)
O1	0.0222 (10)	0.0122 (9)	0.0156 (9)	−0.0001 (7)	0.0037 (8)	−0.0006 (7)
O2	0.0206 (10)	0.0174 (9)	0.0152 (9)	0.0003 (8)	0.0038 (8)	−0.0036 (7)
O3	0.0278 (11)	0.0134 (9)	0.0191 (10)	−0.0017 (8)	0.0045 (8)	−0.0002 (7)
O4	0.0215 (11)	0.0184 (9)	0.0186 (10)	0.0038 (8)	0.0012 (8)	0.0006 (8)
O5	0.0260 (11)	0.0118 (9)	0.0174 (10)	0.0003 (8)	0.0049 (8)	−0.0014 (7)
O6	0.0194 (10)	0.0171 (9)	0.0140 (9)	−0.0001 (8)	0.0029 (8)	0.0002 (7)
O7	0.0319 (12)	0.0251 (11)	0.0185 (10)	−0.0016 (9)	0.0068 (9)	0.0049 (8)
O8	0.0231 (10)	0.0145 (9)	0.0153 (9)	−0.0003 (8)	0.0033 (8)	−0.0008 (7)
O9	0.0178 (10)	0.0175 (9)	0.0129 (9)	0.0003 (7)	0.0024 (7)	0.0008 (7)
O10	0.0226 (11)	0.0151 (9)	0.0177 (10)	0.0021 (8)	0.0047 (8)	−0.0012 (7)
O11	0.0232 (10)	0.0124 (9)	0.0138 (9)	0.0031 (7)	0.0065 (8)	0.0024 (7)
O12	0.0191 (10)	0.0137 (9)	0.0152 (9)	0.0005 (7)	0.0040 (8)	−0.0021 (7)
O13	0.0220 (11)	0.0275 (11)	0.0166 (10)	0.0033 (8)	0.0051 (8)	−0.0034 (8)
O14	0.0208 (10)	0.0141 (9)	0.0129 (9)	0.0003 (7)	0.0044 (8)	−0.0010 (7)
O15	0.0305 (12)	0.0262 (11)	0.0186 (10)	−0.0041 (9)	0.0003 (9)	−0.0016 (8)
O16	0.0293 (12)	0.0288 (11)	0.0228 (11)	−0.0019 (9)	0.0102 (9)	−0.0026 (9)
O17	0.0265 (11)	0.0223 (10)	0.0212 (10)	−0.0065 (8)	0.0038 (9)	−0.0039 (8)
O18	0.0265 (12)	0.0286 (11)	0.0234 (11)	−0.0067 (9)	0.0011 (9)	−0.0002 (9)
O19	0.0295 (12)	0.0187 (10)	0.0242 (11)	−0.0007 (8)	−0.0004 (9)	0.0092 (8)
O20	0.0318 (12)	0.0194 (10)	0.0265 (11)	−0.0004 (9)	0.0051 (9)	0.0097 (8)
O21	0.0251 (12)	0.0306 (11)	0.0300 (12)	0.0017 (9)	0.0071 (9)	−0.0006 (9)
O22	0.0195 (11)	0.0338 (11)	0.0193 (10)	0.0070 (9)	0.0038 (8)	−0.0006 (9)
O23	0.0393 (13)	0.0140 (9)	0.0168 (10)	0.0048 (8)	0.0041 (9)	−0.0022 (8)
O24	0.0290 (12)	0.0263 (11)	0.0199 (10)	0.0043 (9)	0.0009 (9)	0.0032 (8)
O25	0.0250 (11)	0.0230 (10)	0.0190 (10)	−0.0051 (8)	0.0052 (8)	−0.0068 (8)
O26	0.0261 (12)	0.0574 (15)	0.0251 (12)	0.0118 (11)	0.0065 (10)	0.0041 (11)
O27	0.0276 (12)	0.0284 (11)	0.0384 (13)	0.0053 (9)	0.0115 (10)	−0.0062 (10)
O28	0.0385 (15)	0.0349 (13)	0.0314 (14)	−0.0138 (11)	0.0067 (11)	−0.0033 (11)
O29	0.0647 (17)	0.0294 (12)	0.0172 (11)	−0.0113 (11)	0.0042 (11)	0.0056 (9)
O30	0.0465 (15)	0.0233 (11)	0.0307 (13)	−0.0089 (10)	0.0053 (11)	−0.0100 (9)
O31	0.0420 (14)	0.0143 (10)	0.0446 (14)	0.0017 (9)	0.0139 (11)	0.0045 (9)
C1	0.069 (3)	0.050 (3)	0.074 (3)	−0.013 (2)	0.006 (3)	−0.007 (2)
C2	0.078 (4)	0.058 (3)	0.065 (3)	−0.014 (3)	0.013 (3)	−0.011 (2)
C3	0.050 (3)	0.050 (2)	0.060 (3)	0.004 (2)	0.003 (2)	−0.019 (2)
C4	0.044 (2)	0.035 (2)	0.077 (3)	−0.0023 (17)	0.004 (2)	−0.007 (2)
C5	0.040 (2)	0.043 (2)	0.058 (3)	0.0072 (18)	−0.0033 (19)	−0.0094 (19)
C6	0.073 (3)	0.055 (3)	0.049 (3)	−0.008 (2)	0.012 (2)	−0.002 (2)
C7	0.064 (3)	0.042 (2)	0.053 (3)	−0.002 (2)	0.011 (2)	−0.0044 (19)

C8	0.098 (4)	0.061 (3)	0.029 (2)	−0.014 (3)	0.020 (2)	−0.0005 (19)
C9	0.089 (4)	0.044 (2)	0.054 (3)	−0.020 (2)	0.022 (2)	−0.001 (2)
C10	0.046 (2)	0.043 (2)	0.041 (2)	−0.0013 (17)	0.0016 (17)	−0.0095 (17)
C11	0.078 (3)	0.041 (2)	0.0291 (19)	−0.004 (2)	−0.0071 (19)	−0.0022 (16)
C12	0.071 (3)	0.038 (2)	0.039 (2)	−0.0051 (19)	−0.002 (2)	−0.0015 (17)
C13	0.057 (3)	0.0270 (18)	0.047 (2)	−0.0051 (17)	−0.0004 (19)	−0.0091 (16)
C14	0.061 (3)	0.0245 (17)	0.0298 (18)	−0.0071 (16)	−0.0030 (17)	0.0021 (14)
C15	0.041 (2)	0.0199 (15)	0.0293 (17)	−0.0024 (13)	0.0035 (14)	0.0014 (13)
C16	0.066 (3)	0.0323 (18)	0.0298 (19)	−0.0067 (17)	0.0091 (18)	0.0024 (15)
C17	0.066 (3)	0.0314 (19)	0.046 (2)	−0.0029 (18)	0.015 (2)	0.0145 (17)
C18	0.056 (2)	0.0211 (15)	0.0235 (16)	−0.0055 (14)	0.0041 (15)	0.0044 (12)
N1	0.0411 (19)	0.0370 (18)	0.067 (2)	0.0014 (14)	−0.0045 (17)	−0.0176 (16)
N2	0.058 (2)	0.0446 (18)	0.0326 (17)	−0.0088 (15)	0.0037 (15)	−0.0132 (14)
N3	0.0449 (19)	0.0163 (13)	0.064 (2)	−0.0032 (12)	0.0124 (16)	0.0043 (14)
O1W	0.0472 (17)	0.0421 (15)	0.0632 (18)	−0.0007 (12)	0.0034 (14)	0.0031 (14)
O2W	0.060 (2)	0.088 (2)	0.0466 (17)	−0.0260 (17)	0.0040 (16)	0.0269 (16)
O3W	0.088 (3)	0.072 (2)	0.078 (2)	0.0247 (19)	0.020 (2)	0.0180 (19)
O4W	0.236 (14)	0.121 (8)	0.070 (6)	0.002 (9)	0.002 (7)	0.063 (6)
O5W	0.108 (9)	0.268 (17)	0.32 (2)	0.059 (10)	0.078 (11)	0.246 (17)

Geometric parameters (Å, º)

Mo1—O15	1.673 (2)	P4—O31	1.561 (2)
Mo1—O4	1.9276 (19)	O5—H5A	0.8591
Mo1—O11	1.9736 (17)	O8—H8A	0.8411
Mo1—O19	2.0532 (19)	O10—H10A	0.8960
Mo1—O5	2.1062 (19)	O23—H23A	0.8711
Mo1—O14	2.2592 (18)	O26—H26A	1.0107
Mo1—Mo6	2.5782 (3)	O28—H28A	0.68 (5)
Mo2—O16	1.670 (2)	O30—H30A	0.8792
Mo2—O3	1.9487 (19)	O31—H31A	0.9642
Mo2—O1	1.9830 (18)	C1—N1	1.325 (6)
Mo2—O20	2.0290 (19)	C1—C2	1.348 (6)
Mo2—O5	2.0933 (19)	C1—H1	0.9300
Mo2—O14	2.2711 (18)	C2—C3	1.378 (6)
Mo2—Mo3	2.6039 (4)	C2—H2	0.9300
Mo3—O21	1.666 (2)	C3—C4	1.400 (6)
Mo3—O3	1.9408 (19)	C3—C6	1.478 (6)
Mo3—O1	1.9743 (18)	C4—C5	1.379 (6)
Mo3—O17	2.0715 (19)	C4—H4	0.9300
Mo3—O10	2.0789 (19)	C5—N1	1.321 (5)
Mo3—O6	2.3146 (19)	C5—H5	0.9300
Mo4—O7	1.6751 (19)	C6—C7	1.284 (6)
Mo4—O2	1.9419 (18)	C6—H6	0.9300
Mo4—O12	1.9733 (18)	C7—C10	1.474 (5)
Mo4—O13	2.042 (2)	C7—H7	0.9300
Mo4—O8	2.0819 (18)	C8—N2	1.331 (5)
Mo4—O9	2.2948 (18)	C8—C9	1.358 (6)

Mo4—Mo5	2.5890 (4)	C8—H8	0.9300
Mo5—O24	1.670 (2)	C9—C10	1.391 (6)
Mo5—O2	1.9404 (19)	C9—H9	0.9300
Mo5—O12	1.9734 (18)	C10—C11	1.379 (5)
Mo5—O25	2.0494 (19)	C11—C12	1.363 (5)
Mo5—O10	2.0823 (19)	C11—H11	0.9300
Mo5—O6	2.3006 (18)	C12—N2	1.337 (5)
Mo6—O18	1.677 (2)	C12—H12	0.9300
Mo6—O4	1.9295 (19)	C13—N3	1.323 (5)
Mo6—O11	1.9757 (18)	C13—C14	1.369 (5)
Mo6—O22	2.0527 (19)	C13—H13	0.9300
Mo6—O8	2.0953 (18)	C14—C15	1.387 (5)
Mo6—O9	2.3043 (18)	C14—H14	0.9300
Fe1—O1	2.1401 (18)	C15—C16	1.382 (5)
Fe1—O1^{i}	2.1401 (18)	C15—C18	1.469 (4)
Fe1—O12	2.1751 (18)	C16—C17	1.368 (5)
Fe1—O12^{i}	2.1751 (18)	C16—H16	0.9300
Fe1—O11^{i}	2.1857 (18)	C17—N3	1.332 (5)
Fe1—O11	2.1858 (18)	C17—H17	0.9300
P1—O9	1.5277 (19)	C18—C18^{ii}	1.318 (6)
P1—O6	1.528 (2)	C18—H18	0.9300
P1—O14	1.5283 (18)	N1—H1A	0.9462
P1—O23	1.5368 (19)	N2—H2A	1.0241
P2—O25	1.518 (2)	N3—H3A	0.9327
P2—O17	1.523 (2)	O1W—H1WA	0.9441
P2—O26	1.526 (2)	O1W—H1WB	1.0004
P2—O30	1.553 (2)	O2W—H2WA	0.8635
P3—O27	1.505 (2)	O2W—H2WB	0.9157
P3—O22	1.520 (2)	O3W—H3WA	0.8382
P3—O13	1.524 (2)	O3W—H3WB	0.8507
P3—O28	1.570 (2)	O4W—O5W	1.71 (2)
P4—O29	1.506 (2)	O4W—H4WA	0.9049
P4—O20	1.520 (2)	O4W—H4WB	0.8894
P4—O19	1.526 (2)		

O15—Mo1—O4	105.52 (10)	O12—Fe1—O11	95.23 (7)
O15—Mo1—O11	102.31 (9)	O12^{i}—Fe1—O11	84.77 (7)
O4—Mo1—O11	95.54 (8)	O11^{i}—Fe1—O11	180.00 (8)
O15—Mo1—O19	97.53 (9)	O9—P1—O6	108.99 (10)
O4—Mo1—O19	85.38 (8)	O9—P1—O14	110.30 (10)
O11—Mo1—O19	159.09 (8)	O6—P1—O14	109.69 (11)
O15—Mo1—O5	97.28 (9)	O9—P1—O23	111.56 (11)
O4—Mo1—O5	155.78 (8)	O6—P1—O23	110.98 (11)
O11—Mo1—O5	87.33 (7)	O14—P1—O23	105.27 (10)
O19—Mo1—O5	83.63 (8)	O25—P2—O17	113.79 (11)
O15—Mo1—O14	169.09 (9)	O25—P2—O26	108.40 (13)
O4—Mo1—O14	84.60 (7)	O17—P2—O26	112.16 (12)
O11—Mo1—O14	80.33 (7)	O25—P2—O30	108.66 (12)

O19—Mo1—O14	78.96 (7)	O17—P2—O30	104.83 (12)
O5—Mo1—O14	72.15 (7)	O26—P2—O30	108.83 (14)
O15—Mo1—Mo6	100.21 (7)	O27—P3—O22	111.18 (12)
O4—Mo1—Mo6	48.09 (6)	O27—P3—O13	109.22 (12)
O11—Mo1—Mo6	49.28 (5)	O22—P3—O13	112.79 (11)
O19—Mo1—Mo6	133.10 (6)	O27—P3—O28	108.55 (14)
O5—Mo1—Mo6	135.69 (5)	O22—P3—O28	109.08 (13)
O14—Mo1—Mo6	89.55 (5)	O13—P3—O28	105.81 (13)
O16—Mo2—O3	105.39 (9)	O29—P4—O20	111.02 (14)
O16—Mo2—O1	101.99 (9)	O29—P4—O19	110.93 (13)
O3—Mo2—O1	94.97 (8)	O20—P4—O19	112.99 (11)
O16—Mo2—O20	98.39 (9)	O29—P4—O31	110.87 (13)
O3—Mo2—O20	85.17 (8)	O20—P4—O31	107.43 (13)
O1—Mo2—O20	158.79 (8)	O19—P4—O31	103.30 (12)
O16—Mo2—O5	97.47 (9)	Mo3—O1—Mo2	82.29 (7)
O3—Mo2—O5	156.01 (8)	Mo3—O1—Fe1	134.08 (9)
O1—Mo2—O5	87.18 (7)	Mo2—O1—Fe1	134.77 (10)
O20—Mo2—O5	84.40 (8)	Mo5—O2—Mo4	83.65 (7)
O16—Mo2—O14	169.44 (9)	Mo3—O3—Mo2	84.05 (7)
O3—Mo2—O14	84.70 (7)	Mo1—O4—Mo6	83.89 (7)
O1—Mo2—O14	79.81 (7)	Mo2—O5—Mo1	113.48 (8)
O20—Mo2—O14	79.08 (8)	Mo2—O5—H5A	110.0
O5—Mo2—O14	72.14 (7)	Mo1—O5—H5A	108.1
O16—Mo2—Mo3	100.51 (7)	P1—O6—Mo5	126.25 (11)
O3—Mo2—Mo3	47.84 (5)	P1—O6—Mo3	124.88 (10)
O1—Mo2—Mo3	48.71 (5)	Mo5—O6—Mo3	99.06 (7)
O20—Mo2—Mo3	132.49 (6)	Mo4—O8—Mo6	114.22 (8)
O5—Mo2—Mo3	134.85 (5)	Mo4—O8—H8A	108.8
O14—Mo2—Mo3	88.53 (5)	Mo6—O8—H8A	109.4
O21—Mo3—O3	104.65 (9)	P1—O9—Mo4	126.86 (11)
O21—Mo3—O1	102.53 (9)	P1—O9—Mo6	124.54 (10)
O3—Mo3—O1	95.50 (8)	Mo4—O9—Mo6	99.40 (7)
O21—Mo3—O17	98.97 (9)	Mo3—O10—Mo5	115.08 (9)
O3—Mo3—O17	83.31 (8)	Mo3—O10—H10A	108.6
O1—Mo3—O17	158.03 (8)	Mo5—O10—H10A	110.8
O21—Mo3—O10	98.80 (9)	Mo1—O11—Mo6	81.51 (7)
O3—Mo3—O10	155.19 (8)	Mo1—O11—Fe1	133.72 (9)
O1—Mo3—O10	87.13 (7)	Mo6—O11—Fe1	135.33 (9)
O17—Mo3—O10	85.16 (8)	Mo4—O12—Mo5	81.99 (7)
O21—Mo3—O6	170.46 (9)	Mo4—O12—Fe1	135.11 (9)
O3—Mo3—O6	83.39 (7)	Mo5—O12—Fe1	134.54 (9)
O1—Mo3—O6	81.45 (7)	P3—O13—Mo4	133.36 (12)
O17—Mo3—O6	76.62 (7)	P1—O14—Mo1	125.46 (11)
O10—Mo3—O6	72.58 (7)	P1—O14—Mo2	126.90 (11)
O21—Mo3—Mo2	100.37 (8)	Mo1—O14—Mo2	101.63 (7)
O3—Mo3—Mo2	48.11 (6)	P2—O17—Mo3	129.14 (12)
O1—Mo3—Mo2	49.00 (5)	P4—O19—Mo1	135.50 (13)
O17—Mo3—Mo2	130.81 (6)	P4—O20—Mo2	135.79 (12)

O10—Mo3—Mo2	134.93 (5)	P3—O22—Mo6	133.58 (12)
O6—Mo3—Mo2	88.80 (5)	P1—O23—H23A	118.4
O7—Mo4—O2	104.88 (9)	P2—O25—Mo5	130.49 (12)
O7—Mo4—O12	101.90 (9)	P2—O26—H26A	121.5
O2—Mo4—O12	95.48 (8)	P3—O28—H28A	116 (5)
O7—Mo4—O13	96.81 (9)	P2—O30—H30A	111.0
O2—Mo4—O13	85.82 (8)	P4—O31—H31A	118.8
O12—Mo4—O13	160.21 (8)	N1—C1—C2	120.8 (5)
O7—Mo4—O8	98.01 (9)	N1—C1—H1	119.6
O2—Mo4—O8	155.88 (7)	C2—C1—H1	119.6
O12—Mo4—O8	87.04 (7)	C1—C2—C3	120.0 (5)
O13—Mo4—O8	84.00 (8)	C1—C2—H2	120.0
O7—Mo4—O9	170.76 (9)	C3—C2—H2	120.0
O2—Mo4—O9	83.57 (7)	C2—C3—C4	117.8 (4)
O12—Mo4—O9	80.65 (7)	C2—C3—C6	118.3 (4)
O13—Mo4—O9	79.87 (7)	C4—C3—C6	123.9 (4)
O8—Mo4—O9	73.15 (7)	C5—C4—C3	119.9 (4)
O7—Mo4—Mo5	99.81 (7)	C5—C4—H4	120.1
O2—Mo4—Mo5	48.15 (6)	C3—C4—H4	120.1
O12—Mo4—Mo5	49.01 (5)	N1—C5—C4	118.9 (4)
O13—Mo4—Mo5	133.66 (6)	N1—C5—H5	120.5
O8—Mo4—Mo5	135.05 (5)	C4—C5—H5	120.5
O9—Mo4—Mo5	88.58 (5)	C7—C6—C3	125.1 (4)
O24—Mo5—O2	104.78 (9)	C7—C6—H6	117.5
O24—Mo5—O12	101.68 (9)	C3—C6—H6	117.5
O2—Mo5—O12	95.52 (8)	C6—C7—C10	124.0 (4)
O24—Mo5—O25	98.24 (9)	C6—C7—H7	118.0
O2—Mo5—O25	85.71 (8)	C10—C7—H7	118.0
O12—Mo5—O25	158.99 (8)	N2—C8—C9	120.8 (4)
O24—Mo5—O10	98.14 (9)	N2—C8—H8	119.6
O2—Mo5—O10	156.14 (8)	C9—C8—H8	119.6
O12—Mo5—O10	86.12 (7)	C8—C9—C10	119.9 (4)
O25—Mo5—O10	84.53 (8)	C8—C9—H9	120.1
O24—Mo5—O6	170.58 (9)	C10—C9—H9	120.1
O2—Mo5—O6	83.94 (7)	C11—C10—C9	117.8 (4)
O12—Mo5—O6	80.69 (7)	C11—C10—C7	117.9 (4)
O25—Mo5—O6	78.59 (7)	C9—C10—C7	124.2 (4)
O10—Mo5—O6	72.81 (7)	C12—C11—C10	120.2 (4)
O24—Mo5—Mo4	99.57 (7)	C12—C11—H11	119.9
O2—Mo5—Mo4	48.20 (5)	C10—C11—H11	119.9
O12—Mo5—Mo4	49.00 (5)	N2—C12—C11	120.5 (4)
O25—Mo5—Mo4	133.46 (6)	N2—C12—H12	119.8
O10—Mo5—Mo4	134.18 (5)	C11—C12—H12	119.8
O6—Mo5—Mo4	88.89 (5)	N3—C13—C14	119.6 (3)
O18—Mo6—O4	105.76 (9)	N3—C13—H13	120.2
O18—Mo6—O11	102.17 (9)	C14—C13—H13	120.2
O4—Mo6—O11	95.42 (8)	C13—C14—C15	120.1 (3)
O18—Mo6—O22	98.89 (9)	C13—C14—H14	119.9

O4—Mo6—O22	85.10 (8)	C15—C14—H14	119.9
O11—Mo6—O22	157.93 (8)	C16—C15—C14	117.8 (3)
O18—Mo6—O8	98.23 (9)	C16—C15—C18	122.9 (3)
O4—Mo6—O8	154.95 (8)	C14—C15—C18	119.2 (3)
O11—Mo6—O8	86.31 (7)	C17—C16—C15	120.2 (4)
O22—Mo6—O8	84.20 (8)	C17—C16—H16	119.9
O18—Mo6—O9	170.35 (8)	C15—C16—H16	119.9
O4—Mo6—O9	82.86 (7)	N3—C17—C16	119.5 (3)
O11—Mo6—O9	80.92 (7)	N3—C17—H17	120.3
O22—Mo6—O9	77.25 (7)	C16—C17—H17	120.3
O8—Mo6—O9	72.71 (7)	C18^{ii}—C18—C15	125.7 (4)
O18—Mo6—Mo1	100.29 (7)	C18^{ii}—C18—H18	117.2
O4—Mo6—Mo1	48.02 (6)	C15—C18—H18	117.2
O11—Mo6—Mo1	49.21 (5)	C5—N1—C1	122.7 (4)
O22—Mo6—Mo1	132.61 (6)	C5—N1—H1A	124.5
O8—Mo6—Mo1	134.43 (5)	C1—N1—H1A	112.7
O9—Mo6—Mo1	88.67 (5)	C8—N2—C12	120.9 (3)
O1—Fe1—O1^{i}	180.0	C8—N2—H2A	118.0
O1—Fe1—O12	96.66 (7)	C12—N2—H2A	119.6
O1^{i}—Fe1—O12	83.34 (7)	C13—N3—C17	122.7 (3)
O1—Fe1—O12^{i}	83.34 (7)	C13—N3—H3A	125.2
O1^{i}—Fe1—O12^{i}	96.66 (7)	C17—N3—H3A	112.0
O12—Fe1—O12^{i}	180.0	H1WA—O1W—H1WB	97.3
O1—Fe1—O11^{i}	83.23 (7)	H2WA—O2W—H2WB	109.4
O1^{i}—Fe1—O11^{i}	96.77 (7)	H3WA—O3W—H3WB	130.1
O12—Fe1—O11^{i}	84.77 (7)	O5W—O4W—H4WA	143.1
O12^{i}—Fe1—O11^{i}	95.23 (7)	O5W—O4W—H4WB	111.8
O1—Fe1—O11	96.77 (7)	H4WA—O4W—H4WB	105.0
O1^{i}—Fe1—O11	83.23 (7)		

Symmetry codes: (i) $-x+1, -y, -z$; (ii) $-x+1, -y+2, -z+1$.